

FOUNDED 1925
INCORPORATED BY
ROYAL CHARTER 1961

*"To promote the advancement
of radio, electronics and kindred
subjects by the exchange of
information in these branches
of engineering."*

THE RADIO AND ELECTRONIC ENGINEER

The Journal of the Institution of Electronic and Radio Engineers

VOLUME 39 No. 5

MAY 1970

Fitness for Purpose

GOOD functional design and good appearance in a product have been for long regarded as virtually unrelated, if not actually incompatible. Such views are fortunately now being succeeded by an awareness that a pleasing outward appearance in a device which has to be used by people is not solely needed to achieve an initial attraction—to 'sell' it—but ought to be associated with ease and efficiency of operation. The fact that it has taken so long for this to be appreciated, and that the new science of ergonomics has had to be founded, shows that good design is not a natural attribute of man's creations.

The recent announcement by the British Council of Industrial Design of its prize winning awards for 1970 for capital and consumer goods was accompanied by comments from the two panels of judges underlining some of the basic considerations which ought to be more clearly before designers than is all too often the case. The judges have looked primarily for innovation, economic value in terms of purpose and of manufacturing cost, ease of use and maintenance, and good appearance—all attributes with which every design engineer must agree. The observation that 'really concentrated efforts made at the design stage produce greater rewards than those obtained by successive modifications as the need for improvements subsequently become apparent' will raise rueful smiles among those many engineers who have been urged to proceed from design to production against their better judgement.

Out of the twenty-one products named, two out of eight in the capital goods section and one in the consumer goods section are made by the electronics industry. The first two are respectively a new range of computers and peripherals, and an automatic test equipment. The selected products were considered to show that the designers had striven to obtain the greatest value from the materials and manufacturing resources employed while making a contribution not only to current technology—through innovation—but to current economic requirements. The nature of the design process means that the 'ideal' design is unattainable—engineering after all always involves some compromise. In achieving this kind of compromise however, one factor not explicitly stated by the judges but implied in their requirements for a product to have been in service for a year, is that of reliability. Here compromise is hardly possible since 'built-in obsolescence' is a characteristic of few 'consumer goods', least of all of products such as the mobile u.h.f. radiotelephone which received an award in this section: reliability is a factor which must be continually borne in mind right from the initiation of a design with at least the same degree of care as is ease of use and final appearance.

It is hard to think of any product which can be simultaneously stigmatized as being out-of-date, expensive, inconvenient, unreliable and ugly! The positive counterparts of these negative attributes should be apparent to all and although one may find surprising omissions—and inclusions—in the CoID list, this annual critical look at new designs does emphasize that fitness for purpose calls for consideration of all aspects. Just to look good is not enough.

F.W.S.

INSTITUTION NOTICES

C.E.I. Local Committee in Scotland

A C.E.I. Local Committee has now been formed in Scotland and twelve of the fourteen chartered engineering institutions within C.E.I. have already nominated their representatives. The first Chairman is Mr. T. Ridley, B.Sc., C.Eng., D.I.C., F.I.C.E.; the I.E.R.E. is represented by the chairman of the Scottish Section, Mr. David Dick, D.I.C., C.Eng., F.I.E.R.E.

The Committee's objectives will be to stimulate interest in the work of C.E.I. through contact with Government and Local Authorities, the Press and other bodies. It will, in conjunction with its constituent member institutions, promote the interests of professional engineers in Scotland and provide a forum for active contact between the members of these institutions through meetings, public lectures or other functions.

European Register of Engineers

The 18 member countries of FEANI (Fédération Européenne d'Associations Nationales d'Ingenieurs) have introduced a 'European Register of Engineers'. This has been set up by the collaboration of FEANI National Register Committees in each of the member countries. Thus the 650,000 professionally qualified European engineers within FEANI may now be provided with a registration document which will materially help employers throughout the member countries in judging the qualifications of the holder, and thereby assist the interchangeability of engineers.

In the U.K. the Council of Engineering Institutions will act as the agents for the FEANI British National Register Committee. Initially from the U.K. only Chartered Engineers will be eligible for this Register.

Vacation School on R.F. Electrical Measurement Practice

A vacation school on Radio Frequency Electrical Measurement practice is to be held at the University of Kent, Canterbury, from 6th to 18th September, 1970. Organized by the Institution of Electrical Engineers with the association of the British Calibration Service and the I.E.R.E., the aim of the school is to review the latest practices in the field. It will mainly be of interest to senior workers in, and supervisors of, measurements laboratories. A minimum of mathematical treatment is planned, and the emphasis of the school will be on practical aspects of the subject. Some thirty lectures will be given during the vacation school, and these will be supplemented by group discussion periods.

Further details and registration will be available in due course from the Secretary, LS(SE), I.E.E., Savoy Place, London WC2R 0BL.

New Zealand Electronics Convention

NELCON 70, the third convention to be organized by the Institution's New Zealand Section and the New Zealand Electronics Institute, will be held in the School of Engineering, University of Auckland, from 25th to 28th August, 1970. Symposia and sessions comprising about 60 papers will deal with the following:

Electronics in Health; Micro-electronics; Colour Television; Satellite Communications; Components and Instruments; Applied Electronics; Research Electronics; Communications; Computer Systems, Applications and Data Handling.

Further information and registration forms may be obtained from: The Secretariat, NELCON 70, P.O. Box 3266, Auckland, 1.

Mobile Radio Communication Systems Conference

The Society of Electronic and Radio Technicians is holding a three-day conference on Mobile Radio Communication Systems at Brunel University, Uxbridge, from Tuesday, 30th June to Thursday, 2nd July. This is intended for technical staff engaged in the design, manufacture, operation and maintenance of mobile radio communication equipment.

Further information may be obtained from: The Conference Secretary, Society of Electronic and Radio Technicians, Faraday House, 8-10 Charing Cross Road, London, W.C.2. (Telephone 01-240 1152).

Prizes for Innovation

Prizes of £1,500 are being offered by the Royal Society of Arts as part of their continuing effort to further interest in the development of Britain's export trade. The prizes will be awarded for case studies dealing with innovations in industry and British exports, and funds for the prizes have been provided by the BETRO Trust and the Edgar E. Lawley Foundations. There will be two prizes of £500 and two of £250.

The rules of the award say that case studies should illustrate 'the successful use of new designs, innovations or discoveries which in recent years have contributed or in the next few years will contribute significantly to the United Kingdom's export trade or balance of payments'.

Entries may be submitted by any British firm or individual and the judges will be:

Mr. Raymond Baxter; Professor Misha Black; Mr. J. C. Duckworth (Director of the National Research Development Corporation); Mr. Whitney Straight (Deputy Chairman of Rolls Royce Ltd.); and Sir Barnes Wallis.

Further information may be obtained from the Secretary of the Royal Society of Arts, John Adam Street, London, WC2N 6EZ, to whom entries should be sent not later than 30th September, 1970.

Electronic Circuit Analysis using Transformation Matrices in conjunction with the Multi-Node Method

By

R. T. KENNEDY,

B.Sc., C.Eng., M.I.E.E., M.I.E.R.E.†

The representation of a network by its indefinite admittance matrix and the subsequent reduction to a nodal matrix is easily achieved. Any set of linear equations can be reduced by matrix partitioning to a 2×2 matrix; however, it is important to realize that if the easy-to-set-up nodal matrix is reduced, the resultant two-port representation has a node common to the input and output ports.

The reduction procedure can also be applied to two-ports such as lattice networks and difference amplifiers that do not have a node common to the ports of interest. The lack of the common node means that reduction of the nodal matrix is no longer applicable and the nodal equations must therefore be transformed into the required form before the reduction procedure is used.

Transformation matrices are used to transform the nodal equations into a new set of equations that contains voltage and current vectors related to the two ports of interest.

Symbols

[]	arrow indicates current direction at port 2
←	
[a]	transmission matrix
[Y]	short circuit admittance matrix
[] _T	transpose of the matrix
[A]	voltage transformation matrix
[Y _E]	equivalent 2×2 matrix
[E*]	conjugate of [E]
Y _{11E} , Y _{12E}	elements of equivalent 2×2 matrix
Y _{21E} , Y _{22E}	
g _m	mutual conductance
μ	amplification factor
r _a	anode slope resistance
y _{ib} , y _{rb}	transistor common base admittance parameters
y _{fb} , y _{ob}	
y _{ie} , y _{re}	transistor common emitter admittance parameters
y _{fe} , y _{oe}	
g _{fs}	f.e.t. transconductance
r _d	f.e.t. output resistance

$$\text{voltage gain} = -\frac{Y_{21E}}{Y_{22E}}$$

$$y_{re} = \frac{h_{fe}}{h_{ie}}$$

1. Introduction

In a previous paper¹ it has been stated that the multi-node method applies to a variety of networks,

† Department of Electrical and Electronic Engineering, College of Technology, Huddersfield, HD1 3DH.

active or passive. It could further be stated that it is directly applicable to networks having a common



Fig. 1. Network with common input and output node.

input and output node such as Fig. 1. All networks do not fall into this category, examples being:

- (1) The lattice network of Fig. 2.
- (2) The difference amplifier of Fig. 3.
- (3) Amplifiers with series voltage feedback as shown in Fig. 9.
- (4) Unilateralized networks as shown in Fig. 8.

One of the advantages of representing a network by a matrix is that the characteristics can then be easily determined. If the more conventional interconnected two-port method is used with the above circuits the following are some of the disadvantages that arise:

- (1) Validity of the two-port interconnexions must be verified.
- (2) The arrangement of interconnected two ports is not always obvious and can therefore be

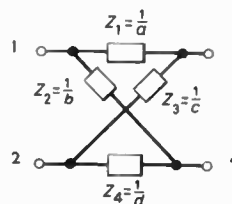
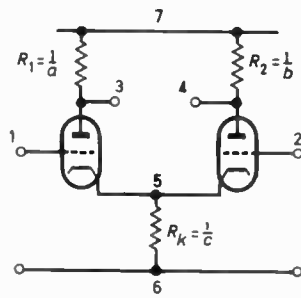
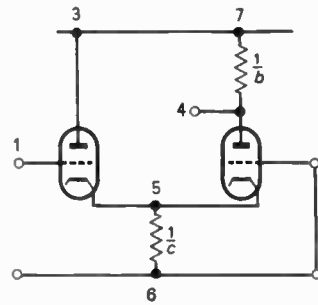


Fig. 2. Lattice network.



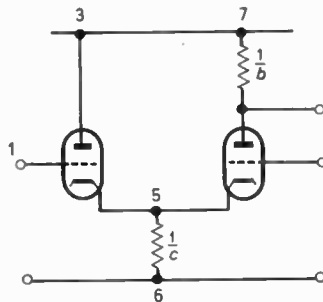
(a) Differential output, differential input

NODES 6 AND 7
ARE COMMON
WITH RESPECT
TO A.C.



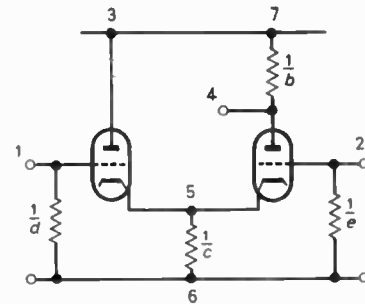
(d) Single-ended output, single-ended input

NODES 2,3,6,7
ARE COMMON
WITH RESPECT
TO A.C.

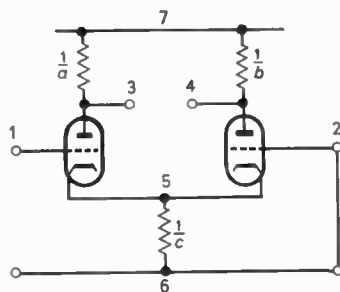


(b) Single-ended output, differential input

NODES 3,6,7
ARE COMMON
WITH RESPECT
TO A.C.



(e) As (b) but with grid admittances included



(c) Differential output, single-ended input

NODES 2,6,7
ARE COMMON
WITH RESPECT
TO A.C.

Fig. 3. Thermionic difference amplifier configurations.

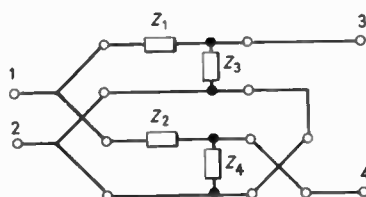


Fig. 4. Lattice network in the form of interconnected two-ports.

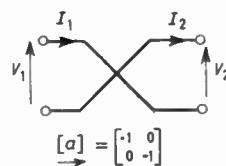


Fig. 5. Crossover matrix used in Fig. 4

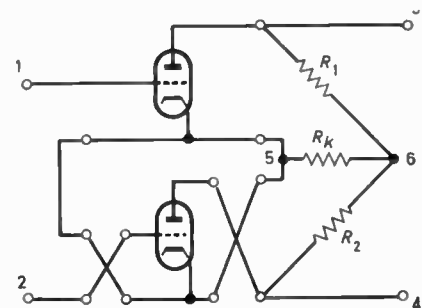


Fig. 6. The circuit of Fig. 3(a) as interconnected two-ports. (The T network can be replaced by a π equivalent.)

difficult to set up as shown in Fig. 6. In some cases an arrangement may not exist.

- (3) The matrices required for the interconnexions may not exist as is the case when the impedance matrix for a valve is required.
- (4) Several matrices are required as is the case with the lattice network. This is shown in Fig. 4.

The form of the nodal matrix is given by

$$[I] = [Y][E]$$

and can be considered as

$$[I_{old}] = [Y_{old}][E_{old}]$$

If the ports of the network are rearranged such that there is no direct connexion between input and output then the terms of the equation will change but the form of the equation will remain unaltered, thus

$$[I_{new}] = [Y_{new}][E_{new}]$$

The result is an admittance matrix $[Y_{new}]$ which is referred to the new voltages $[E_{new}]$, and can be reduced as before to a 2×2 matrix related to the new input and output. The method of obtaining the new admittance matrix is described.

Example. The nodal matrix for the difference amplifier of Fig. 3, having nodes 6 and 7 common with respect to a.c. and taken as the reference, is of the form given by

$$\begin{bmatrix} I_1 - I_7 \\ I_2 - I_7 \\ I_3 - I_7 \\ I_4 - I_7 \\ I_5 - I_7 \end{bmatrix} = \begin{bmatrix} Y_{11} & Y_{12} & \cdot & \cdot & Y_{15} \\ \cdot & \cdot & \cdot & \cdot & \cdot \\ \cdot & \cdot & \cdot & \cdot & \cdot \\ \cdot & \cdot & \cdot & \cdot & \cdot \\ Y_{51} & \cdot & \cdot & \cdot & Y_{55} \end{bmatrix} \begin{bmatrix} E_1 - E_7 \\ E_2 - E_7 \\ \cdot \\ \cdot \\ E_5 - E_7 \end{bmatrix}$$

The voltage gain formula can be used to relate any two voltage vectors in this equation; however, if a relationship is required between the differential input ($E_1 - E_2$) and the differential output ($E_3 - E_4$), then the equation cannot be used directly and thus reduction of the admittance matrix will not provide the required solution. Rearrangement of the equation to a more suitable form is achieved by the introduction of transformation matrices. The use of such transformations is discussed with respect to impedances by Kron.²

2. Mathematical Basis

Consider a network N_1 represented by

$$\begin{bmatrix} I_1 \\ I_2 \\ \vdots \\ I_n \end{bmatrix} = [Y_0] \begin{bmatrix} E_1 \\ E_2 \\ \vdots \\ E_n \end{bmatrix}$$

or $[I_0] = [Y_0][E_0]$ (1)

Power in the circuit can be represented by

$$\begin{aligned} P_0 &= E_1^* I_1 + E_2^* I_2 + \dots + E_n^* I_n \\ &= [E_1^* E_2^* \dots E_n^*] \begin{bmatrix} I_1 \\ I_2 \\ \vdots \\ I_n \end{bmatrix} \\ &= [E_0^*]_{\text{T}} [I_0] \end{aligned} \quad \text{.....(2)}$$

Let the network be transformed such that

$$[I_n] = [Y_n][E_n]$$

and

$$P_n = [E_n^*]_{\text{T}} [I_n] \quad \text{.....(3)}$$

If the power remains invariant then equations (2) and (3) are equal, thus

$$[E_0^*]_{\text{T}} [I_0] = [E_n^*]_{\text{T}} [I_n^*] \quad \text{.....(4)}$$

If the original voltages are transformed into new voltages given by

$$[E_0] = [A][E_n] \quad \text{.....(5)}$$

then

$$[E_0]_{\text{T}} = ([A][E_n])_{\text{T}}$$

and

$$[E_0]_{\text{T}} = [E_n]_{\text{T}} [A]_{\text{T}}$$

or

$$[E_0^*]_{\text{T}} = [E_n^*]_{\text{T}} [A]_{\text{T}} \quad \text{.....(6)}$$

Substituting the result of equation (5) into equation (1)

$$[I_0] = [Y_0][A][E_n]$$

Premultiply both sides by $[E_0^*]_{\text{T}}$

$$[E_0^*]_{\text{T}} [I_0] = [E_0^*]_{\text{T}} [Y_0][A][E_n]$$

using the result of equation (4)

$$[E_n^*]_{\text{T}} [I_n] = [E_0^*]_{\text{T}} [Y_0][A][E_n]$$

$$[I_n] = [E_n^*]^{-1} [E_0^*]_{\text{T}} [Y_0][A][E_n]$$

substituting the result of equation (6) for $[E_0^*]_{\text{T}}$

$$[I_n] = [E_n^*]_{\text{T}}^{-1} [E_n^*]_{\text{T}} [A]_{\text{T}} [Y_0][A][E_n]$$

Thus

$$[I_n] = [A]_{\text{T}} [Y_0][A][E_n]$$

and

$$[Y_n] = [A]_{\text{T}} [Y_0][A] \quad \text{.....(7)}$$

3. Theoretical Analysis and Numerical Verification

3.1. Lattice Network

Consider the network of Fig. 2. The indefinite admittance matrix is given by

$$[Y_1] = \begin{bmatrix} a+b & 0 & -a & -b \\ 0 & c+d & -c & -d \\ -a & -c & a+c & 0 \\ -b & -d & 0 & b+d \end{bmatrix}$$

The nodal admittance matrix with node 2 as the reference is given by

$$[Y_N] = \begin{bmatrix} a+b & -a & -b \\ -a & a+c & 0 \\ -b & 0 & b+d \end{bmatrix} \dots\dots(8)$$

the original voltages related to node 2 are represented by

$$[E_{old}] = \begin{bmatrix} E_1 - E_2 \\ E_3 - E_2 \\ E_4 - E_2 \end{bmatrix}$$

the new voltages must include $E_1 - E_2$ and $E_3 - E_4$, and as in equation (5),

$$[E_{old}] = [A][E_{new}]$$

$$\begin{bmatrix} E_1 - E_2 \\ E_3 - E_2 \\ E_4 - E_2 \end{bmatrix} = \begin{bmatrix} 1 & 0 & 0 \\ 0 & 0 & 1 \\ 0 & -1 & 1 \end{bmatrix} \begin{bmatrix} E_1 - E_2 \\ E_3 - E_4 \\ E_3 - E_2 \end{bmatrix}$$

hence

$$[A] = \begin{bmatrix} 1 & 0 & 0 \\ 0 & 0 & 1 \\ 0 & -1 & 1 \end{bmatrix} \dots\dots(9)$$

and

$$[A]_T = \begin{bmatrix} 1 & 0 & 0 \\ 0 & 0 & -1 \\ 0 & 1 & 1 \end{bmatrix} \dots\dots(10)$$

Substituting the results of equations (8), (9) and (10) in equation (7):

$$[Y_{new}] = \begin{bmatrix} 1 & 0 & 0 \\ 0 & 0 & -1 \\ 0 & 1 & 1 \end{bmatrix} \begin{bmatrix} a+b & -a & -b \\ -a & a+c & 0 \\ -b & 0 & b+d \end{bmatrix} \begin{bmatrix} 1 & 0 & 0 \\ 0 & 0 & 1 \\ 0 & -1 & 1 \end{bmatrix}$$

$$= \begin{bmatrix} a+b & -a & -b \\ b & 0 & -b-d \\ -a-b & a+c & b+d \end{bmatrix} \begin{bmatrix} 1 & 0 & 0 \\ 0 & 0 & 1 \\ 0 & -1 & 1 \end{bmatrix}$$

$$= \begin{bmatrix} a+b & b & -a-b \\ b & b+d & -b-d \\ -a-b & -b-d & a+c \\ & & b+d \end{bmatrix}$$

Using the reduction procedure¹ (see Appendix)

$$Y_{21E} = b(a+c+b+d) - (-a-b)(-b-d)$$

$$= bc - ad$$

$$Y_{22E} = (b+d)(a+c+b+d) - (-b-d)^2$$

$$= (a+c)(b+d)$$

$$\text{voltage gain} = \frac{E_3 - E_4}{E_1 - E_2} = \frac{-Y_{21E}}{Y_{22E}}$$

$$= \frac{ad - bc}{(b+d)(a+c)}$$

If $a=d$ and $b=c$

$$\text{voltage gain} = \frac{a-b}{a+b}$$

These results can be verified from textbooks.

3.2. Thermionic Difference Amplifiers

Four common configurations of difference amplifier are shown in Figs. 3(a) (b), (c) and (d) and can be classified as follows:

1. Fig. 3(a) differential output, differential input.
2. Fig. 3(b) single-ended output, differential input.
3. Fig. 3(c) differential output, single-ended input.
4. Fig. 3(d) single-ended output, single-ended input.

Condition 4 has a common input and output node (6) and thus the multi-node method can be used directly. This example is the cathode-coupled amplifier already discussed.¹

The indefinite admittance matrix for the overall network of Fig. 3(a) assuming identical valves is given by:

$$[Y_I] = \begin{bmatrix} & 1 & 2 & 3 & 4 & 5 & 6 & 7 \\ 1 & 0 & 0 & 0 & 0 & 0 & 0 & 0 \\ 2 & 0 & 0 & 0 & 0 & 0 & 0 & 0 \\ 3 & g_m & 0 & \frac{1}{r_a} + a & 0 & -g_m - \frac{1}{r_a} & 0 & -a \\ 4 & 0 & g_m & 0 & \frac{1}{r_a} + b & -g_m - \frac{1}{r_a} & 0 & -b \\ 5 & -g_m & -g_m & -\frac{1}{r_a} & -\frac{1}{r_a} & 2g_m + \frac{2}{r_a} + c & -c & 0 \\ 6 & 0 & 0 & 0 & 0 & -c & c & 0 \\ 7 & 0 & 0 & -a & -b & 0 & 0 & a+b \end{bmatrix} \dots\dots(11)$$

3.2.1. Analysis of Fig. 3(c)

The nodal matrix can be obtained from equation (11) by removing rows and columns 2, 6 and 7:

$$\underline{[Y_N]} = \begin{bmatrix} 0 & 0 & 0 & 0 \\ g_m & \frac{1}{r_a} + a & 0 & -g_m - \frac{1}{r_a} \\ 0 & 0 & \frac{1}{r_a} + b & -g_m - \frac{1}{r_a} \\ -g_m & -\frac{1}{r_a} & -\frac{1}{r_a} & 2g_m + \frac{2}{r_a} + c \end{bmatrix} = \underline{[Y_{old}]}$$

$$\underline{[E_{old}]} = [A] \underline{[E_{new}]} \\ \begin{bmatrix} E_1 - E_6 \\ E_3 - E_6 \\ E_4 - E_6 \\ E_5 - E_6 \end{bmatrix} = \begin{bmatrix} 1 & 0 & 0 & 0 \\ 0 & 1 & 1 & 0 \\ 0 & 0 & 1 & 0 \\ 0 & 0 & 0 & 1 \end{bmatrix} \begin{bmatrix} E_1 - E_6 \\ E_3 - E_4 \\ E_4 - E_6 \\ E_5 - E_6 \end{bmatrix}$$

$$[A] = \begin{bmatrix} 1 & 0 & 0 & 0 \\ 0 & 1 & 1 & 0 \\ 0 & 0 & 1 & 0 \\ 0 & 0 & 0 & 1 \end{bmatrix}$$

and

$$[A]_T = \begin{bmatrix} 1 & 0 & 0 & 0 \\ 0 & 1 & 0 & 0 \\ 0 & 1 & 1 & 0 \\ 0 & 0 & 0 & 1 \end{bmatrix}$$

Using

$$\underline{[Y_{new}]} = [A]_T \underline{[Y_{old}]} [A]$$

$$\underline{[Y_{new}]} = \begin{bmatrix} 1 & 0 & 0 & 0 \\ 0 & 1 & 0 & 0 \\ 0 & 1 & 1 & 0 \\ 0 & 0 & 0 & 1 \end{bmatrix} \begin{bmatrix} 0 & 0 & 0 & 0 \\ g_m & \frac{1}{r_a} + a & 0 & -g_m - \frac{1}{r_a} \\ 0 & 0 & \frac{1}{r_a} + b & -g_m - \frac{1}{r_a} \\ -g_m & -\frac{1}{r_a} & -\frac{1}{r_a} & 2g_m + \frac{2}{r_a} + c \end{bmatrix} \begin{bmatrix} 1 & 0 & 0 & 0 \\ 0 & 1 & 1 & 0 \\ 0 & 0 & 1 & 0 \\ 0 & 0 & 0 & 1 \end{bmatrix}$$

$$\underline{[Y_{new}]} = \begin{bmatrix} 0 & 0 & 0 & 0 \\ g_m & \frac{1}{r_a} + a & 0 & -g_m - \frac{1}{r_a} \\ g_m & \frac{1}{r_a} + a & \frac{1}{r_a} + b & -2g_m - \frac{2}{r_a} \\ -g_m & -\frac{1}{r_a} & -\frac{1}{r_a} & 2g_m + \frac{2}{r_a} + c \end{bmatrix} \begin{bmatrix} 1 & 0 & 0 & 0 \\ 0 & 1 & 1 & 0 \\ 0 & 0 & 1 & 0 \\ 0 & 0 & 0 & 1 \end{bmatrix}$$

$$\underline{[Y_{new}]} = \begin{bmatrix} 0 & 0 & 0 & 0 \\ g_m & \frac{1}{r_a} + a & \frac{1}{r_a} + a & -g_m - \frac{1}{r_a} \\ g_m & \frac{1}{r_a} + a & \frac{2}{r_a} + a + b & -2g_m - \frac{2}{r_a} \\ -g_m & -\frac{1}{r_a} & -\frac{2}{r_a} & 2g_m + \frac{2}{r_a} + c \end{bmatrix}$$

Using the reduction procedure

$$Y_{21E} = \begin{bmatrix} g_m & \frac{1}{r_a} + a & -g_m - \frac{1}{r_a} \\ g_m & \frac{2}{r_a} + a + b & -2g_m - \frac{2}{r_a} \\ -g_m & -\frac{2}{r_a} & 2g_m + \frac{2}{r_a} + c \end{bmatrix}$$

$$Y_{21E} = g_m a \left(g_m + \frac{1}{r_a} \right) + g_m b \left(g_m + \frac{1}{r_a} + c \right) + g_m \frac{c}{r_a}$$

$$Y_{22E} = \begin{bmatrix} \frac{1}{r_a} + a & \frac{1}{r_a} + a & -g_m - \frac{1}{r_a} \\ \frac{1}{r_a} + a & \frac{2}{r_a} + a + b & -2g_m - \frac{2}{r_a} \\ -\frac{1}{r_a} & -\frac{2}{r_a} & 2g_m + \frac{2}{r_a} + c \end{bmatrix}$$

$$Y_{22E} = \left(\frac{1}{r_a} + a \right) \left(2g_m + \frac{2}{r_a} \right) b + \left(\frac{c}{r_a} + ac \right) \times \left(\frac{1}{r_a} + b \right) - \left(g_m - \frac{1}{r_a} \right) \left(-\frac{a}{r_a} + \frac{b}{r_a} \right)$$

3.2.2. Analysis of Fig. 3(b)

The nodal matrix for Fig. 3(b) is obtained from equation (11) by removing rows and columns 3, 6 and 7:

$$[Y_N] = \begin{bmatrix} 0 & 0 & 0 & 0 \\ 0 & 0 & 0 & 0 \\ 0 & g_m & \frac{1}{r_a} + b & -g_m - \frac{1}{r_a} \\ -g_m & -g_m & -\frac{1}{r_a} & 2g_m + \frac{2}{r_a} + c \end{bmatrix} \dots\dots(12)$$

The voltage transformation matrix is obtained:

$$\begin{bmatrix} E_1 - E_6 \\ E_2 - E_6 \\ E_4 - E_6 \\ E_5 - E_6 \end{bmatrix} = \begin{bmatrix} 1 & 0 & 1 & 0 \\ 0 & 0 & 1 & 0 \\ 0 & 1 & 0 & 0 \\ 0 & 0 & 0 & 1 \end{bmatrix} \begin{bmatrix} E_1 - E_2 \\ E_4 - E_6 \\ E_2 - E_6 \\ E_5 - E_6 \end{bmatrix} \dots\dots(13)$$

Thus

$$[A]_T = \begin{bmatrix} 1 & 0 & 0 & 0 \\ 0 & 0 & 1 & 0 \\ 1 & 1 & 0 & 0 \\ 0 & 0 & 0 & 1 \end{bmatrix} \dots\dots(14)$$

The new admittance matrix is obtained from the result of equation (7):

$$[Y_{new}] = \begin{bmatrix} 1 & 0 & 0 & 0 \\ 0 & 0 & 1 & 0 \\ 1 & 1 & 0 & 0 \\ 0 & 0 & 0 & 1 \end{bmatrix} \begin{bmatrix} 0 & 0 & 0 & 0 \\ 0 & 0 & 0 & 0 \\ 0 & g_m & \frac{1}{r_a} + b & -g_m - \frac{1}{r_a} \\ -g_m & -g_m & -\frac{1}{r_a} & 2g_m + \frac{2}{r_a} + c \end{bmatrix} \begin{bmatrix} 1 & 0 & 1 & 0 \\ 0 & 0 & 1 & 0 \\ 0 & 1 & 0 & 0 \\ 0 & 0 & 0 & 1 \end{bmatrix}$$

$$[Y_{new}] = \begin{bmatrix} 0 & 0 & 0 & 0 \\ 0 & \frac{1}{r_a} + b & g_m & -g_m - \frac{1}{r_a} \\ 0 & 0 & 0 & 0 \\ -g_m & -\frac{1}{r_a} & -2g_m & 2g_m + \frac{2}{r_a} + c \end{bmatrix} \dots\dots(15)$$

It is apparent from equation (15) that the gain in terms of Y_{21E} and Y_{22E} is indeterminate by this method. This problem can be overcome by the following methods.

- (1) Determine $(E_4 - E_6)/(E_1 - E_2)$ with node 2 common to node 6 and $(E_4 - E_6)/(E_1 - E_2)$ with node 1 common to node 6

and use the superposition theorem.

- (2) Introduce grid admittances d and e as shown in Fig. 3(e). Since the latter is the quicker method it will be considered here.

If $a = b = \frac{1}{R_L}$ and $c = \frac{1}{R_K} \rightarrow 0$

$$\text{gain} = \frac{E_3 - E_4}{E_1 - E_2} = \frac{-Y_{21E}}{Y_{22E}} = \frac{\mu R_L}{r_a + R_L}$$

This result can be verified from textbooks.³

The transformation matrices from equations (13) and (14) remain the same; but additional terms are needed in the matrix of equation (11) as follows:

$$\begin{array}{c}
 1 \\
 2 \\
 3 \\
 4 \\
 5 \\
 6 \\
 7
 \end{array}
 \begin{array}{c}
 1 \quad 2 \quad 3 \quad 4 \quad 5 \quad 6 \quad 7 \\
 \hline
 \begin{array}{ccccccc}
 d & & & & & & -d \\
 & e & & & & & -e \\
 & & & & & & \\
 & & & & & & \\
 & & & & & & \\
 -d & -e & & & & & d+e \\
 & & & & & &
 \end{array}
 \end{array}
 \dots\dots(16)$$

Equation (12) is now modified to

$$\underline{[Y_N]} = \begin{bmatrix} d & 0 & 0 & 0 \\ 0 & e & 0 & 0 \\ 0 & g_m & \frac{1}{r_a} + b & -g_m - \frac{1}{r_a} \\ -g_m & -g_m & -\frac{1}{r_a} & 2g_m + \frac{2}{r_a} + c \end{bmatrix}$$

Hence

$$\begin{aligned}
 \underline{[Y_{new}]} &= \begin{bmatrix} 1 & 0 & 0 & 0 \\ 0 & 0 & 1 & 0 \\ 1 & 1 & 0 & 0 \\ 0 & 0 & 0 & 1 \end{bmatrix} \begin{bmatrix} d & 0 & 0 & 0 \\ 0 & e & 0 & 0 \\ 0 & g_m & \frac{1}{r_a} + b & -g_m - \frac{1}{r_a} \\ -g_m & -g_m & -\frac{1}{r_a} & 2g_m + \frac{2}{r_a} + c \end{bmatrix} \begin{bmatrix} 1 & 0 & 1 & 0 \\ 0 & 0 & 1 & 0 \\ 0 & 1 & 0 & 0 \\ 0 & 0 & 0 & 1 \end{bmatrix} \\
 &= \begin{bmatrix} d & 0 & 0 & 0 \\ 0 & g_m & \frac{1}{r_a} + b & -g_m - \frac{1}{r_a} \\ d & e & 0 & 0 \\ -g_m & -g_m & -\frac{1}{r_a} & 2g_m + \frac{2}{r_a} + c \end{bmatrix} \begin{bmatrix} 1 & 0 & 1 & 0 \\ 0 & 0 & 1 & 0 \\ 0 & 1 & 0 & 0 \\ 0 & 0 & 0 & 1 \end{bmatrix} \\
 &= \begin{bmatrix} d & 0 & d & 0 \\ 0 & \frac{1}{r_a} + b & g_m & -g_m - \frac{1}{r_a} \\ d & 0 & d+e & 0 \\ -g_m & -\frac{1}{r_a} & -2g_m & 2g_m + \frac{2}{r_a} + c \end{bmatrix}
 \end{aligned}$$

Using the previous method

$$Y_{21E} = -g_m d \left(2g_m + \frac{2}{r_a} + c \right) - g_m \left(g_m + \frac{1}{r_a} \right) (-d+e)$$

If $d = e$

$$= -g_m d \left(2g_m + \frac{2}{r_a} + c \right)$$

$$Y_{22E} = 2d \left\{ \left(2g_m + \frac{2}{r_a} \right) \left(\frac{1}{r_a} + b \right) - \left(g_m + \frac{1}{r_a} \right) \left(\frac{1}{r_a} \right) \right\}$$

$$\text{gain} = \frac{-Y_{21E}}{Y_{22E}}$$

$$\text{gain} = \frac{g_m d \left(2g_m + \frac{2}{r_a} + c \right)}{2d \left\{ \left(2g_m + \frac{2}{r_a} \right) \left(\frac{1}{r_a} + b \right) - \left(g_m + \frac{1}{r_a} \right) \left(\frac{1}{r_a} \right) \right\}}$$

If R_K tends to be large then $c \rightarrow 0$

$$\text{gain} = \frac{g_m}{\frac{1}{r_a} + 2b}$$

$$\text{If } b = \frac{1}{R_L}$$

$$\text{gain} = \frac{\mu R_L}{2r_a + R_L}$$

This result can be verified from Ref. 3.

3.2.3. Analysis of Fig. 3(a)

Since the input is again differential and since the circuit involves valves, it is again necessary to introduce the grid admittances d and e . Referring to equations (11) and (16) the nodal matrix for the circuit

of Fig. 3(a) is formed by removing rows and columns 6 and 7:

$$[Y_N] = \begin{bmatrix} & 1 & 2 & 3 & 4 & 5 \\ 1 & d & 0 & 0 & 0 & 0 \\ 2 & 0 & e & 0 & 0 & 0 \\ 3 & g_m & 0 & \frac{1}{r_a} + a & 0 & -g_m - \frac{1}{r_a} \\ 4 & 0 & g_m & 0 & \frac{1}{r_a} + b & -g_m - \frac{1}{r_a} \\ 5 & -g_m & -g_m & -\frac{1}{r_a} & -\frac{1}{r_a} & 2g_m + \frac{2}{r_a} + c \end{bmatrix}$$

As before,

$$\begin{bmatrix} E_1 - E_6 \\ E_2 - E_6 \\ E_3 - E_6 \\ E_4 - E_6 \\ E_5 - E_6 \end{bmatrix} = \begin{bmatrix} 1 & 0 & 1 & 0 & 0 \\ 0 & 0 & 1 & 0 & 0 \\ 0 & 1 & 0 & 1 & 0 \\ 0 & 0 & 0 & 1 & 0 \\ 0 & 0 & 0 & 0 & 1 \end{bmatrix} \begin{bmatrix} E_1 - E_2 \\ E_3 - E_4 \\ E_2 - E_6 \\ E_4 - E_6 \\ E_5 - E_6 \end{bmatrix}$$

Thus

$$[A]_T = \begin{bmatrix} 0 & 0 & 0 & 0 \\ 0 & 0 & 1 & 0 & 0 \\ 1 & 1 & 0 & 0 & 0 \\ 0 & 0 & 1 & 1 & 0 \\ 0 & 0 & 0 & 0 & 1 \end{bmatrix}$$

$$[Y_{new}] = \begin{bmatrix} 1 & 0 & 0 & 0 & 0 \\ 0 & 0 & 1 & 0 & 0 \\ 1 & 1 & 0 & 0 & 0 \\ 0 & 0 & 1 & 1 & 0 \\ 0 & 0 & 0 & 0 & 1 \end{bmatrix} \begin{bmatrix} d & 0 & 0 & 0 & 0 \\ 0 & e & 0 & 0 & 0 \\ g_m & 0 & \frac{1}{r_a} + a & 0 & -g_m - \frac{1}{r_a} \\ 0 & g_m & 0 & \frac{1}{r_a} + b & -g_m - \frac{1}{r_a} \\ -g_m & -g_m & -\frac{1}{r_a} & -\frac{1}{r_a} & 2g_m + \frac{2}{r_a} + c \end{bmatrix} \begin{bmatrix} 1 & 0 & 1 & 0 & 0 \\ 0 & 0 & 1 & 0 & 0 \\ 0 & 1 & 0 & 1 & 0 \\ 0 & 0 & 0 & 1 & 0 \\ 0 & 0 & 0 & 0 & 1 \end{bmatrix}$$

$$= \begin{bmatrix} d & 0 & 0 & 0 & 0 \\ g_m & 0 & \frac{1}{r_a} + a & 0 & -g_m - \frac{1}{r_a} \\ d & e & 0 & 0 & 0 \\ g_m & g_m & \frac{1}{r_a} + a & \frac{1}{r_a} + b & -2g_m - \frac{2}{r_a} \\ -g_m & -g_m & -\frac{1}{r_a} & -\frac{1}{r_a} & 2g_m + \frac{2}{r_a} + c \end{bmatrix} \begin{bmatrix} 1 & 0 & 1 & 0 & 0 \\ 0 & 0 & 1 & 0 & 0 \\ 0 & 1 & 0 & 1 & 0 \\ 0 & 0 & 0 & 1 & 0 \\ 0 & 0 & 0 & 0 & 1 \end{bmatrix}$$

$$= \begin{bmatrix} d & 0 & d & 0 & 0 \\ g_m & \frac{1}{r_a} + a & g_m & \frac{1}{r_a} + a & -g_m - \frac{1}{r_a} \\ d & 0 & d+e & 0 & 0 \\ g_m & \frac{1}{r_a} + a & 2g_m & \frac{2}{r_a} + a + b & -2g_m - \frac{2}{r_a} \\ -g_m & -\frac{1}{r_a} & -2g_m & -\frac{2}{r_a} & 2g_m + \frac{2}{r_a} + c \end{bmatrix}$$

If $a = b$; $d = e$ and $c \rightarrow 0$

$$Y_{21E} = 4g_m da \left(g_m + \frac{1}{r_a} \right)$$

$$Y_{22E} = 4da \left(\frac{1}{r_a} + a \right) \left(g_m + \frac{1}{r_a} \right)$$

$$\text{gain} = \frac{-\mu R_L}{r_a + R_L}$$

This result can be verified from Ref. 3.

3.3. Transistor Difference Amplifiers

Transformation matrices together with use of the multi-node method are applicable to transistor amplifiers without introducing input admittances as in the previous case.

Consider the differential input, differential output transistor amplifier of Fig. 7(a).

The indefinite admittance matrix is given by

$$[Y_{\leftarrow}] = \begin{bmatrix} & 1 & 2 & 3 & 4 & 5 & 6 & 7 \\ \begin{matrix} 1 \\ 2 \\ 3 \\ 4 \\ 5 \\ 6 \\ 7 \end{matrix} & \begin{matrix} y_{ie} & 0 & y_{re} & 0 & -y_{ie} - y_{re} & 0 & 0 \\ 0 & y_{ie} & 0 & y_{re} & -y_{ie} - y_{re} & 0 & 0 \\ y_{fe} & 0 & y_{oe} + a & 0 & -y_{fe} - y_{oe} & 0 & -a \\ 0 & y_{fe} & 0 & y_{oe} + a & -y_{fe} - y_{oe} & 0 & -a \\ -y_{ie} - y_{fe} & -y_{ie} - y_{fe} & -y_{re} - y_{oe} & -y_{re} - y_{oe} & 2y_{ie} + 2y_{re} + 2y_{fe} + 2y_{oe} + b & -b & 0 \\ 0 & 0 & 0 & 0 & -b & b & 0 \\ 0 & 0 & -a & -a & 0 & 0 & 2a \end{matrix} \end{bmatrix}$$

If y_{re} and y_{oe} are considered to be zero the nodal matrix with nodes 6 and 7 common and taken as the reference is given by:

$$[Y_N] = \begin{bmatrix} y_{ie} & 0 & 0 & 0 & -y_{ie} \\ 0 & y_{ie} & 0 & 0 & -y_{ie} \\ y_{fe} & 0 & a & 0 & -y_{fe} \\ 0 & y_{fe} & 0 & a & -y_{fe} \\ -y_{ie} - y_{fe} & -y_{ie} - y_{fe} & 0 & 0 & 2y_{ie} + 2y_{fe} + b \end{bmatrix}$$

Using the result $[E_{old}] = [A][E_{new}]$

$$\begin{bmatrix} E_1 - E_6 \\ E_2 - E_6 \\ E_3 - E_6 \\ E_4 - E_6 \\ E_5 - E_6 \end{bmatrix} = \begin{bmatrix} 1 & 0 & 1 & 0 & 0 \\ 0 & 0 & 1 & 0 & 0 \\ 0 & 1 & 0 & 1 & 0 \\ 0 & 0 & 0 & 1 & 0 \\ 0 & 0 & 0 & 0 & 1 \end{bmatrix} \begin{bmatrix} E_1 - E_2 \\ E_3 - E_4 \\ E_2 - E_6 \\ E_4 - E_6 \\ E_5 - E_6 \end{bmatrix}$$

Thus

$$[A]_T = \begin{bmatrix} 1 & 0 & 0 & 0 & 0 \\ 0 & 0 & 1 & 0 & 0 \\ 1 & 1 & 0 & 0 & 0 \\ 0 & 0 & 1 & 1 & 0 \\ 0 & 0 & 0 & 0 & 1 \end{bmatrix}$$

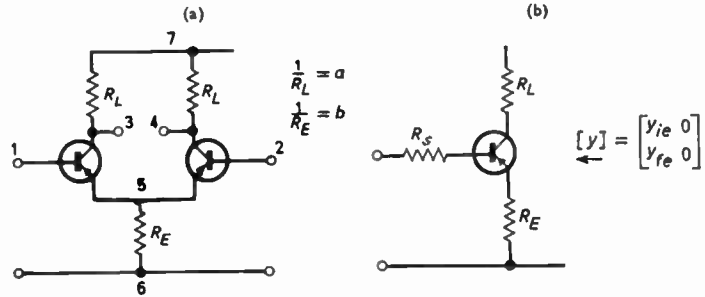


Fig. 7. Differential input, differential output transistor amplifier.

$$[Y_{new}] = [A]^{-1} [Y_{old}] [A]$$

$$\begin{aligned}
 [Y_{new}] &= \begin{bmatrix} 1 & 0 & 0 & 0 & 0 \\ 0 & 0 & 1 & 0 & 0 \\ 1 & 1 & 0 & 0 & 0 \\ 0 & 0 & 1 & 1 & 0 \\ 0 & 0 & 0 & 0 & 1 \end{bmatrix} \begin{bmatrix} y_{ie} & 0 & 0 & 0 & -y_{ie} \\ 0 & y_{ie} & 0 & 0 & -y_{ie} \\ y_{fe} & 0 & a & 0 & -y_{fe} \\ 0 & y_{fe} & 0 & a & -y_{fe} \\ -y_{ie}-y_{fe} & -y_{ie}-y_{fe} & 0 & 0 & 2y_{ie}+2y_{fe}+b \end{bmatrix} \begin{bmatrix} 1 & 0 & 1 & 0 & 0 \\ 0 & 0 & 1 & 0 & 0 \\ 0 & 1 & 0 & 1 & 0 \\ 0 & 0 & 0 & 1 & 0 \\ 0 & 0 & 0 & 0 & 1 \end{bmatrix} \\
 &= \begin{bmatrix} y_{ie} & 0 & 0 & 0 & -y_{ie} \\ y_{fe} & 0 & a & 0 & -y_{fe} \\ y_{ie} & y_{ie} & 0 & 0 & -2y_{ie} \\ y_{fe} & y_{fe} & a & a & -2y_{fe} \\ -y_{ie}-y_{fe} & -y_{ie}-y_{fe} & 0 & 0 & 2y_{ie}+2y_{fe}+b \end{bmatrix} \begin{bmatrix} 1 & 0 & 1 & 0 & 0 \\ 0 & 0 & 1 & 0 & 0 \\ 0 & 1 & 0 & 1 & 0 \\ 0 & 0 & 0 & 1 & 0 \\ 0 & 0 & 0 & 0 & 1 \end{bmatrix} \\
 &= \begin{bmatrix} y_{ie} & 0 & y_{ie} & 0 & -y_{ie} \\ y_{fe} & a & y_{fe} & a & -y_{fe} \\ y_{ie} & 0 & 2y_{ie} & 0 & -2y_{ie} \\ y_{fe} & a & 2y_{fe} & 2a & -2y_{fe} \\ -y_{ie}-y_{fe} & 0 & -2y_{ie}-2y_{fe} & 0 & 2y_{ie}+2y_{fe}+b \end{bmatrix}
 \end{aligned}$$

$$\text{voltage gain} = \frac{E_3 - E_4}{E_1 - E_2} = -\frac{Y_{21E}}{Y_{22E}}$$

$$Y_{21E} = \begin{vmatrix} y_{fe} & y_{fe} & a & -y_{fe} \\ y_{ie} & 2y_{ie} & 0 & -2y_{ie} \\ y_{fe} & 2y_{fe} & 2a & -2y_{fe} \\ -y_{ie}-y_{fe} & -2y_{ie}-2y_{fe} & 0 & 2y_{ie}+2y_{fe}+b \end{vmatrix}$$

$$Y_{21E} = 2ab y_{ie} y_{fe}$$

$$Y_{22E} = \begin{vmatrix} a & y_{fe} & a & -y_{fe} \\ 0 & 2y_{ie} & 0 & -2y_{ie} \\ a & 2y_{fe} & 2a & -2y_{fe} \\ 0 & -2y_{ie}-2y_{fe} & 0 & 2y_{ie}+2y_{fe}+b \end{vmatrix}$$

$$Y_{22E} = 2a^2 b y_{ie}$$

$$\text{voltage gain} = -\frac{2ab y_{ie} y_{fe}}{2a^2 b y_{ie}}$$

$$= -\frac{y_{fe}}{a}$$

$$= -y_{fe} R_L$$

$$= -\frac{h_{fe} R_L}{h_{ie}}$$

If input resistances R_s are included as in Fig. 7(b) these can be directly added to h_{ie} .

Thus

$$\text{voltage gain} = -\frac{h_{fe} R_L}{(h_{ie} + R_s)}$$

These results can be verified from Ref. 7.

3.3.1. Special case—f.e.t. difference amplifier

Special consideration is required with the field effect transistor as similarity to the thermionic valve

exists with respect to performance, equivalent circuit and matrix representation.

The admittance matrix for the f.e.t. is given by

$$[Y] = \begin{bmatrix} 0 & 0 \\ g_{fs} & \frac{1}{r_d} \end{bmatrix}$$

It is therefore apparent that a singular matrix exists and thus input admittances have to be inserted as previously discussed in the section on thermionic difference amplifiers.

3.4. Unilateralization

The simple transistor circuit of Fig. 8 can be designed for unilateral transmission if the input port is 1, 4 and the output port is 2, 3. This is therefore an

example that would require transformation matrices.

$$\begin{bmatrix} E_1 - E_3 \\ E_2 - E_3 \\ E_4 - E_3 \end{bmatrix} = \begin{bmatrix} 1 & 0 & 1 \\ 0 & 1 & 0 \\ 0 & 0 & 1 \end{bmatrix} \begin{bmatrix} E_1 - E_4 \\ E_2 - E_3 \\ E_4 - E_3 \end{bmatrix}$$

$$[A] = \begin{bmatrix} 1 & 0 & 1 \\ 0 & 1 & 0 \\ 0 & 0 & 1 \end{bmatrix}$$

$$[A]_T = \begin{bmatrix} 1 & 0 & 0 \\ 0 & 1 & 0 \\ 1 & 0 & 1 \end{bmatrix}$$

The original nodal matrix with node 3 as the reference is

$$[Y_N] = \begin{bmatrix} y_{ib} & y_{rb} & 0 \\ y_{fb} & y_{ob} + a & -a \\ 0 & -a & a + b \end{bmatrix}$$

$$[Y_{new}] = \begin{bmatrix} 1 & 0 & 0 \\ 0 & 1 & 0 \\ 1 & 0 & 1 \end{bmatrix} \begin{bmatrix} y_{ib} & y_{rb} & 0 \\ y_{fb} & y_{ob} + a & -a \\ 0 & -a & a + b \end{bmatrix} \begin{bmatrix} 1 & 0 & 1 \\ 0 & 1 & 0 \\ 0 & 0 & 1 \end{bmatrix}$$

$$= \begin{bmatrix} y_{ib} & y_{rb} & 0 \\ y_{fb} & y_{ob} + a & -a \\ y_{ib} & y_{rb} - a & a + b \end{bmatrix} \begin{bmatrix} 1 & 0 & 1 \\ 0 & 1 & 0 \\ 0 & 0 & 1 \end{bmatrix}$$

$$[Y_{new}] = \begin{bmatrix} y_{ib} & y_{rb} & y_{ib} \\ y_{fb} & y_{ob} + a & y_{fb} - a \\ y_{ib} & y_{rb} - a & y_{ib} + a + b \end{bmatrix}$$

$$Y_{12E} = y_{rb}(y_{ib} + a + b) - (y_{rb} - a)(y_{ib})$$

$$Y_{12E} = y_{rb}a + y_{rb} \cdot b + ay_{ib}$$

For unilateralization

$$Y_{12E} = 0,$$

which requires that

$$y_{rb}a + y_{rb}b + ay_{ib} = 0.$$

This answer can be verified from Ref. 4.

3.5. Amplifier with Series Voltage Feedback

Consider the amplifier of Fig. 9.

The indefinite admittance matrix is given by

$$[Y_I] = \begin{bmatrix} & 1 & 2 & 3 & 4 & 5 \\ 1 & 0 & 0 & 0 & 0 & 0 \\ 2 & g_m & cs + \frac{1}{R_L} + \frac{1}{r_a} + \frac{1}{r} & -cs - g_m - \frac{1}{r_a} & -\frac{1}{r} & -\frac{1}{R_L} \\ 3 & -g_m & -\frac{1}{r_a} - cs & cs + \frac{1}{R} + g_m + \frac{1}{r_a} & -\frac{1}{R} & 0 \\ 4 & 0 & -\frac{1}{r} & -\frac{1}{R} & \frac{1}{r} + \frac{1}{R} & 0 \\ 5 & 0 & -\frac{1}{R_L} & 0 & 0 & \frac{1}{R_L} \end{bmatrix}$$

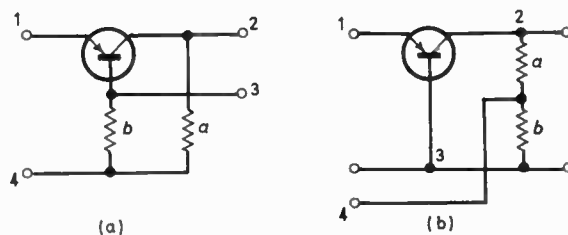


Fig. 8. Unilateralized networks.

With respect to a.c. nodes 5 and 3 are common therefore the nodal matrix is given by

$$[Y_N] = \begin{bmatrix} 0 & 0 & 0 \\ cs + \frac{1}{r_a} & \frac{1}{R_L} + \frac{1}{r} & -\frac{1}{r} \\ 0 & -\frac{1}{r} & \frac{1}{r} + \frac{1}{R} \end{bmatrix}$$

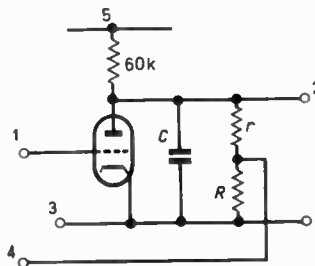


Fig. 9. Amplifier with series voltage feedback. $r + R$ 120 kΩ; g_m 5 mA/V; r_a very large.

Let

$$x = cs + \frac{1}{r_a} + \frac{1}{R_L} + \frac{1}{r}$$

$$\begin{bmatrix} E_1 - E_3 \\ E_2 - E_3 \\ E_4 - E_3 \end{bmatrix} = \begin{bmatrix} 1 & 0 & 1 \\ 0 & 1 & 0 \\ 0 & 0 & 1 \end{bmatrix} \begin{bmatrix} E_1 - E_4 \\ E_2 - E_3 \\ E_4 - E_3 \end{bmatrix}$$

$$\left[\leftarrow Y_{new} \right] = \begin{bmatrix} 1 & 0 & 0 \\ 0 & 1 & 0 \\ 1 & 0 & 1 \end{bmatrix} \begin{bmatrix} 0 & 0 & 0 \\ g_m & x & -\frac{1}{r} \\ 0 & -\frac{1}{r} & \frac{1}{r} + \frac{1}{R} \end{bmatrix} \begin{bmatrix} 1 & 0 & 1 \\ 0 & 1 & 0 \\ 0 & 0 & 1 \end{bmatrix}$$

$$= \begin{bmatrix} 0 & 0 & 0 \\ g_m & x & -\frac{1}{r} \\ 0 & -\frac{1}{r} & \frac{1}{r} + \frac{1}{R} \end{bmatrix} \begin{bmatrix} 1 & 0 & 1 \\ 0 & 1 & 0 \\ 0 & 0 & 1 \end{bmatrix}$$

$$= \begin{bmatrix} 0 & 0 & 0 \\ g_m & x & g_m - \frac{1}{r} \\ 0 & -\frac{1}{r} & \frac{1}{r} + \frac{1}{R} \end{bmatrix} \dots\dots(17)$$

$$Y_{21E} = g_m \left(\frac{1}{r} + \frac{1}{R} \right)$$

$$Y_{22E} = x \left(\frac{1}{r} + \frac{1}{R} \right) + \frac{1}{r} \left(g_m - \frac{1}{r} \right)$$

Resubstitute for x

$$\text{gain} = \frac{-Y_{21E}}{Y_{22E}} = \frac{-g_m \left(\frac{1}{r} + \frac{1}{R} \right)}{\left(cs + \frac{1}{60} \times 10^{-3} + \frac{1}{r_a} + \frac{1}{r} \right) \left(\frac{1}{r} + \frac{1}{R} \right) + \frac{1}{r} \left(g_m - \frac{1}{r} \right)}$$

Let r_a be very large hence $1/r_a \rightarrow 0$

$$\text{gain} = \frac{-g_m \left(\frac{1}{r} + \frac{1}{R} \right)}{cs \left(\frac{1}{r} + \frac{1}{R} \right) + \frac{1}{60} \times 10^{-3} + \frac{1}{60R} \times 10^{-3} + \frac{1}{rR} + \frac{g_m}{r}}$$

$$= \frac{-g_m(R+r)}{cs(R+r) + \frac{R+r}{60 \times 10^3} + 1 + g_m R}$$

Substituting values

$$\text{gain} = \frac{-200}{\left(1 + \frac{5}{6}R \right) + (4 \times 10^4 cs)}$$

This result can be verified from Ref. 5.

It is appreciated that the simple circuit of Fig. 9 could be solved by conventional methods. However,

the method used has the following advantages:

1. The effect of r_a can be more easily introduced.
2. The matrix of equation (17) will also give the input impedance and the output impedance without additional analysis.
3. The sign of the feedback voltage is automatically taken care of.
4. The feedback factor is not required and in some circuits this is difficult to assess.

4. Conclusions

The use of transformation matrices in conjunction with the multi-node approach provides a unified approach to active and passive circuit analysis for a wide range of network topology. The equivalent 2×2 matrix yields the two-port characteristics of input impedance, output impedance and voltage and current transfer functions and thus reduces the amount of work required for the complete analysis on a two-port basis. The fact that validity tests are not required is another major advantage.

5. References and Bibliography

1. Kennedy, R. T., 'Two-port representation of multi-node networks by matrix partitioning', *The Radio and Electronic Engineer*, 37, No. 2, pp. 109-16, February 1969.
2. Kron, G., 'Tensor Analysis of Networks', pp. 103-4 (Macdonald, London, 1965).
3. Ryder, J. D., 'Engineering Electronics', pp. 264-6 (McGraw-Hill, New York, 1967).

7. Stewart, H. E., 'Engineering Electronics', pp. 518-23 (Allyn & Bacon, Boston, Mass., 1969).
8. Rogers, F. E., 'Topology and Matrices in the Solution of Networks, pp. 30-3, 175-9, 65-6, 85-8, 132 (Iliffe, London, 1965).
9. Fairbrother, L. R. and Bassett, H. G., 'A computer program for analysing networks containing three-terminal active devices, characterized by their two-port parameters', *The Radio and Electronic Engineer*, 29, No. 2, pp. 85-92, February 1965.
10. Stignant, S. A., 'The Elements of Determinants, Matrices and Tensors for Engineers' (Macdonald, London, 1963).

6. Appendix: Multi-node Method¹

A multi-node network having two ports of interest can be represented by an equivalent 2x2 matrix relevant to the ports of interest and having the form

$$[Y_E] = \frac{1}{K} \begin{bmatrix} Y_{11E} & Y_{12E} \\ Y_{21E} & Y_{22E} \end{bmatrix}$$

The terms of the equivalent matrix can be found directly by considering the determinant of the original matrix with appropriate rows and columns removed as follows:

Term	To be removed	
	Column	Row
K	1, 2	1, 2
Y _{11E}	2	2
Y _{12E}	1	2
Y _{21E}	2	1
Y _{22E}	1	1

The validity of the method requires that the input and output nodes be selected as nodes 1 and 2 respectively. The terminal characteristics can then be obtained as follows:

voltage transfer function = $-\frac{Y_{21E}}{Y_{22E}}$

input impedance = $\frac{KY_{22E}}{Y_{11E}Y_{22E} - Y_{12E}Y_{21E}}$

output impedance = $\frac{K}{Y_{22E}}$

Manuscript first received by the Institution on 8th January 1969 and in revised form on 1st December 1969. (Paper No. 1319/CC 73).

© The Institution of Electronic and Radio Engineers, 1970

STANDARD FREQUENCY TRANSMISSIONS—April 1970

(Communication from the National Physical Laboratory)

April 1970	Deviation from nominal frequency in parts in 10 ¹¹ (24-hour mean centred on 0300 UT)			Relative phase readings in microseconds N.P.L.—Station (Readings at 1500 UT)		April 1970	Deviation from nominal frequency in parts in 10 ¹¹ (24-hour mean centred on 0300 UT)			Relative phase readings in microseconds N.P.L.—Station (Readings at 1500 UT)	
	GBR 16 kHz	MSF 60 kHz	Droitwich 200 kHz	*GBR 16 kHz	†MSF 60 kHz		GBR 16 kHz	MSF 60 kHz	Droitwich 200 kHz	*GBR 16 kHz	†MSF 60 kHz
1	-300.0	-0.1	+0.1	624	551.0	17	-299.9	0	+0.1	621	567.1
2	-299.9	-0.1	+0.1	623	558.2	18	-299.9	+0.1	+0.2	620	566.5
3	-299.9	-0.1	+0.1	622	559.0	19	-299.9	0	+0.1	619	566.1
4	-300.1	0	+0.1	623	559.4	20	-300.0	+0.1	+0.2	619	565.3
5	-300.0	-0.1	+0.1	623	560.4	21	-299.9	0	+0.1	618	565.6
6	-300.0	0	+0.1	623	560.4	22	-300.0	0	+0.1	618	565.6
7	-300.0	0	+0.1	623	560.6	23	-300.0	-0.1	+0.1	618	566.2
8	-300.1	-0.1	+0.1	624	562.0	24	-300.0	0	+0.1	618	566.2
9	-300.0	-0.1	+0.1	624	562.8	25	-300.0	0	+0.1	618	566.4
10	-300.0	-0.1	+0.1	624	563.8	26	-300.0	0	+0.1	618	566.8
11	-300.0	-0.1	+0.1	624	565.1	27	-300.1	-0.1	+0.1	619	567.6
12	-300.0	0	+0.1	624	565.1	28	-300.0	0	+0.1	619	566.6
13	-300.0	-0.1	0	624	566.0	29	-300.0	0	+0.2	619	566.2
14	-300.0	-0.1	+0.1	624	566.5	30	-300.0	-0.1	+0.2	619	565.0
15	-299.9	-0.1	+0.1	623	567.1	31	-	-	-	-	-
16	-299.9	0	+0.2	622	567.1						

All measurements in terms of H.P. Caesium Standard No. 334, which agrees with the N.P.L. Caesium Standard to 1 part in 10¹¹.

* Relative to UTC Scale; (UTC_{NPL} - Station) = + 500 at 1500 UT 31st December 1968.

†Relative to AT Scale; (AT_{NPL} - Station) = + 468.6 at 1500 UT 31st December 1968.

As from the 5th April 1970 the maintenance shutdown for MSF is the first Tuesday in the month from 1000 - 1400 GMT. The GBR transmission is shut down each Tuesday from 1000 - 1400 GMT.

Contributors to this Issue



C. E. E. Stewart graduated in chemistry at the University of London in 1959. From 1960 to 1963 he was concerned with the growth of germanium and silicon crystals at the Hirst Research Centre, Wembley. In 1963 he joined Standard Telecommunication Laboratories, Harlow, where he has been working on the vapour phase crystal growth of semiconductors for solid-state electroluminescent devices.



J. R. Peters graduated from London University in physics and chemistry in 1944. He has been engaged in several fields in the electrical and semiconductor industry, specializing since 1962 in the device technology of III/V semiconductor compounds. He is at present a senior research engineer at Standard Telecommunication Laboratories, responsible for gallium arsenide-phosphide device research.



Professor Sankara Venkateswaran received his B.Sc. and M.A. degrees in physics from Madras University. In 1961 he obtained his Ph.D. degree in transistor electronics from London University and his D.I.C. in electrical engineering from Imperial College. He initially held a Metropolitan-Vickers Bursary and later a Ministry of Aviation Fellowship.

Professor Venkateswaran gained his early practical training from All-India Radio, and in radar from the Indian Air Force. He taught basic and equipment courses at the School of Signals, Mhow, and communications and electronics at the University of Ceylon and the University College of Swansea, South Wales. He joined the Indian Institute of Technology, Kanpur, in 1963, where he now holds a Chair in Electrical Engineering.

Professor Venkateswaran has been a member of several Government of India Committees connected with the

growth of education in Electronics and Communications at Polytechnics and Universities of the northern Indian region. He is a Member of the Editorial Panel of the joint *I.E.E.-I.E.R.E. Proceedings—India*, and has contributed several papers to *The Radio and Electronic Engineer*.



Vinod Purushottam Namjoshi took his B.Tech.(Hons.) degree in electrical engineering at the Indian Institute of Technology, Bombay, in 1966. He was a junior research assistant at the Indian Institute of Technology, Kanpur, for two years and is now completing his studies and research for the M.Tech. degree. His field of interest is solid-state circuits and computer applications.



R. T. Kennedy (M. 1966), a graduate of Heriot-Watt University, Edinburgh, is a senior lecturer in electrical engineering at the Huddersfield College of Technology. Previous appointments have included a lectureship at the University of Science and Technology, Kumasi, Ghana; senior design engineer, Plessey Co. Ltd.; member of scientific staff, G.E.C. Hirst Research Centre.

Mr. Kennedy is at present writing his thesis on thyristor parameters under conditions of pulse operation for submission to Heriot-Watt University for a Master's Degree.



Y. A. Bedri received his B.E.E. from the American University of Beirut in 1963. Between 1963 and 1967 he lectured on Electronics at the Khartoum Polytechnic, Sudan, and worked as a part-time engineer with El Nasr Engineering Co. On coming to England in 1968 he was for some time with the Post Office, receiving training on colour television. At present he is doing research

on active RC networks at the West Ham College of Technology.

A note on Dr. T. Debiyannis' career was published in the March 1970 issue.

The E.M.I. Four-Tube Colour Television Camera

By

I. J. P. JAMES,

B.Sc., C.Eng., F.I.E.E., F.I.E.R.E.,†

D. G. PERKINS, C.Eng., M.I.E.E.,†

P. J. PYKE,‡

E. W. TAYLOR, M.A.,‡

D. E. KENT, C.Eng., M.I.E.E.†

and

I. A. FAIRBAIRN, B.Sc.‡

Presented at a meeting of the Institution's Communications Group in London on 29th May 1968.

The first part of the paper describes the background to the decision taken on the number and type of pickup tubes used in the camera. The argument for the use of a separate luminance tube is presented together with an explanation of the delta-L system for providing accurate colorimetry in a four-tube camera.

Part 2 covers the considerations leading to the particular optical and mechanical arrangement adopted and the advantages which result from this arrangement. The key part of the design is the use of a pre-aligned beam splitter system, and the way in which this was achieved is described.

Part 3 deals with the design of the more important circuits used. General requirements such as stability, serviceability and ease of adjustment are discussed first. This is followed by a description of the scanning circuits and the monitoring arrangements used for adjusting registration. The video circuits are then discussed in detail with particular reference to such problems as the tracking of the master gain and gamma correction controls applied to the four signals. Luminance correction is applied by the delta-L system and its practical realization in a form which gives three output signals suitable for direct monitoring and encoding is described. The final section deals with power supplies and in particular the stabilizer module which is used for all the low-voltage supplies including the camera supplies which are required to work through 600 m of cable by remote sensing.

List of Symbols

A	circuit gain	Y_{H}	high frequency components of Y
i	video signal current	R, G, B	red, green, blue video signals
G	diode conductance	R_N, G_N, B_N	narrow-band R, G, B
q	charge on the electron	y	narrow-band luminance signal derived from R, G and B
k	Boltzmann's constant ($= 1.38 \times 10^{-23}$ J/degK)	h_{ob}	common-base output admittance
T	temperature, °K	h_{re}	common-emitter reverse voltage transfer ratio
I	direct current	h_{fe}	common-emitter forward current transfer ratio
Y	wide-band luminance signal		

Part 1. THE DESIGN PHILOSOPHY

I. J. P. JAMES

1. Introduction

Before the mechanical and electrical detailing of a colour television camera design can be started, important decisions must be taken as to the number and type of pickup tubes to be employed and the types of optical, mechanical and electrical systems to be used. The success of the project depends heavily on reaching correct conclusions at this stage, as the complexity of the development process makes mistakes both costly and time-consuming.

† E.M.I. Electronics Ltd., Hayes, Middlesex.

‡ Research Laboratories of Electric & Musical Industries Ltd., Hayes, Middlesex.

2. General Design Considerations

2.1. Choice of Pickup Tube

Many parameters must be considered when the pickup tubes for a colour camera are to be chosen. Among these may be listed registration, shading, signal/noise ratio, resolution, lag, stability, sensitivity, size, weight and ease of operation.

When the camera design was started, the pickup tubes of interest were the image orthicon, the vidicon and the newly introduced Plumbicon.§ While many years of operating experience in America had shown

§ Trade mark of N.V. Philips, Eindhoven.

the practicability of cameras based on the image orthicon, the size and weight of these cameras remained an embarrassment. The vidicon offered small size, but lag and low sensitivity ruled it out for broadcast use. The Plumbicon in effect achieved the sensitivity and low lag of an image orthicon in an envelope little larger than a vidicon. Since it also had the advantages of a fixed black level, practically no shading errors and a (linear) transfer characteristic which was independent of picture content, it became the obvious choice for colour work.

2.2. Number of Tubes

Colour cameras have been designed with anything from one to four tubes, but for broadcast work the choice lay between either three or four tubes. Earlier experience with an experimental image orthicon plus three vidicon camera had shown the inadvisability of mixing tubes but had convincingly demonstrated the virtues of the four-tube arrangement. The use of a separate luminance tube ensures that luminance detail is rendered crisply despite misregistration. As a result the four-tube camera is markedly more tolerant of registration error. So long as advantage is not taken of this fact to ease stability requirements, colour fringing caused by misregistration becomes less evident under practical operating conditions.

A further important practical feature of the arrangement is concerned with lag. It is found in practice that coloured lag caused by unequal signal currents in the pickup tubes is much more visible than balanced or monochrome lag. In the four-tube format it is possible to achieve a reasonable balance of signal current in the colour tubes without reducing the overall sensitivity as in the three-tube system. Under studio conditions the improved lag performance of the four-tube camera enables it to be worked at a higher operational sensitivity, thus offsetting its greater capital cost and complexity.

2.3. Optical System

The art of making wide-range zoom lenses had advanced sufficiently for the camera to be conceived as a zoom camera rather than a turret camera modified to take a zoom lens. Although it meant a more complex development programme, a pre-aligned direct-imaging beam splitter was chosen in preference to a relay system. This resulted in a compact optical system and allowed the pickup tubes to be disposed in such a way that tubes could be changed without the scanning yokes being disturbed. The short length of the system also helped in the decision to make the zoom lens integral with the camera rather than having it project from the front as in previous cameras. This arrangement considerably reduced the moment

of inertia, with the result that the camera is lighter to handle than many monochrome cameras.

2.4. Colorimetry

The N.T.S.C. and the (subsequent) PAL and SECAM systems were designed basically around three-tube colorimetry and so it was necessary to solve the problems of colorimetry associated with the use of a fourth separate luminance tube.

The outcome of the study was: (a) a specification for the optimum colour analysis characteristics for the beam splitter, which not only included the relative characteristics, but also the absolute values; and (b) the development of the signal processing method known as delta-L (described later in Section 2.5), which ensured extremely accurate colorimetry.

Having determined the theoretical prism characteristics it was necessary to obtain practical dichroic and glass filter characteristics to match them. This was achieved with a fair degree of success, even allowing for the Plumbicon characteristic, which cuts sharply at approximately 640 nm.

In order to maintain the accuracy of colour matching between cameras, a comprehensive measuring equipment was designed to measure the spectral characteristics of the prism outputs.

2.5. The Delta-L System of Signal Processing

The signal coding process developed in the U.S.A. by N.T.S.C. (and subsequently applied to the PAL and SECAM systems) consisted in taking the three gamma-corrected tristimulus signals $R^{1/\gamma}$, $G^{1/\gamma}$, and $B^{1/\gamma}$ and by linear matrixing changing them into three other signals:

- (a) a wideband monochrome signal

$$Y' = 0.3R^{1/\gamma} + 0.59G^{1/\gamma} + 0.11B^{1/\gamma}.$$

- (b) two narrowband colour-difference signals

$$(R_N^{1/\gamma} - y')(B_N^{1/\gamma} - y')$$

where

$$y'_N = 0.3R_N^{1/\gamma} + 0.59G_N^{1/\gamma} + 0.11B_N^{1/\gamma}.$$

At the receiver, the three signals R , G and B were recovered by matrixing, thus:

$$\left. \begin{aligned} Y' + (R_N^{1/\gamma} - y') &= R_N^{1/\gamma} + (Y' - y') = R_N^{1/\gamma} \\ Y' + (G_N^{1/\gamma} - y') &= G_N^{1/\gamma} + (Y' - y') = G_N^{1/\gamma} \\ Y' + (B_N^{1/\gamma} - y') &= B_N^{1/\gamma} + (Y' - y') = B_N^{1/\gamma} \end{aligned} \right\} + Y'_H.$$

$(G_N^{1/\gamma} - y')$ was obtained from the matrix

$$(G_N^{1/\gamma} - y') = -0.51(R_N^{1/\gamma} - y') - 0.19(B_N^{1/\gamma} - y').$$

Y'_H is the mixed high-frequency monochrome signal.

In the case of the separate luminance tube in a colour camera the output signal is

$$Y = 0.3R + 0.59G + 0.11B,$$

which when gamma-corrected gives

$$Y^{1/\gamma} = (0.3R + 0.59G + 0.11B)^{1/\gamma}.$$

$Y^{1/\gamma}$ does not equal Y' except for the case $R = G = B$, which corresponds to white, or neutral (grey) tones. If the gamma-corrected luminance signal $Y^{1/\gamma}$ is used in place of the monochrome signal Y' , then the recovered signals at the receiver will be in error since:

$$\begin{aligned} Y^{1/\gamma} + (R_N^{1/\gamma} - y') &= R_N^{1/\gamma} + (Y^{1/\gamma} - y') \\ &= R_N^{1/\gamma} + (y^{1/\gamma} - y') + (Y^{1/\gamma})_{II} \\ Y^{1/\gamma} + (G_N^{1/\gamma} - y') &= G_N^{1/\gamma} + (Y^{1/\gamma} - y') \\ &= G_N^{1/\gamma} + (y^{1/\gamma} - y') + (Y^{1/\gamma})_{II} \\ Y^{1/\gamma} + (B_N^{1/\gamma} - y') &= B_N^{1/\gamma} + (Y^{1/\gamma} - y') \\ &= B_N^{1/\gamma} + (y^{1/\gamma} - y') + (Y^{1/\gamma})_{II} \end{aligned}$$

where

$$y^{1/\gamma} = (0.3R_N + 0.59G_N + 0.11B_N)^{1/\gamma}.$$

It is seen that the three output tristimulus signals have an added error term $(y^{1/\gamma} - y')$. For neutral colours the error is nil, but for saturated colours the error becomes appreciable.

This error can be avoided by subtracting from the gamma-corrected luminance signal $Y^{1/\gamma}$, a luminance-difference correction signal $\Delta L = (y^{1/\gamma} - y')$ formed by matrixing from the band-limited R, G and B signals, and this is the basis of the delta-L correction system. The monochrome signal transmitted is therefore $Y^{1/\gamma} - \Delta L = Y^{1/\gamma} - (y^{1/\gamma} - y')$.

At the receiver the relevant equations are:

$$\left. \begin{aligned} Y^{1/\gamma} - (y^{1/\gamma} - y') + (R_N^{1/\gamma} - y') \\ &= R_N^{1/\gamma} + Y^{1/\gamma} - y^{1/\gamma} = R_N^{1/\gamma} \\ Y^{1/\gamma} - (y^{1/\gamma} - y') + (G_N^{1/\gamma} - y') \\ &= G_N^{1/\gamma} + Y^{1/\gamma} - y^{1/\gamma} = G_N^{1/\gamma} \\ Y^{1/\gamma} - (y^{1/\gamma} - y') + (B_N^{1/\gamma} - y') \\ &= B_N^{1/\gamma} + Y^{1/\gamma} - y^{1/\gamma} = B_N^{1/\gamma} \end{aligned} \right\} + (Y^{1/\gamma})_{II}$$

The delta-L correction signal is formed from the narrow band (1.6 MHz) R, G and B signals by suitable gamma-correcting and matrixing circuits. With grey scale scenes $y^{1/\gamma} = y'$, and the signal remaining is that from the separate luminance tube only. The system thus contains first-order noise cancellation in respect of the correction signal.

It is not essential that the signal $y^{1/\gamma}$ be formed with the normal coefficients, i.e.

$$y^{1/\gamma} = (0.3R_N + 0.59G_N + 0.11B_N)^{1/\gamma}.$$

If, for example, a Plumbicon tube deficient in red response is employed as a separate luminance tube, then it is possible to modify the coefficients in forming y to correct, to some extent, for this deficiency.

The delta-L system enables the four signals to be matrixed into three signals, without the advantages of the fourth tube being lost. The three signals obtained are suitable for immediate application to a RGB monitor, or encoder. Details of one method of realizing the delta-L system are given in Part 3 dealing with the electrical design of the camera.

In general it can be said that because of the extra information derived from the fourth tube the colorimetry can be more accurate than that of a three-tube analysis, especially so if luminance matrix correction is employed.

Part 2: THE OPTICAL AND MECHANICAL DESIGN

D. G. PERKINS and P. J. PYKE

3. The Optical Splitter

After the initial decisions regarding the number and type of pickup tubes to be used, the basic form of the camera emerged during the design of the four-way direct-imaging optical splitter.

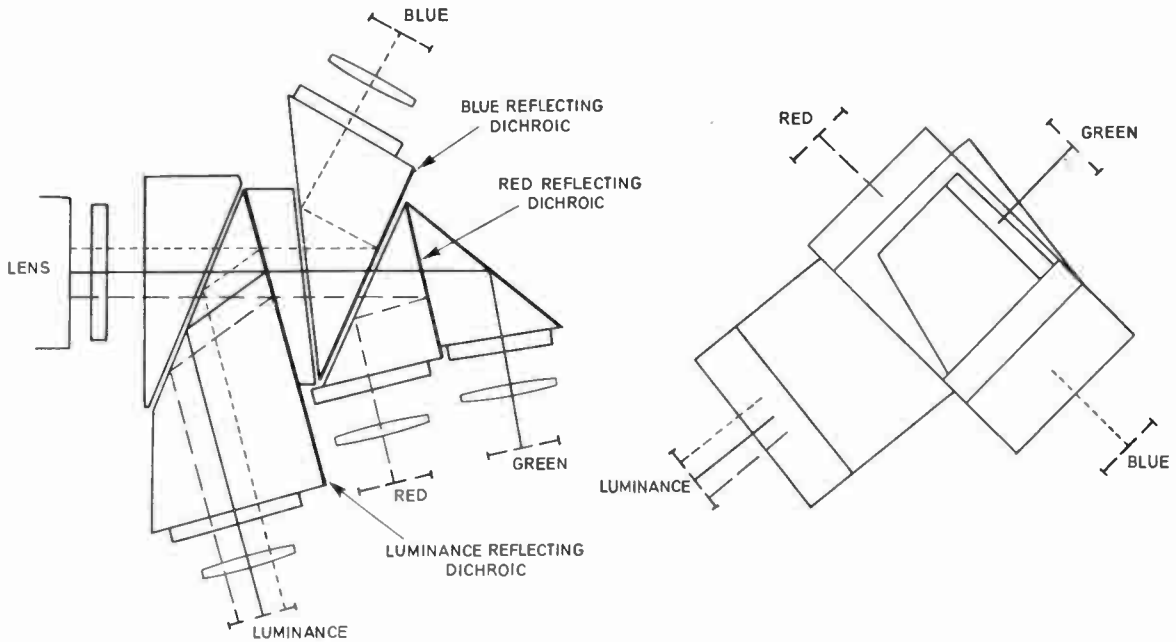
The optical design criteria for the splitter were that it should:

- (a) have an optical path length that could be accommodated within the back focal length of suitable zoom lenses;
- (b) be large enough to cover the pickup tube format and accept an $f/2$ cone without vignetting;

- (c) have favourable dichroic angles to minimize shading and polarization effects.

The mechanical design criteria were that it should:

- (a) allow the camera to be compact for easy handling;
- (b) allow good access for pickup tube changing;
- (c) allow the component prisms, filters, etc., to be cemented together to form one dustproof, rigid assembly;
- (d) allow its incorporation in the camera in a way that would ensure a rigid structure for supporting the optical components (lens, splitter and scanning yokes plus pickup tubes);



(a) Some prisms have been rotated about the inlet axis in order to show the light paths within the glass.

(b) View from rear of camera—actual angles of prisms.

Fig. 1. The final optical arrangement of the splitter.

(e) allow for thermal effects and avoid microphony.

A number of configurations were considered with minimum optical path length as the main objective. This dictated that full advantage be taken of the aspect ratio of the image, and the resulting configurations required a camera larger than was considered acceptable: furthermore, in most cases, at least one of the pickup tubes came in a relatively inaccessible position.

4. Tube Positioning

In order to accommodate the pickup tubes within an acceptable camera size, thought was given to placing the tubes on the diagonals of the camera cross-section. No advantage could then be taken of the aspect ratio of the image and consequently a longer optical path length would result.

Consultation with the lens manufacturers indicated that they could supply a range of zoom lenses which would have high quality performance provided that a simple field-correcting lens could be incorporated in a position near to the pickup tube. This eliminated the need for absolute minimum optical path length, and a splitter was devised with the tubes on the camera diagonals. This in itself did not completely solve the camera size problem because the luminance tube, the light for which was split off first, projected rather more from the main optical axis than did the

other three tubes. By having the luminance tube as one of the bottom tubes and by rotating the luminance splitter prism 8° from the true diagonal, it was possible to make the luminance tube base come at the same height as the other bottom tube (blue) and thus to project only sideways. This sideways projection of approximately 6.5 cm ($2\frac{1}{2}$ in) was accommodated within an extension on the side of the camera into which were also fitted connectors for the camera cable, for zoom rate control, talkback and auxiliary mains. The basic cross-section, determined by the dimensions over the red, green and blue tubes is 38 cm (15 in) square, with the main optical axis in the centre.

Figure 1 shows diagrammatically the final optical arrangement of the splitter which is cemented together to form one compact assembly. This assembly is clamped permanently into an aluminium casting, after which four seatings—one for each of the focus-scanning yoke assemblies—are machined into the casting, accurately positioned with respect to the emergent light rays as described later. This method of assembly allows the scanning yokes to be rigidly fixed to the central prism casting as shown in Fig. 2. The only optical alignment adjustments are rotation of the scanning coil and a small amount of axial movement of the pickup tube for differential optical focusing. With this prism configuration, the tube

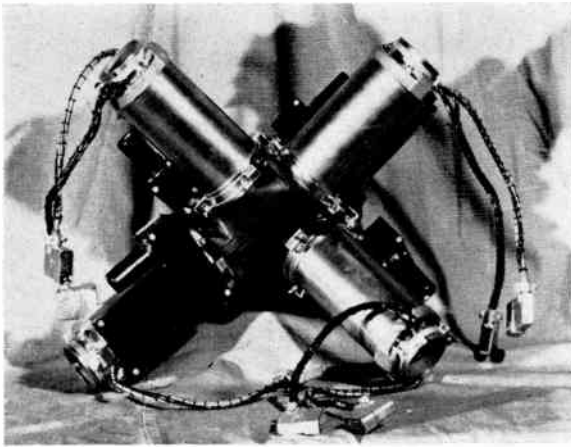


Fig. 2. The central prism casting showing yoke fixing.

bases appear in the corners of the camera and permit easy access for tube changing after the camera covers have been opened.

In order to minimize the camera's moment of inertia, the short length of the splitter plus scanning yoke assembly was fully exploited by keeping the camera length behind the prism assembly to a minimum. This length was determined by that required for the viewfinder tube, the neck of which was placed between the two top pickup tubes. With the length so determined there was insufficient room at the rear of the camera for all of the circuits and positioning of these at the sides of the zoom lens was considered. Investigation of zoom lens sizes showed this to be practical, there being approximately 7.5 cm (3 in) width available on each side of the largest zoom lens likely to be used, provided that the lens servo amplifiers were incorporated as part of the camera. The box-like structure of the compartment into which the zoom package slides provides a stiff central 'chassis' which prevents twisting and mechanical deformation of the camera generally.

With the basic form of the camera determined, the remaining decision was how best to fit in the rest of the camera parts, preferably without increasing the size beyond that required for the optical splitter and pickup tube assembly, the studio zoom lens and the viewfinder tube.

5. Other Physical Considerations

Apart from physically accommodating the parts within the prescribed volume, it was desirable to satisfy many conditions: all controls, adjusters, etc. should be conveniently positioned for the camera operator to use; all parts should be easily accessible for servicing; circuits should if at all possible be on

plug-in printed boards of the same standard size as used throughout the rest of the camera channel; the viewfinder should be capable of being tilted and of being operated remotely from the camera; the 'shot box' should be incorporated in the camera in a position that places the shot buttons and controls near to the cameraman's right hand; a 'turret' with optical filters would have to be positioned between the zoom lens and the prism assembly; adequate carrying handles would be required; it should be possible to stand the camera on a flat surface with cables connected; the camera should be showerproof; the weight of the camera should be kept to a minimum consistent with adequate strength; it should be possible to change zoom lenses easily and quickly; and finally, of course, all this would have to be achieved in a design which would permit production at a competitive price.

With the foregoing conditions in mind, areas of the camera were allocated to the various parts and assemblies; the top back of the camera for the viewfinder, the bottom right-hand corner at the back for the shot box and focus control, the volume to the left of the zoom lens for the four video amplifier boards and camera cable terminating tag panels (to keep short connections to the camera cable connector), leaving the volume to the right of the zoom for the servo amplifier chassis and the heater supply stabilizer chassis, and the space at the back under the viewfinder for miscellaneous camera circuits (pickup tube line scan, talkback, beam current stabilizers, etc.). The engineers working on these various parts were thus able to design them to fit into the available space while the camera carcass was being designed. At this stage, industrial design consultants were called in to advise on the styling of the camera. The pickup tubes had already determined the cross-section size of the camera and it was quite clear that the best

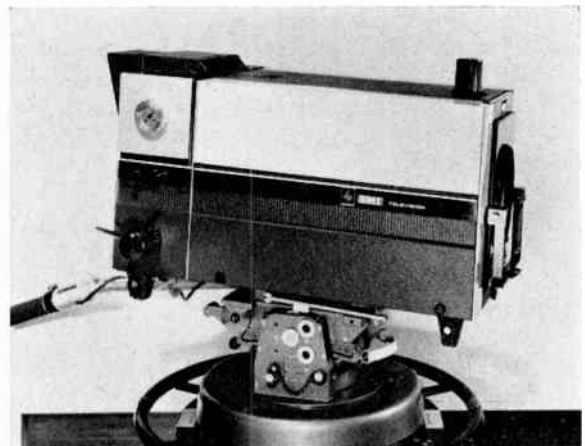


Fig. 3. A side view of the complete camera.

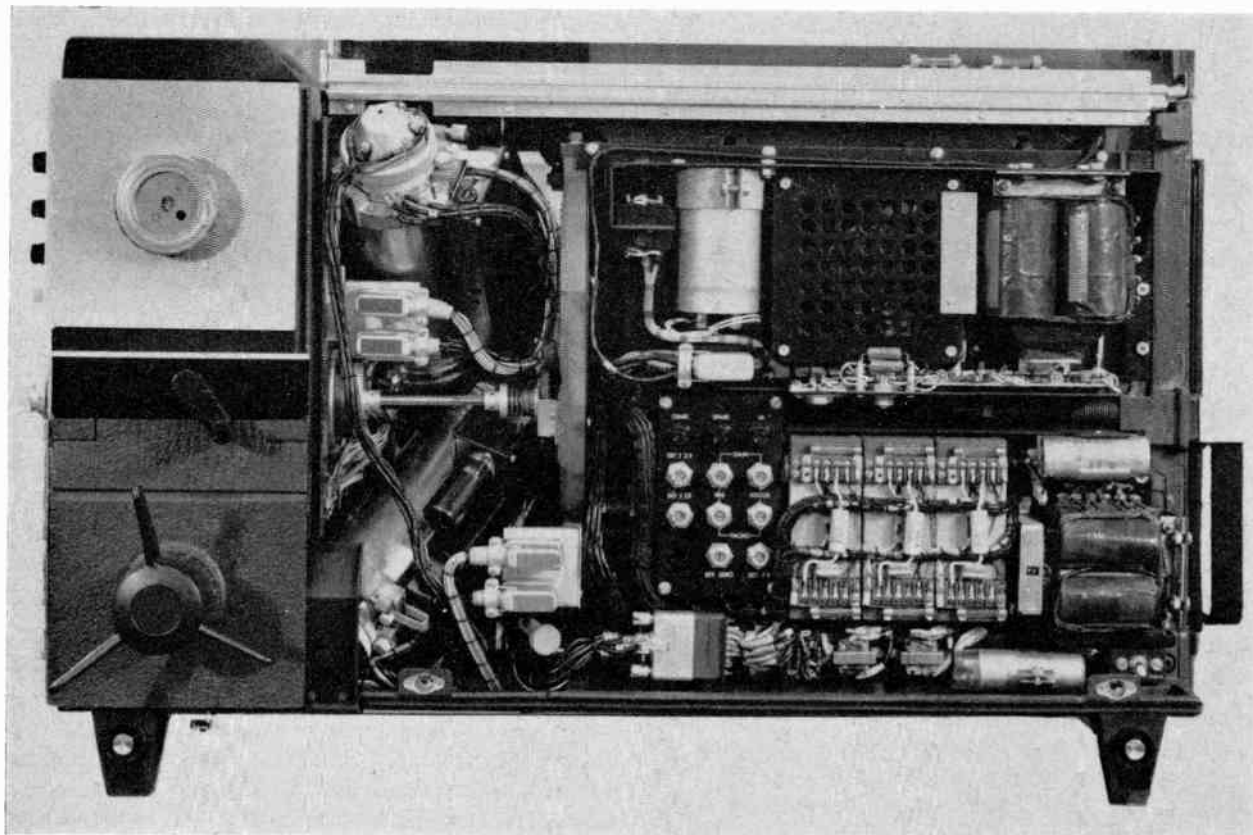


Fig. 4. Camera right-hand side with covers off.

shape to accommodate the component parts was a cubic form and that any shaping for styling purposes could only be achieved by an undesirable increase in the volume of the camera. The appearance of the camera was made interesting by breaking up the cubic shape with shallow contouring and different surface finishes and textures.

6. The Final Design

One by one the design problems were solved and the Type 2001 camera came into being (Figs. 3, 4, 5 and 6). With the studio zoom lens fitted, it is 53.7 cm (29 in) long, with an all-up weight of approximately 91 kg (210 lb). All operational controls (apart from the zoom rate control which is positioned on the panning bar for operation by the left hand) are grouped for operation by the cameraman's right hand. The head amplifiers, lens servo amplifiers and heater stabilizer are the only circuits that are not on standard plug-in printed circuit boards. The viewfinder is fully tilting and may be operated up to 9 m (30 ft) away from the camera. The shot box may be readily removed with the optical focus control attached for remote operation. The eight-position filter turret placed between the lens and the prism

block and operated by a control on the rear of the camera via a shaft is thus totally enclosed within the camera, and is therefore rainproof and, to a very high degree, dustproof. The four retractable carrying handles built into the four feet at the corners of the camera are particularly useful for lifting the camera on to a tripod because of their low position and wide spacing. The angle of the camera cable entry and the height of the feet allow the camera to be operated when standing on a flat surface; the pickup tubes may also be changed when in this position. The use of rain-tight hinges for the camera covers, and of gutters formed in the camera castings, provides a high degree of shower protection.

The camera carcass consists of a number of aluminium alloy castings which are anodized and painted before being bolted together. The wiring harness is preformed complete with all connectors, the tube bases, the cameraman's panel and the main tag panel, leaving just the camera cable connector to be wired to the main tag panel after the harness is fitted into the camera carcass.

The zoom lens package slides into the camera on runners (Fig. 7) and is pulled up on to dowel pins to

ensure accurate alignment. It is secured in the camera by a simple catch mechanism, incorporating powerful springs that force the lens package back against an adjustable stop, the control knob of which is situated just inside the right-hand camera cover; by this means the position of the lens may be readily adjusted to achieve focus tracking.

In order to enable rapid balancing of the camera with interchange of zoom lenses, for example, a slide mechanism is built into the camera between the wedge mounting plate and the base casting; by adjusting a simple knob (operating through a lead screw) the cameraman can balance the camera to his liking without the use of tools.

7. Development of the Prism Unit

The camera layout, as described above, determined within narrow limits the design of the prism unit. The optical path length was made as short as possible consistent with the requirement for passing an

unobstructed cone of light from a zoom lens having an aperture of $f/2$. Long term reliability was one of the main considerations in the camera design, and it was considered desirable that the prism unit should not require adjustment. At an early stage it became clear that this could only be achieved by a cemented prism assembly housed in a casting which would have machined seatings for the scan-focus coil units. In turn, the pickup tubes would have to be very accurately located in the coil units.

Prisms made to a high order of accuracy by hand finishing methods are very expensive and available only in limited quantities. Each unit requires six prisms for its construction, and it was therefore necessary to consider the use of prisms made to commercial tolerances. These are manufactured in relatively large batches and have a high quality surface finish, but dimensions and angles can vary by ± 0.0127 mm (0.005 in) and ± 5 minutes respectively. If the errors in an assembly happen to be cumulative, then the worst angular error of an exit

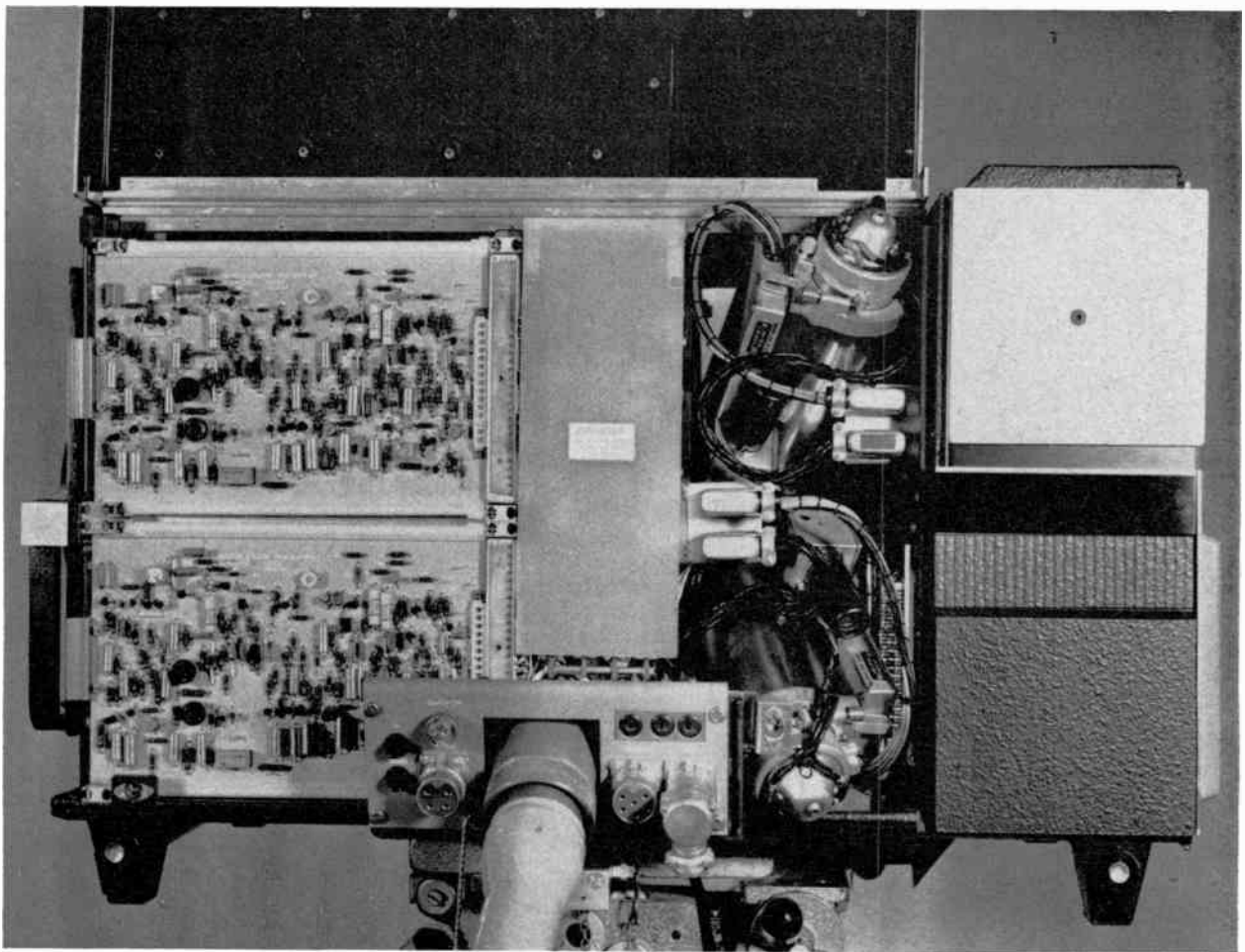


Fig. 5. Camera left-hand side with covers off.

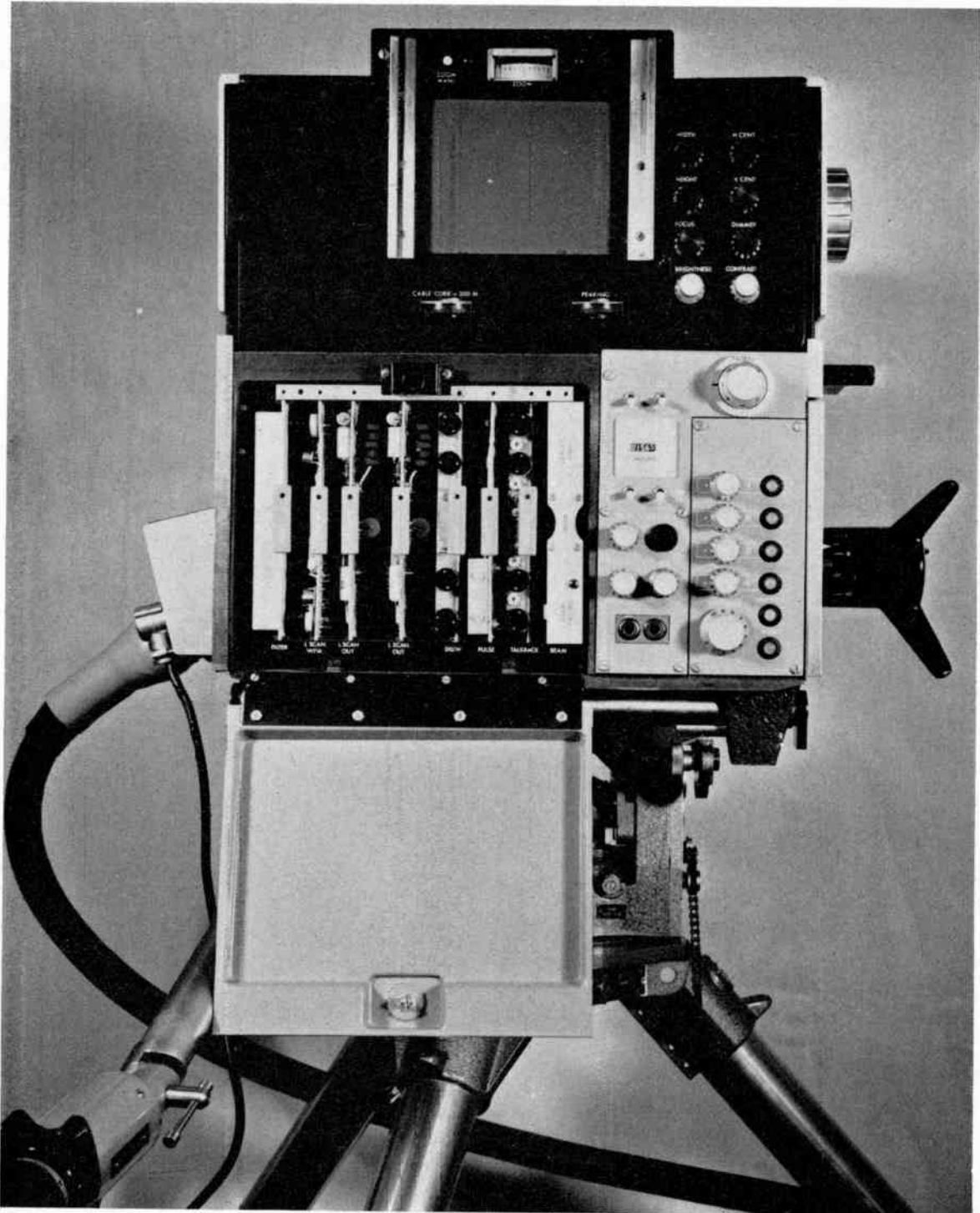


Fig. 6. Cameraman's view showing viewfinder and shot box.

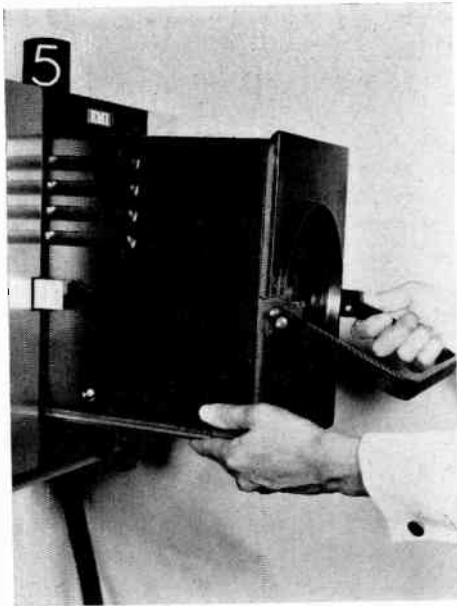


Fig. 7. Zoom lens package withdrawal.

axis could be of the order of 1° ; the image tilt caused by this error would be quite intolerable. A technique of machining the coil seating with reference to the exit axes was devised to accommodate these variations.

Figure 1 shows the light paths within the prism unit; three surfaces are coated with multiple dielectric (dichroic) layers, each reflecting only a part of the incoming light. First the luminance portion is split off, and then the blue and red respectively, allowing the green light to pass out via the last prism. All other air/glass surfaces are anti-reflection coated for the appropriate wavelengths. The broad divisions of the spectrum produced by the dichroic mirrors are

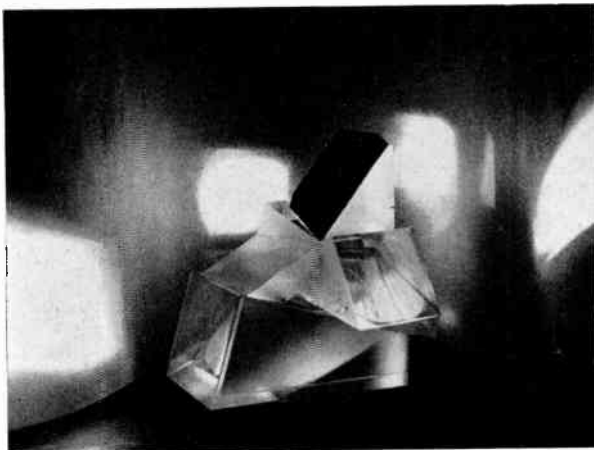


Fig. 8. A prism unit before trimming filters are cemented in place. Light enters the inlet face from below.

shaped to the required characteristics by colour glass trimming filters cemented to the outlet faces of the unit. Two prism interfaces require to be fully cemented, and three require air-gaps in order that light reflected from the dichroic coatings may be reflected out of the unit by total internal reflection. Since light must pass through the air gaps before reflection, the gaps are maintained at 0.025 mm (0.001 in) so that coma and astigmatism are kept to acceptable levels.

Assembly jigs were designed to locate the outlet faces in their correct positions, one for the first pair of prisms comprising the luminance section, and a more complex arrangement to complete the assembly of the colour sections.

The formation of the air-gap is achieved by using very soft metal wire, laid around the perimeter of the required gap on the surface of the first prism; the second prism is placed in position and pressure applied to flatten the wire, forming a seal around the gap area. Epoxy cement is then introduced into the gap outside the metal seal and cured by heating. After cooling, the first pair of prisms is transferred to the main assembly jig. The third prism is positioned and cemented so that variations in the height of the luminance section are corrected. The upper face then provides a new reference surface for the assembly of the remaining three prisms comprising the colour section. Air-gaps for the blue and red outputs are formed as before, and the sixth prism is cemented in place. Figure 8 shows the assembly after reinforcing plates have been cemented to the sides of the unit in the region of the air-gap joints and a bridge piece cemented between the luminance and colour sections. Finally, the trimming filters are cemented to their respective outlet faces and the unit painted black to absorb any stray light.

The aluminium alloy castings are given a preliminary machining operation in which the bores for the coil units are left undersize. One hole and slot are formed in the base of the casting at an early stage in the machining, and are used throughout all subsequent operations as the locating reference, finally serving to position the unit in the camera. The prism

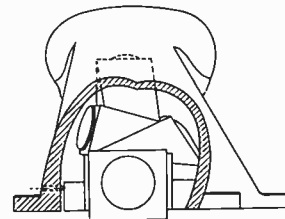


Fig. 9. Part-sectional diagram of a prism unit in a casting showing the method of clamping the unit in position.

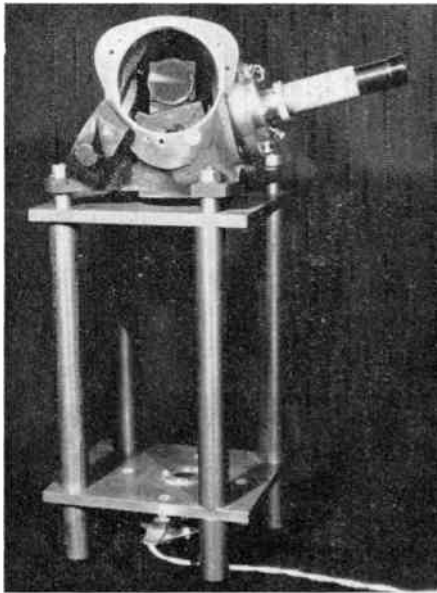


Fig. 10. The jig used for determining image positions prior to final machining, and also for inspection.

unit is clamped in position in the casting on a seating previously machined with reference to the hole and slot, a simple jig serving to position the projecting entry face of the unit at 0.635 mm (0.025 in) from the casting base (Fig. 9).

In addition to the previously described variations of position and angle of the exit axes, slight differences will exist in the path lengths through the unit and hence in the image positions along the axes. The jig used for determining the image positions is shown in Fig. 10. It serves two purposes—firstly to determine the actual image position in each of the four channels prior to machining the coil seatings, and secondly as an inspection jig to establish that the final machining has been carried out correctly for image position and centring. It consists of an illuminated graticule and a lens adjusted to produce an accurately centred

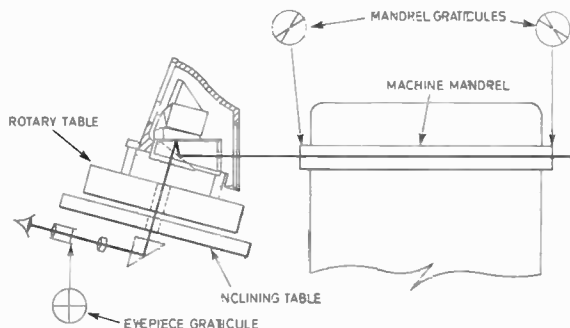


Fig. 11. The optical arrangements for alignment of the prism unit axes with the machine axis.

image at the theoretically correct distance from the casting base. From the image positions measured on the jig, the required depth of seating is obtained.

Machining of the bores and seatings is carried out on a precision universal milling machine equipped with an optical arrangement to align each exit axis of the prism unit with the machine axis in turn. Figure 11 shows the prism casting located by means of its reference holes so that its inlet axis is exactly aligned with the axis of rotation of a rotary table. A special fitting allows the rotary table to be inclined with respect to the mandrel. Below the table is a telescope having a cross-wire in its eye piece, thus defining its axis. A small prism allows the telescope axis to be aligned with the rotary table and prism inlet axis, and brings the eye piece to a convenient viewing position. Situated at each end of the machine mandrel are two accurately centred graticules, and behind the machine (not shown) is a source of light.

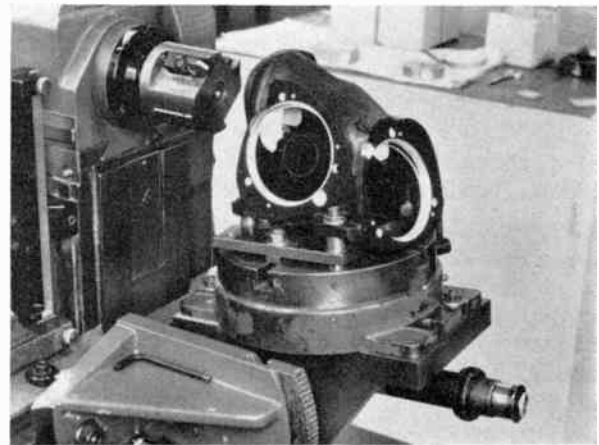


Fig. 12. Machining in progress—two faces have been finished and the multipoint cutter is being used to form the seating of the third face.

In use, the exit axis of the unit and the axis of the machine are brought into alignment by adjustment of the machine settings until both mandrel graticules are coincident with the telescope graticule.

The mandrel graticules are then replaced by a multipoint tool. In a single operation the bore is machined to a tolerance of ± 0.0127 mm (0.005 in) on diameter, and a counterbore is formed to the previously measured depth (Fig. 12). Immediately after the boring operation, holes are drilled to accept threaded steel inserts for clamping screws. Interposed between the machined seatings and the coil units are magnetic shields which carry field flattener lenses. Plastic gaskets hold the lenses in place and provide a dust seal between the lenses and the outlet faces of the prism unit.

Part 3: THE ELECTRICAL DESIGN

E. W. TAYLOR, D. E. KENT and I. A. FAIRBAIRN

8. General Design Considerations

8.1. Performance

The requirement for high performance in colour television equipment does not need to be stressed. Factors which are considered of particular importance in determining the overall performance of the equipment are head amplifier signal/noise ratio, master gain control tracking, gamma corrector tracking, four-signal to three-signal conversion (delta-L system) and registration. These aspects received particular attention in the development programme and are discussed in detail.

8.2. Long Term Stability

In a practical situation the achievement of high performance is of little value if it is marred by instabilities which make it difficult to keep the equipment at peak performance for more than short periods. Feedback techniques involving high loop gains and ultra-stable resistors (± 5 parts/ 10^6 deg $^{-1}$ C) are used throughout. Certain control functions require very stable voltage supplies and a power supply module of 0.1% long-term accuracy was developed for this purpose.

8.3. Long Camera Cable

The channel is required to operate with up to 600 m (2000 ft) of cable between the camera and its control unit. It is necessary to allow for the effect of this cable on all the circuits passing through it. This has been done successfully and the camera operates at the full cable length without noticeable degradation of performance.

9. Practical Considerations

9.1. All Controls at Camera Control Unit (c.c.u.)

It is held to be desirable to place as many controls as possible at the c.c.u. Exceptions made to this rule are the mechanical controls for yoke rotation and differential optical focus adjustment, and the electrical controls for target voltage and skew correction. These controls normally only require adjustment when a pickup tube is changed.

9.2. Separate Power Supply Unit

The power supply is separated from the c.c.u. in order to keep the latter small and make it possible to operate several cameras from a single control position. Power to the camera itself is mainly fed through the cable at low voltage and stabilized by remote sensing. This approach has been adopted to keep circuitry at the camera to a minimum. It is inefficient but the total load of the channel is less

than 550 VA so the power loss is not serious. It was anticipated that hum problems might arise with a remote sensing loop 1200 m long and care was taken with the choice of conductor pairs with the result that no difficulties have been encountered.

9.3. Remote Controls

In line with monochrome practice, the original design allowed for optional remote control of lens iris and master black level. Later modifications have introduced optional remote trimming of black level and gain in the red, green and blue colour channels to facilitate accurate colour balancing.

9.4. Plug-in Cards

Wherever possible, circuits are mounted on plug-in printed cards, with access for servicing by means of an extender board. To avoid some of the problems of instability caused by the extender board, this is not made in printed circuit form but is composed mainly of coaxial leads with a few heavy gauge conductors for earth returns. Each circuit is broken on the extender board and completed by a link, thus allowing signal injection and continuity checking. The use of plug-in cards enables good packing density to be achieved but the large number of plug and socket connections involved requires a very reliable connector if overall reliability is not to be prejudiced. For this reason it was decided not to use printed edge contacts but to rely on the prefabricated i.s.e.p. connector. This connector is available with heavily gold plated contacts and is used in this form throughout the channel. Many thousands are now in service with an excellent reliability record.

9.5. Monitoring Facilities

The channel has been designed to include sufficient monitoring facilities to permit setting-up to be carried out with a minimum of special equipment. The extra equipment required consists of a good quality monochrome picture monitor and a waveform monitor or oscilloscope.

10. Scanning Circuits

Figure 13 is a much-simplified block diagram intended to give a general idea of the arrangement of the channel.

10.1. Horizontal Scanning Circuits

In the 625-line television system there are approximately 500 picture elements along a line. Measurements have shown the permissible misregistration between channels for just-noticeable degradation of

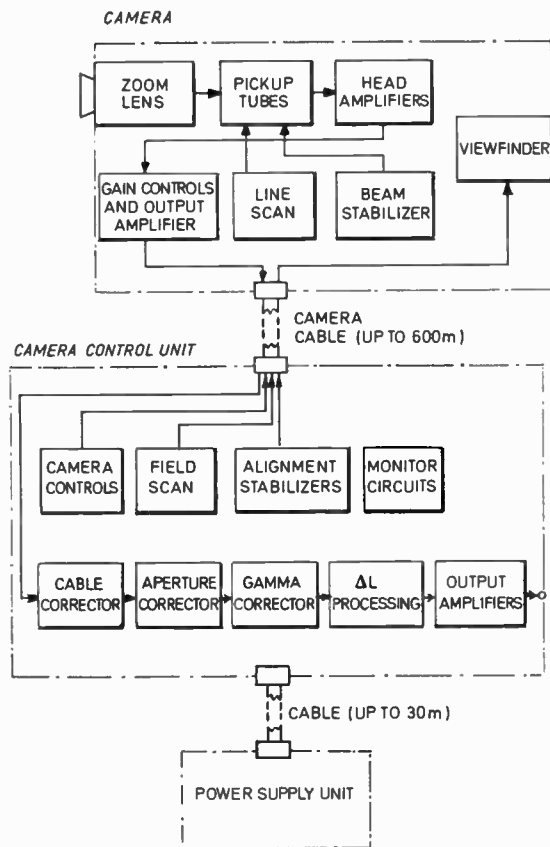


Fig. 13. General arrangement of camera circuits.

the image from a four-tube camera to be of the order of half a picture point. If half of this error is allowed per channel the required stability is of the order of one part in 2000. This consideration has led many designers to use a common scan generator with the scan coils connected in parallel, differential width control being obtained by variable inductors in series with each coil. Unfortunately the variable inductors upset the L/R ratio of the coil and cause linearity errors. Correction of the linearity errors causes differential width errors and the width and linearity controls become interdependent.

In order to avoid this problem, the system shown in Fig. 14 was developed. This system has the further advantage of permitting accurate remote control so that it is possible to place the differential width controls at the c.c.u. although the scan generator must for practical reasons be at the camera. The coils are fed from a common waveform generator via independent gain controls and output amplifiers. The output amplifiers have unity gain and a very high level of internal feedback so that they meet the stability criterion without difficulty. The gain controls are

diode circuits† of the form described in the video amplifier section of this paper and they have a control range of $\pm 2.5\%$. With a total gain range of 5%, the stability required from the gain control is 1% in order to meet the overall stability criterion. With proper design the diode gain control circuit can meet this requirement. Light-controlled resistors were initially tried for this function and a suitable circuit was in fact evolved. It was more complex than that finally used, however, because of the additional circuitry required to overcome the device instability.

Some limitations of the circuit as illustrated should be mentioned. Errors may be caused by the coil resistances, and the L/R ratio of the coils must be closely similar. In practice the coil inductance is not noticeably temperature dependent but the coil resistance is, and this will cause errors in registration if the yokes are at different temperatures. For this reason a small circulating fan is incorporated within the camera. Calculation shows that a temperature differential of 10 degC between yokes is permissible. With the fan in operation this is not exceeded. Overall temperature variations cause absolute linearity errors but these are small and can be ignored.

In the interest of operational simplicity, the system does not contain differential linearity controls. Some differential errors do occur in practice, particularly due to errors in setting of the beam alignment controls. Also some tubes show errors which vary with tube rotation, possibly due to slight asymmetry in the wall anode structure. The resultant errors are small and do not significantly degrade the picture.

The d.c. blocking capacitors in series with the output amplifiers were initially made large in value

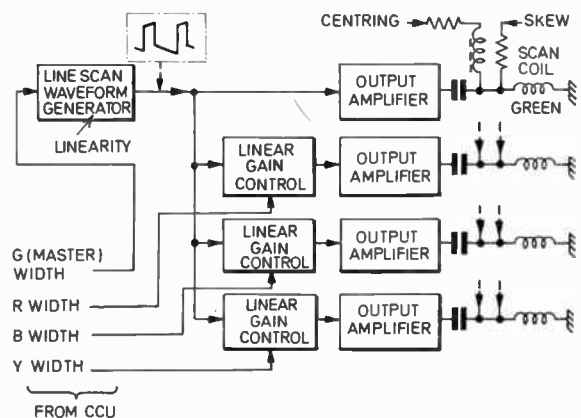


Fig. 14. Line scan system.

† Bray, D. and Hayden-Pigg, G. E., 'Video circuits for transistor television cameras', *J. Soc. Motion Pict. Television Engrs*, 72, p. 853, November 1963.

so that their impedance at line scan frequency could be ignored. In practice this results in the system being unduly sensitive to hum because the scan coils have a very low impedance at mains frequency. It is therefore necessary to use a smaller capacitor and control its effect by using a close tolerance component with good long-term stability and low temperature coefficient. This had the incidental effect of making it easier to inject skew correction currents. These consist of small amounts of positive or negative polarity field scan and are fed directly into the line coils via a stand-off resistor as shown in Fig. 14. Skew correction allows for lack of orthogonality in the scanning coils which are otherwise subject to an impractical requirement for accuracy.

The centring currents are generated in the camera from a control voltage passed through the camera cable from the c.c.u. By this means the effect of resistance variation in the cable is eliminated, and the shift currents eliminated from the camera cable. Centring currents of $\pm 10\%$ of the scan current are made available so that there is a total range of centring control corresponding to 20% of picture width. To meet the one part in 2000 criterion mentioned above, the centring current must therefore be stable to one part in 400. This requires voltage rails at the c.c.u. which are stable to better than $\frac{1}{4}\%$. To avoid using up the whole tolerance they have in fact been made stable to 0.1%. The control voltage is referred to the common earth of the camera and c.c.u. and, since with long cables the earth return impedance between camera and c.c.u. becomes significant, it is important to prevent large unbalance currents from flowing in this earth return. For this reason the main low voltage supplies to the camera are derived from independent floating supplies which are only earthed at the camera. For the same reason relay and talkback supplies are only earthed at a single point in the c.c.u.

10.2. Vertical Scanning Circuits

The system used for the field scan is shown in Fig. 15. As with the line scan, the first step is to generate the required waveform, and this is then applied to a unity gain output amplifier with heavy feedback. In this case, both normal and reverse polarity waveforms are generated and since flyback spike is almost absent at field frequency, the output amplifier can handle either equally well. By reversing the scan at this point, vertical picture reversal is obtained without upsetting registration or introducing relay or switch contacts into the coil circuits. Resistors in series with the scan coils are included mainly to swamp resistance variations in the camera cable but they also improve linearity by reducing the time constant of the coils. The centring currents are generated in a similar manner to that described for

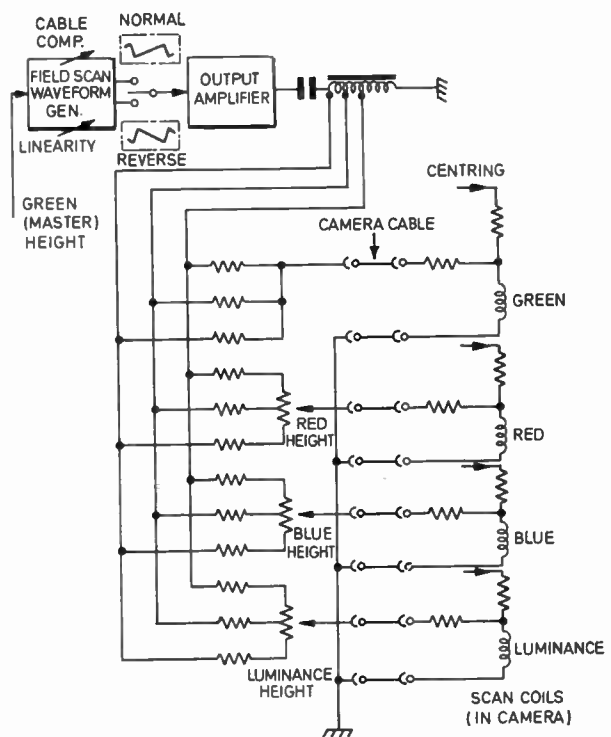


Fig. 15. Field scan system.

the line circuits but in this case the magnitude of current involved is much lower and they are allowed to pass through the cable, returning to the camera via the common earth. The differential height adjustments for red, blue and luminance are derived from 'live' low impedance potentiometers which are connected in nearly constant resistance networks. The low impedance feeds to these networks are derived from the output amplifier by an auto-transformer.

In both line and field scans the master height and width controls are the only controls affecting the green channel, which is therefore adjusted first. Differential corrections are then applied to red, blue and luminance (in that order) to obtain registration. This arrangement is not fortuitous but arises from the fact that errors in red to green registration are found to give the most objectionable effects on picture. The system is therefore arranged to compel the operator to use green as the reference channel when adjusting registration.

10.3. Registration Monitoring Facility

The registration process is made much more critical by adding the signal from the channel to be adjusted to a negative polarity green signal. With perfect registration it would be possible to obtain complete cancellation on a monochrome signal.

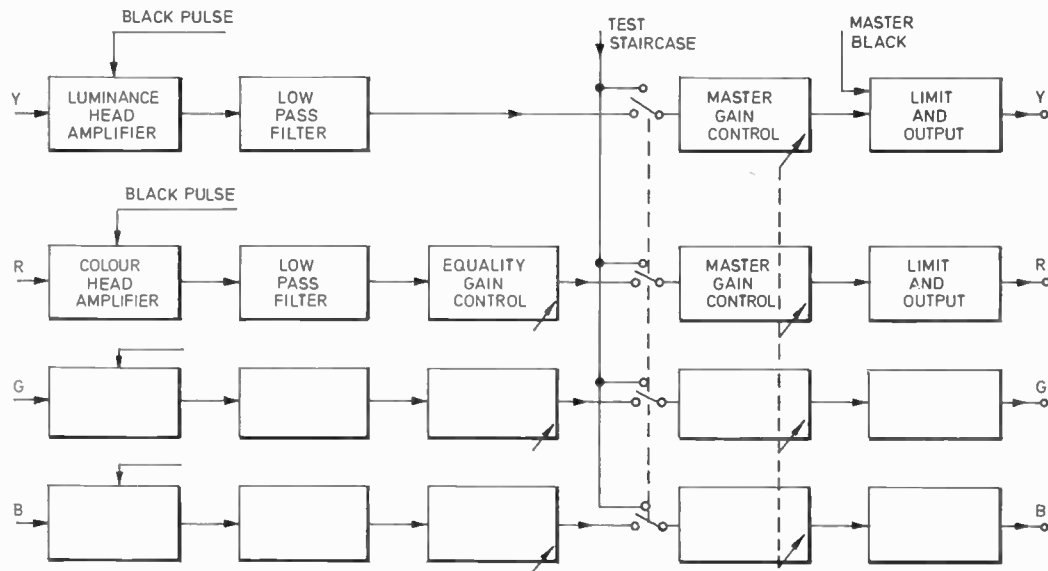


Fig. 16. Camera video block schematic.

With this arrangement, small errors in registration produce large transient edges which enable very small errors to be seen clearly.

11. Video Signal Processing in the Camera

Although such factors as space available and simplicity make it desirable to process the video signal as little as possible in the camera, performance must not be sacrificed. To minimize cross-talk in the camera cable, it is desirable to maintain a high signal level under all conditions of gain, hence the inclusion of all gain control stages in the camera.

The inherently linear characteristic of the pickup tube makes it possible for scene highlights, such as specular reflections, to generate signals with amplitude several times that of normal peak white. The problem of driving these signals along the camera cable into 75 ohms is avoided by including a limiter set to clip at about 3 dB above nominal peak white.

Figure 16 is a schematic diagram of the camera video circuits.

11.1. Head Amplifier

The head amplifier first designed for the camera used a valve in the input stage but this is now replaced by a new amplifier employing field effect transistors in the input. The valve version of the luminance head amplifier has an equivalent noise input current of less than 1.5 nA r.m.s. in a bandwidth of 5.5 MHz, that is, a signal/noise ratio better than 46 dB relative to a signal current of 300 nA. The new luminance head amplifier has an equivalent noise input current of about 1 nA r.m.s. corresponding to a signal/noise ratio of nearly 50 dB for the same conditions.

Both versions of the amplifier have sufficient feedback throughout the video band to make the frequency response insensitive to variations in pickup tube capacitance. It is therefore possible to omit the usual C-R correction control.

Pulses, remotely controlled from the c.c.u., are fed into the head amplifiers to compensate for the effect of line scan pickup spikes occurring during clamping period. A calibration step wedge waveform is also fed in at the same point.

11.2. Low-pass Filters

To remove high frequency noise and unwanted signal information, the channel frequency responses

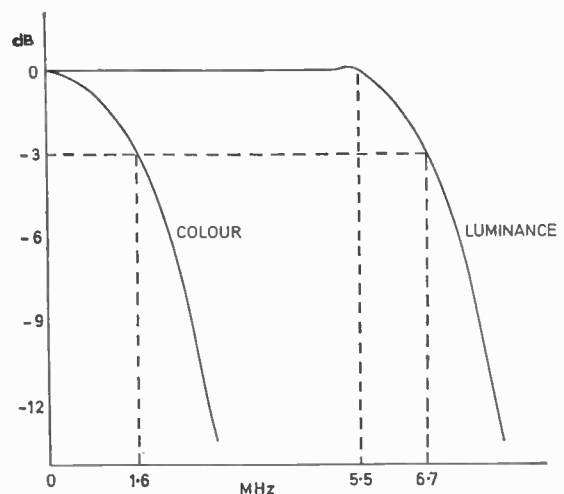


Fig. 17. Amplitude-frequency response.

are shaped by low pass filters immediately following the head amplifiers. The responses are shown in Fig. 17.

11.3. Gain Controls

The equality and master gain amplifiers are all controlled remotely from the c.c.u. The equality gain amplifiers have a range of approximately ± 9 dB and are adjusted to equalize the amplitudes of the four signals at the input to the master gain amplifier for a grey scale scene. The master gain control range is about 20 dB and the four amplifiers are tracked within 0.1 dB throughout the range.

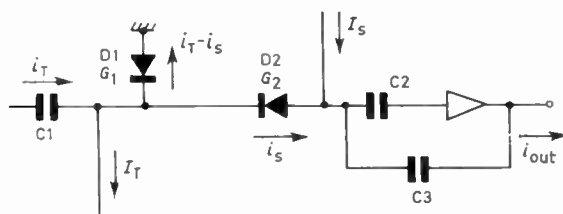


Fig. 18. Remote gain control circuit.

The gain control circuits† use two high conductance type diodes as shown in Fig. 18, their d.c. operating conditions being controlled remotely from the c.c.u.

The two diodes D1 and D2 with conductances G_1 and G_2 are d.c. isolated from the video path by capacitors C1, C2 and C3. Two direct current sources I_T and I_S keep the two diodes in conduction. The video signal is fed through C1 as a current, i_T , which divides between the diodes; the output video current, i_s , passes through D2 to the next amplifier stage. This amplifier is a high loop gain feedback amplifier, the feedback being applied via C3 to form a 'virtual-earth' point at the anode of diode D2.

The signal input current, i_T , divides between the two diodes in the ratio of their conductances.

Therefore, the circuit gain, A , is given by:

$$A = \frac{i_s}{i_T} = \frac{G_2}{G_1 + G_2}$$

For normal forward conduction of a diode, conductance,

$$G \approx \frac{q}{2kT} \cdot I,$$

where $q/2k$ is constant,

T is temperature in degK,

I is diode current.

† Bray and Hayden-Pigg, *loc. cit.*

In the circuit shown in Fig. 18,

$$G_1 = \frac{q}{2kT} \cdot (I_T - I_S)$$

and

$$G_2 = \frac{q}{2kT} \cdot I_S$$

Therefore, gain

$$A = \frac{\frac{q}{2kT} \cdot I_S}{\frac{q}{2kT} \cdot I_T} = \frac{I_S}{I_T}$$

The total direct current, I_T , is kept constant and I_S is varied to adjust gain.

The circuit is linear, even for large amplitude video current swings, because the video current always divides between the two diodes such as to keep the ratio of their conductances, and therefore the circuit gain, constant.

The temperature stability of the circuit is excellent as the temperature dependent components in the gain equation cancel.

Relays controlled from the c.c.u. connect the inputs to the master gain amplifiers together and insert a test staircase. This signal is used for tracking the master gain amplifier and all subsequent video processing.

11.4. Black Level Clamp

In order to peak limit the camera output signals their black levels must first be clamped. This clamp, and every other clamp in the camera channel, uses a double emitter transistor as the switch.

The clamp circuit is shown in Fig. 19. The clamp pulse is applied as a current to the base-collector junction of the double emitter transistor, TR1, causing a low impedance between the two emitters. When the base-collector junction is reverse biased a very high impedance exists between the two emitters, and thus the transistor behaves as a nearly perfect switch.

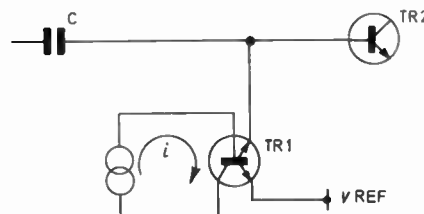


Fig. 19. Black level clamp circuit.

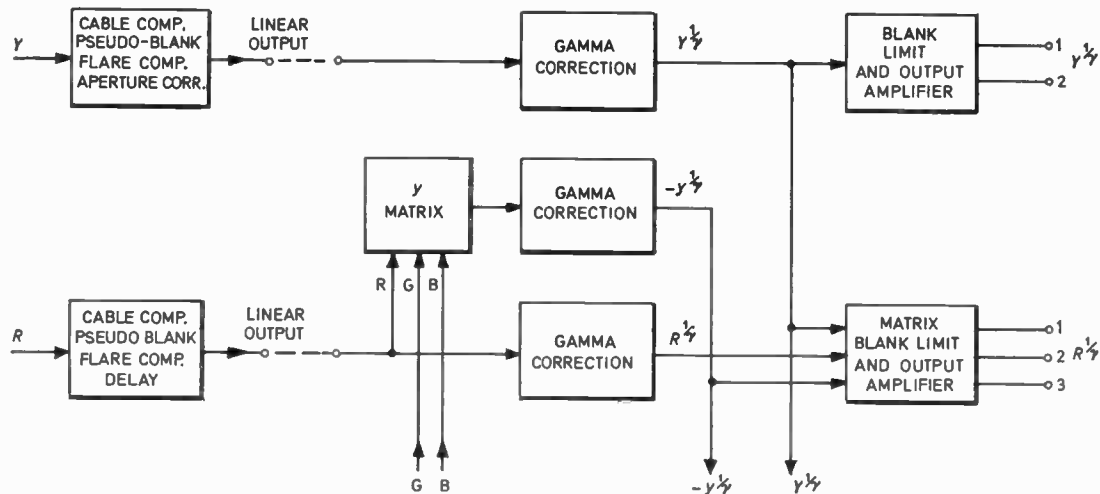


Fig. 20. Camera control unit video block schematic.

12. Video Signal Processing in the Camera Control Unit

Most of the video signal processing is carried out in the c.c.u. Figure 20 is a block diagram of the video circuits including the four-to-three signal process known as delta-L correction (which is described in Section 2.5).

12.1. Cable Compensation

The video signals arriving from the camera are first compensated for losses in the camera cable. Gain and frequency response are corrected for up to 600 m (2000 ft) of camera cable in ten switched steps, each step corresponding to 60 m (200 ft) of cable. There is one switch for each of the four video paths; the switch in the luminance amplifier also adjusts the timing of advanced line drive pulses to compensate for delay in the camera cable.

12.2. Pseudo-blanking

The four signals are blanked at line rate to remove spurious spikes due to line scan pickup. This simplifies the signal processing, particularly after the gamma correctors which would amplify such spikes to very high levels.

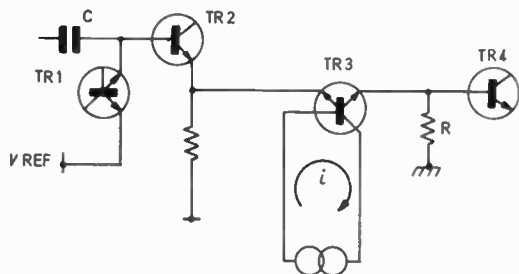


Fig. 21. Pseudo-blanking circuit.

The pseudo-blanking circuit (Fig. 21) uses a double emitter switching transistor in series with the video path. The video signal appears across R at TR4 base while the switch is closed, but when the switch is open TR4 base is at earth potential. The reference voltage for the double emitter clamp TR1 is adjusted such that signal black level is normally at earth potential at TR2 emitter and therefore also at TR4 base.

12.3. Flare Compensation

Flare is caused by stray light associated with scatter in the optical system, and multiple reflexions in the face plate of the pickup tube. The stray light arrives at the target layer as a fairly uniform illumination and the effect is to sit up the signal black levels; unfortunately each colour signal may be affected by different amounts depending upon picture content such as colour of background. The lead-oxide vidicon target is particularly reflective at the red end of the spectrum, and therefore for a white scene illumination, the gamma-corrected red signal black level may be lifted by as much as 20% of peak white but the blue signal by only 4%.

The flare compensation circuit generates a pulse with the same timings as clamp pulse and amplitude proportional to the d.c. component of the video signal. The pulse is fed back into the video path with polarity such as to cause the black level clamp to sit the video black level down. A control on the circuit enables the pulse amplitude to be adjusted to compensate for the sit-up effect of flare. This adjustment may be made while observing the waveform from a scene with a definite dark area of, say, less than 2% of peak white illumination. When the flare compensation is correctly adjusted this 'black' area

should remain at a constant level on the signal waveform as the camera iris is varied over a wide range.

12.4. Aperture Correction

Aperture correction is applied to the luminance signal only, but delays are included in the colour signal paths to maintain accurate relative timings. The aperture correction is of the delay line type giving a cosine law frequency response peaked at about 4 MHz. An onset control adjusts the level above black at which the correction becomes effective, thus enabling resolution to be improved without worsening noise at black level. A maximum boost of about 15 dB at 4 MHz is available, this being considerably more than is normally required.

12.5. Linear Outputs

At this stage in the video processing the linear signals are taken to sockets at the rear of the c.c.u. where they are available for extra processing. The four signals are equal in amplitude for a grey scale scene and the outputs are nominally 0.7 V into 75 Ω for peak white.

Vertical aperture correction is normally applied to the luminance signal at this point and, if required, linear matrixing of the three colour signals may be carried out.

On returning to the c.c.u. the three colour signals are added in a linear matrix to form a narrow band luminance signal y , where $y = 0.3R + 0.59G + 0.11B$. This is the first part of the delta-L signal processing.

12.6. Gamma Correction

The five video signals (G, R, B, Y, y) are all applied to accurately tracked gamma correction circuits. Three gamma laws are available ($1/\gamma = 0.72, 0.55$ or 0.45), the desired law being selected by operating a switch on the c.c.u. front panel; a linear law may also be selected for setting-up purposes.

Accurate and stable tracking of the gamma laws of the five signals over the full contrast range of at least 40 : 1 is most important and great care has been taken to achieve this. The circuit used is shown in Fig. 22 and gives a smoothly curved gamma characteristic. The video signal is black level clamped at TR2 base by means of the double emitter switch TR1. The signal is then applied as a current through R1 and R2 to produce a linear law signal across R3 and an exponential law signal across the diode D1. The portion of the exponential law used is determined by adjustment of the clamp reference potential V_{REF} . R3 is then adjusted such that black to peak white amplitude is equal at both ends of R4. The gamma laws required are produced by adding appropriate proportions of linear and exponential signals, a good approximation to a pure power law being

obtained over a large contrast range. Thus, when the output signal is taken from the wiper of R4, the gamma law changes as the wiper moves along R4 but the amplitude of peak white remains constant.

In the circuit used, all important resistors are precision high stability types and R4 is replaced by four resistors, the tapping point being selected by relays. The diode characteristic is stabilized against changes in ambient temperature by means of a miniature oven. As a result of the care taken it has been found that not only is it possible to adjust for accurate tracking but also the setting remains stable for periods of many weeks.

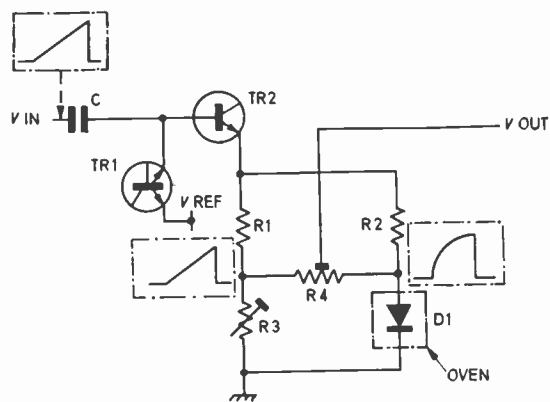


Fig. 22. Gamma correction circuit.

12.7. Output Amplifiers

The colour outputs are formed by adding equal parts of the appropriate colour signal, the separate wide-band luminance signal $Y^{1/\gamma}$ and the inverted matrixed luminance signal $-y^{1/\gamma}$. Thus, the red output signal, $R' = R^{1/\gamma} + Y^{1/\gamma} - y^{1/\gamma}$. These signals are black and white limited and blanked. Three outputs of each of the colour signals and two outputs of the separate luminance signal are provided.

12.8. Operational Control Panel

Coarse and fine iris and master black level controls may be operated remotely from the operational control panel. Fine iris and master black controls are combined in a joystick control. Movement of the control in a quadrant mode varies the iris by plus and minus one stop about the coarse setting determined by an edge control alongside the joystick. The coarse and fine iris controls can be moved simultaneously so that mid-position of the fine iris control range can be adjusted on-air without disturbing the picture. Rotation of the joystick knob controls master black level.

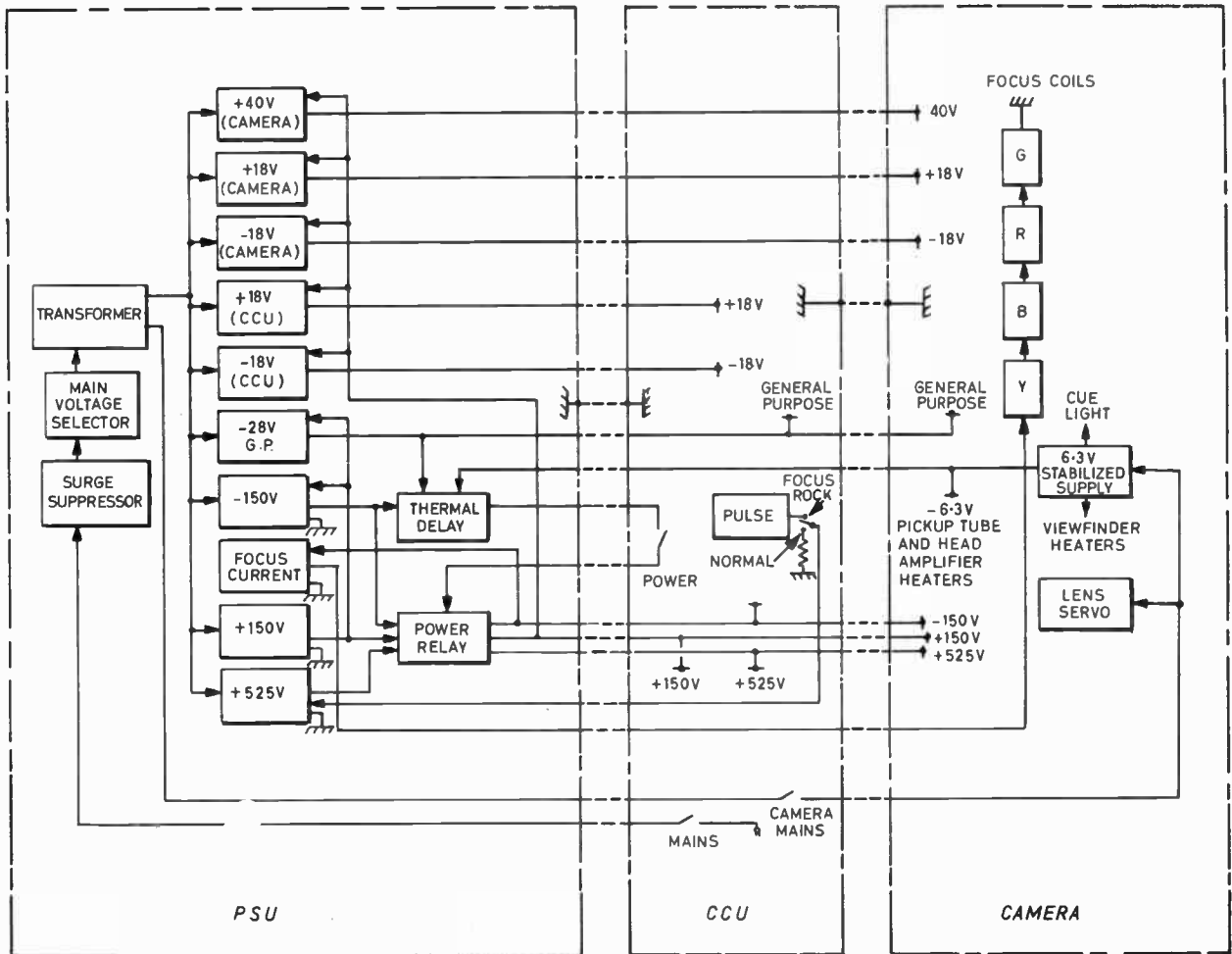


Fig. 23. Power supply system.

12.9. Colour Balance Panel

A colour balance panel is available, if required, for remote adjustment of gain and black balance of the colour signals. The two joystick controls are mounted on a panel 20 cm by 8 cm (8 in by 3¼ in). Using this panel it is possible to correct for changes in lighting conditions or to make fine adjustments to accurately match two or more picture sources.

12.10. Amplifier Monitoring Facility

Operational adjustments of amplifier gain and black level are carried out by comparing the red, green and blue signals with the Y signal on a monochrome subject. The comparison is performed by an electronic switch operating at 12.5 Hz. When viewed on a waveform monitor the low frequency of switching produces a strong flicker if the signals do not coincide. This adjustment will normally be carried out by placing a grey scale chart in front of the camera. Initial preset amplifier adjustments are carried out

on an electronically-generated step wedge which enables master gain and gamma tracking to be adjusted with great accuracy.

To enable peak white to be adjusted, an output consisting of a non-additive mix of the three outputs of the channel is supplied. Observation of this output on a waveform monitor indicates if any of the outputs is hitting the white limit.

13. Power Supplies

A block diagram of the power supply system is shown in Fig. 23. With one exception, all supplies are located in the power supply unit (p.s.u.). The exception is a 6.3 V d.c. stabilizer unit which is placed at the camera to provide a local d.c. heater supply for the pickup tubes and, in the original arrangement, for the head amplifier input stages. The same chassis provides a.c. supplies for the viewfinder heaters, the circulating fan and the remotely-switched cue light supply. In order to ensure that the heaters are up to

temperature before d.c. power is applied to the camera, the 6.3 V d.c. rail is fed back to the p.s.u. to operate a thermal delay circuit giving a delay of approximately one minute. This delay re-sets before the application of power but is arranged to hold for several seconds to avoid unnecessary recycling with temporary mains drop-outs. Although additional switching is provided for test purposes, the channel is normally operated by the mains switch only. During the delay period (or when the power switch is open) the low voltage supplies (other than -28 V general purpose) are disabled electronically, but the high voltage supplies are disconnected by means of a relay. Operation of the power switch removes the d.c. supplies without the necessity for recycling the thermal delay. If the camera mains switch is opened, the 6.3 V d.c. supply is removed and the thermal delay circuit opens. In this condition the -28 V general purpose supply remains available to the camera to allow the use of talkback. Not shown on the diagram is a utility mains circuit between a connector on the rear of the c.c.u. and a socket on the side of the camera.

All supplies are self-protecting and self-resetting against overload or short circuit. Comprehensive metering allows rapid fault location.

13.1. Low Voltage Supplies

All the low voltage supplies are generated in identical low voltage stabilizer modules, the appropriate reconnections being made in the back-wiring of the socket. The use of a single module in this way greatly simplifies manufacture and servicing. The load functions carried out by this module are listed in Table 1. Except for the -28 V supply, the voltage is in each case stabilized by remote sensing.

Figure 24 is a block diagram of the module. The heavy lines show the path of the load current from the transformer winding, via the rectifier and smoothing capacitor, to the collector of the series regulator transistor. From the emitter of this transistor the current passes through a current sensing resistance and is supplied to the load via the p.s.u.-c.c.u. interconnecting cable and the camera cable. The current is returned from the load through the cables and finds its way back to the transformer winding via the smoothing capacitor and rectifier.

The impedance of the total cable between p.s.u. and camera can be as high as 18 Ω for 30 m (100 ft) of p.s.u.-c.c.u. cable and 600 m (2000 ft) of camera cable. Thus, in the case of supplying 1 A at 18 V to the camera, another 18 V must be supplied to the cable. The module must be capable of absorbing this extra power when short cables are used. The voltage drop problem has been alleviated to some

Table 1. D.c. supplies required by the channel.

Supply	Approximate load	Module	Function
+40 V	1½ A	low voltage stabilizer	camera circuits
+18 V	1 A	low voltage stabilizer	camera circuits
-18 V	1½ A	low voltage stabilizer	camera circuits
+18 V	2 A	low voltage stabilizer	c.c.u. circuits and aperture corrector
-18 V	2 A	low voltage stabilizer	c.c.u. circuits and aperture corrector
-28 V	1½ A	low voltage stabilizer	relays and talkback
+150 V	300 mA	} high voltage positive	circuits and tube supplies circuits and tube supplies
+525 V	300 mA		
-150 V	17 mA	} high voltage negative	circuits and tube supplies focus current
100 mA	90 V		
-6.3 V	2½ A	6.3 V stabilizer	tube heaters

extent in the case of the +40 V, 1½ A supply to the camera by using paired conductors in the cable.

The reference amplifier achieves the high loop gain necessary to compensate for the cable resistance by means of a long-tailed pair with an external high voltage supply (+150 V) to the collector load resistor. Analysis shows that transistors with high h_{ob} and h_{re} , and low h_{fe} give gains approaching a theoretical limit of $19 \times V_{LOAD}$. However, transistors with low h_{fe} require large base currents, and therefore in order to maintain good temperature stability, low impedance base circuits would have to be used. This would create problems caused by high currents in the sensing leads, and a design compromise is used giving a reduced gain which is still more than adequate for the purpose. The temperature stability for the c.c.u. supplies of 0.1% for 20 degC change is achieved by using low temperature coefficient resistors and a high quality reference diode in the feedback path. The transistors forming the long-tailed pair are mounted in a common heat-sink.

Frequency compensating elements are incorporated in the amplifier in order to maintain a low output impedance over the video frequency range, and prevent supply oscillation, despite indeterminate

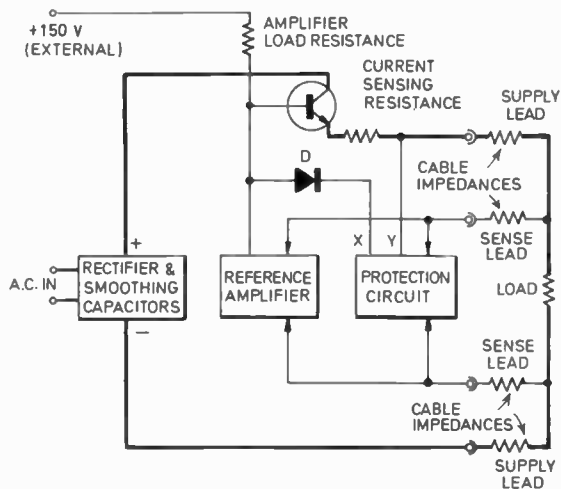


Fig. 24. Low voltage stabilizer.

time-constants in the feedback path. These components were selected after practical tests on modules driving various lengths and types of cable. The tests were carried out by observing the transient response of the stabilizer with a pulsed current load.

The output transistor and heat-sink were designed to be large enough for the range of powers involved in normal operation. In order to deal with overloads without increasing the size or cost of these components, a reducing-current method of protection was adopted. Referring to Fig. 24, point Y follows the output voltage of the supply. The protection circuit sets up a voltage between X and Y which is a function of the voltage across the load. The diode D is cut off in normal operation, but as more current

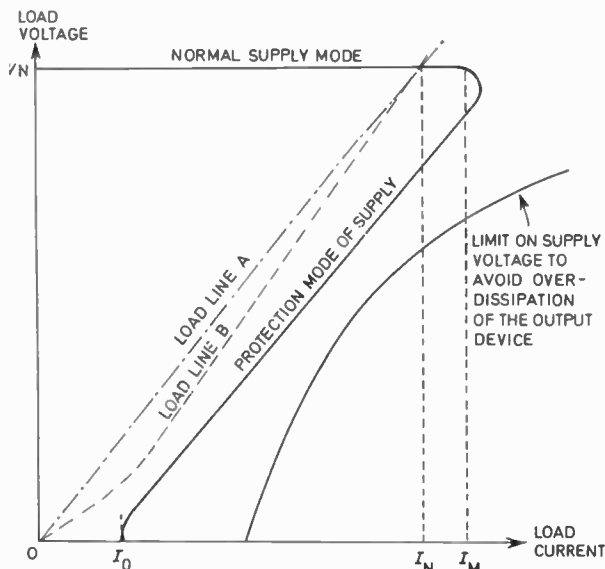


Fig. 25. Overload protection characteristic.

is demanded by the load, the voltage at the base of the emitter follower rises until it is higher in potential than X. This causes the diode to conduct, and current from the amplifier load is diverted into the protection circuit. The reference amplifier is then unable to control the load voltage. Any further reduction in load resistance causes the load voltage to drop. The protection circuit senses this and responds by reducing the voltage between X and Y, thus causing the current to reduce. In the event of a short circuit the current is reduced to a minimum. Figure 25 shows the constraints on the trip current I_m and the short circuit current I_0 . The supply locus must avoid the area of over-dissipation of the output device and when in the protection mode must avoid intersection with load lines of the type shown as B. Intersection with such a load line causes bistable or tristable working even for permissible loads.

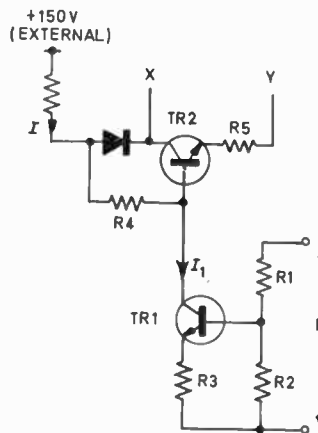


Fig. 26. Protection circuit.

Figure 26 gives details of the protection circuit. The transistor TR1 generates a collector current, I_1 , proportional to the load voltage. This current causes a proportionate voltage to be developed across R4 and defines the voltage at X relative to the base of TR2, and thus also X relative to point Y. The voltage at XY therefore varies linearly with the load voltage. For a short-circuited load, TR1 cuts off, TR2 bottoms and $V_{xy} \approx IR_5$.

13.2. High Voltage Supplies

The +150 V and -150 V supplies are nearly identical to each other and employ a modified version of the low voltage supply circuit. The -150 V supply shares a printed circuit board and heat-sink with the focus current supply whilst the +150 V supply is similarly paired with the +525 V supply.

A shunt regulator is used for the +525 V supply as shown in Fig. 27. The voltage to be handled by the

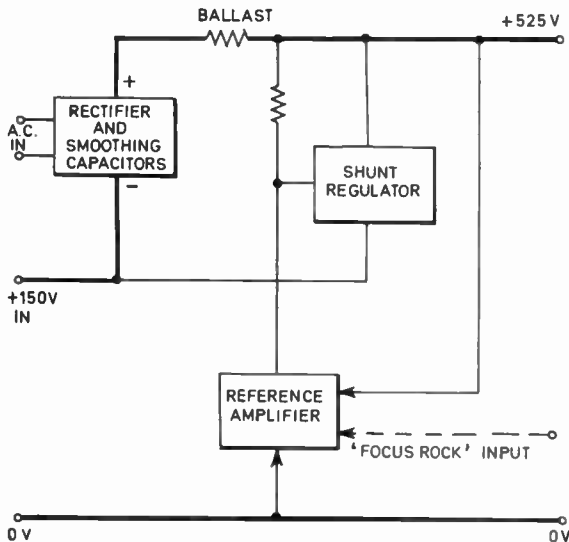


Fig. 27. +525 V supply.

rectifier, smoothing capacitor and regulator is reduced by utilization of the +150 V supply. The supply is stabilized independently of the +150 V supply. This allows simple d.c. connection of 12.5 Hz pulses into the reference amplifier feedback path in order to provide 'focus rock' modulation of the output voltage for alignment purposes.

Figure 28 shows the circuit used for the shunt regulator. The Zener diode shares the voltage between the two transistors TR2 and TR3. This method allows the use of readily available transistors without risk of second breakdown, and also provides more gain than a simple Darlington pair.

13.3. Focus Current Supply

A current of approximately 100 mA at a stability of 0.05% for 20 degC temperature change is required for the focus coils. The output impedance must be high enough to stabilize the current against changes in the resistance of the focus coils while they are warming up. The circuit developed is fully pro-

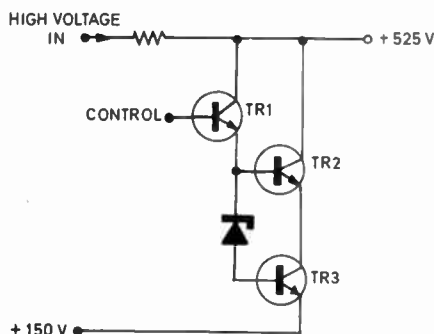


Fig. 28. Shunt regulator.

tected against short-circuit or open circuit and more than satisfies the stability requirements.

Figure 29 is a schematic diagram of the focus current supply. The current generator supplies rather more current than is required by the focus coils, the excess current being passed by emitter followers represented by TR1. TR1 allows the focus current stabilizing transistor TR2 and the reference amplifier to sit at the voltage of the focus coils. The power in excess of that required by the focus coils is thus handled by TR1 and the current generator, leaving only a small and constant power to be dissipated in TR2. This configuration gives a very rugged supply capable of keeping the focus current within specification even if, for instance, three of the four coils were to be short circuited.

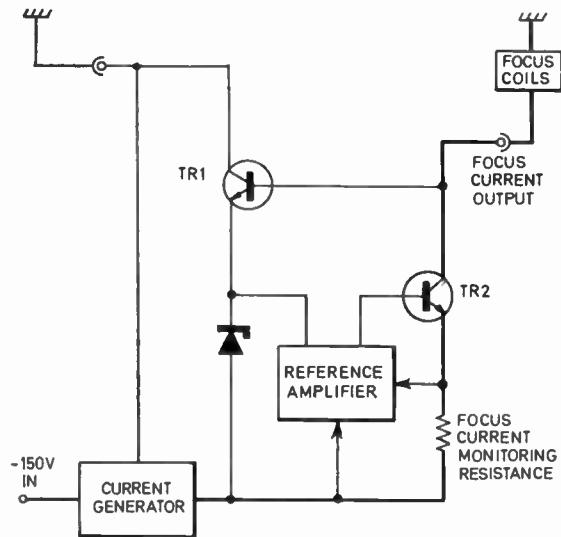


Fig. 29. Focus current supply.

The focus current, tube heaters voltage, camera mains voltage and the voltage and current of each of the d.c. supplies can be measured on the p.s.u. meter. The components associated with the meter are on a printed circuit board in the p.s.u. This board is wired into the main p.s.u. loom but can easily be withdrawn for servicing without unsoldering.

The main use of the meter is as an initial fault-finding tool. The supplies can be quickly checked for fault conditions such as open circuit or short circuit; for example, if there is a short circuit, the defective board can be located by removing boards in turn until the meter shows that the short circuit has been removed.

14. Acknowledgments

A large number of people made contributions to the development of this camera channel and the

authors thank all concerned. In particular they would mention Mr. N. F. Cottrill who did much of the detailing of the scanning circuits, Mr. A. E. H. Pullinger who dealt with pulse processing and Mr. B. W. Curtis who detailed the monitoring and talk-back facilities. Thanks are also due to the Directors of the E.M.I. Research Laboratories and E.M.I. Electronics Limited for permission to publish this paper.

15. Conclusions

The E.M.I. Colour Camera Type 2001 is a four-tube colour camera based on the use of an integral zoom lens and direct-imaging optics, and its advanced optical and mechanical design features of the camera

have been described. The camera was designed to accept four 30 mm Plumbicon tubes and the high quality of pictures obtained is in large measure due to the remarkable characteristics of this tube. In carrying through the design, no effort was spared in the attempt to obtain the best performance possible. Modifications which have been introduced have been mainly for the inclusion of additional facilities. The camera has been in quantity production since the middle of 1967 and has been well received.

Manuscript first received by the Institution on 22nd October 1969 and in final form on 20th February 1970. (Paper No. 1320/Com. 29.)

© The Institution of Electronic and Radio Engineers, 1970

The Authors



I. J. P. James (F. 1961) graduated from the University of Bristol in 1933 and in 1936 joined the Patent Department of Electric and Musical Industries Ltd., Hayes. During the war years he worked on military projects in the Company's Research Laboratories, and since July 1945 he has been concerned almost exclusively with television. Recently, following company reorganiza-

tion, he became Director—Technical of the Television Equipment Division of E.M.I. Electronics Ltd.

He serves on the I.E.E. Electronics Divisional Board and on the I.E.R.E. Communications Group Committee.



D. G. Perkins joined the Research Laboratories of E.M.I. Ltd. in 1936 as an assistant in a laboratory investigating television problems. After the war years, he returned to television and joined a group engaged on high-definition television systems. He is now Manager of a development group in the Television Equipment Division of E.M.I. Electronics Ltd.



E. W. Taylor was educated at Queens' College, Cambridge. Following national service in the Royal Air Force as a radar instructor, he joined the Research Laboratories of E.M.I. Ltd. in 1949. He was senior circuit designer on the E.M.I. colour camera and is now in charge of a circuit development section.



P. J. Pyke has been associated with a variety of high-quality mechanical, optical and electronic design projects primarily concerned with developments in television since joining the E.M.I. Research Laboratories. These have included precise elements of electronic camera tubes, and the development of vacuum deposition techniques for the production of beam splitters for colour television.



D. E. Kent joined the Research Laboratories of E.M.I. Ltd. as trainee in 1948. After a period teaching circuit theory in the R.A.F., he returned to the Colour Television Research Department in 1956. He is now Deputy Manager of a development group of the Television Equipment Division of E.M.I. Electronics Ltd.



I. A. Fairbairn graduated from Manchester University in 1960 with honours in physics. Since then he has worked on television circuit design in the Research Laboratories of E.M.I. Ltd.

Realization of a Quadratic with a Positive Real Zero

By

Y. BEDRI, B.Sc.†

and

T. DELIYANNIS, B.Sc., Ph.D.†

The network described uses one operational amplifier and has very low sensitivity to variations in RC component values.

In realizing certain low-pass non-minimum-phase-delay functions¹ as the cascade connexion of second-order stages, one is involved with the realization of a quadratic with a positive real zero, i.e. with the function

$$F(s) = \frac{k(\alpha - s)}{s^2 + \beta s + \gamma} \quad \dots\dots(1)$$

In Ref. 1 this function was realized by a RC active network of low sensitivity using two operational amplifiers.

It is also possible to realize $F(s)$ by active networks using only one operational amplifier. For example, one may connect the operational amplifier as a i.n.i.c. and use it in the Yanagisawa network² to realize $F(s)$. However, to the authors' knowledge, all up-to-date available active networks with one operational amplifier, suitable for realizing $F(s)$, have the denominator of their transfer function split into the difference of two large quantities and therefore can be highly sensitive to variations in their component values. The purpose of this note is to present a RC active network, which can realize $F(s)$ using one operational amplifier and has very low sensitivity to variations in the values of its components.

The network is shown in Fig. 1. Its transfer voltage ratio is

$$\frac{V_o}{V_i} = \frac{\frac{g_1}{C_2} \left(\frac{g_a \cdot g_2}{g_b \cdot C_1} - s \right)}{s^2 + g_2 \frac{C_1 + C_2}{C_1 C_2} s + \frac{g_2}{C_1 C_2} \left[\left(1 + \frac{g_a}{g_b} \right) g_1 + g_a \right]} \quad \dots\dots(2)$$

The values of the components of the network realizing $F(s)$ (equation (1)) can be found by equating coefficients of equal powers of s in equations (1) and (2). Since the number of the unknowns is larger than the number of the resulting equations, the values of any two components can be selected arbitrarily.

It can be shown that the constant k cannot assume any high value. If, for example, the values of C_1 and C_2 be selected arbitrarily, for the solution of the

simultaneous equations to give positive component values k will have to be

$$k < \frac{\gamma}{\alpha + \beta \frac{C_2}{C_1 + C_2}} \quad \dots\dots(3)$$

It can also be shown that the Q -factor sensitivities, where

$$Q = \frac{\sqrt{\gamma}}{\beta},$$

are as follows:

$$\begin{aligned} S_{g_1}^Q, S_{g_a}^Q, (-S_{g_b}^Q) &< \frac{1}{2} \\ S_{g_2}^Q &= -\frac{1}{2} \\ S_{C_1}^Q = S_{C_2}^Q &= 0 \quad \text{if } C_1 = C_2 \\ S_A^Q &\rightarrow 0 \quad \text{as } A \rightarrow \infty \end{aligned}$$

where A is the open-loop gain of the operational amplifier.

It can be seen that the Q -factor sensitivities are extremely low and independent of the Q -factor. Also the Q -factor is insensitive to variations in the values of the two capacitances, if $C_1 = C_2$. Therefore this condition can be the starting-point in the design of the stage.

This circuit is used to realize the low-pass quadratic term in the delay function $C-R_{3,4}$,¹ where

$$\begin{aligned} C-R_{3,4} &= \frac{0.2814(5.902-s)}{(s^2 + 4.117s + 6.9963)} \times \\ &\times \frac{(s^2 - 10.2464s + 111.4253)}{(s^2 + 3.4528s + 26.4506)} \quad \dots\dots(4) \end{aligned}$$

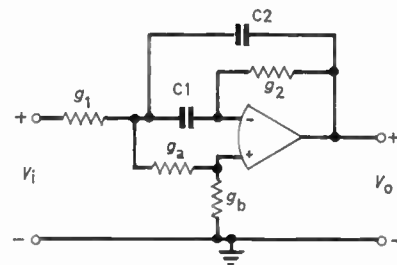


Fig. 1. Proposed network for the realization of $F(s)$, equation (1).

† West Ham College of Technology, Department of Electrical Engineering, London, E.15.

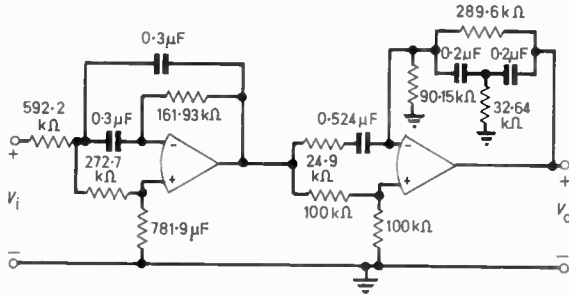


Fig. 2. Network realizing $C-R_{3,4}$ (0.1 s delay).

The biquadratic is realized first using network 1 in Ref. 3. This is achieved to within a constant multiplier of 0.5. Thus for the $C-R_{3,4}$ to be realized to within unity constant multiplier the network in Fig. 1 should realize the function

$$F(s) = \frac{0.5628(5.902 - s)}{s^2 + 4.117s + 6.9963} \dots\dots(5)$$

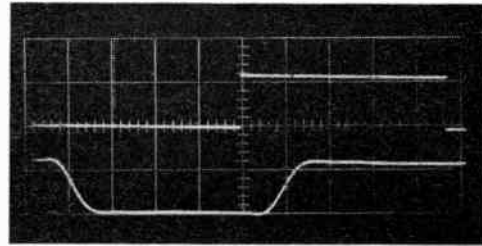
Selecting

$$C_1 = C_2 = 1F,$$

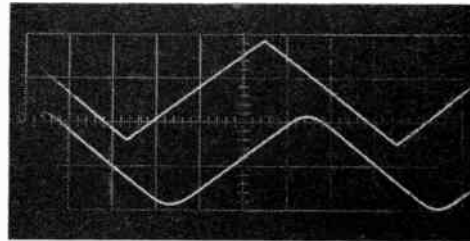
we have inequality (3) satisfied. Therefore, $C-R_{3,4}$ can be realized to within unity constant multiplier. The values of the other components will be found from the four simultaneous equations, which result from coefficient matching in equations (2) and (5).

The overall network realizing $C-R_{3,4}$ is shown in Fig. 2. This has been denormalized to an impedance level of $\frac{1}{3} \times 10^6 \Omega$ and 0.1 second delay.

The network was built using Burr-Brown 3057/01 operational amplifiers, polystyrene capacitors and resistors of various types selected to within 1% of their nominal values. The frequency response (magnitude and phase) of the network was found to be very close to the theoretical one. Figures 3(a) and (b) show the network responses to step and triangular wave inputs respectively.



(a)



(b)

Fig. 3. Network responses: (a) to a step input, (b) to a triangular wave input. Time base 0.1 s/cm. In both photographs the upper trace is the input waveform and the lower trace is the output.

References

1. Deliyannis, T., 'Six new delay functions and their realization using active RC networks', *The Radio and Electronic Engineer*, 39, No. 3, pp. 139-44, March 1970.
2. Yanagisawa, T., 'RC active networks using current inversion type negative-impedance converters', *I.R.E. Trans. on Circuit Theory*, CT-4, No. 3, pp. 140-4, 1957.
3. Deliyannis, T., 'RC active allpass sections', *Electronics Letters*, 1969, 5, No. 3, pp. 59-60, 6th February 1969.

Manuscript received by the Institution on 5th January 1970. (Short contribution No.132/CC74).

© The Institution of Electronic and Radio Engineers, 1970

Sixth-order Non-Minimum-Phase Delay Functions with Adjustable Magnitude

By

T. DELIYANNIS,

B.Sc., Ph.D.†

Two sixth-order all-pole delay functions, the Bessel and a Chebyshev, are modified according to Budak's technique to acquire five right-half s -plane zeros. The magnitude of the resulting functions is then adjusted to have the same half-power frequency as the corresponding Padé delay function, and the three functions are compared to each other in terms of various quantities associated with their frequency and step response. These quantities are next studied for various bandwidths in the case of the modified Chebyshev delay function.

It has been shown‡ that useful non-minimum phase delay functions with three zeros and four poles can be obtained from the all-pole Chebyshev delays of orders 3 and 4 using Budak's technique. These modified delays were found to be superior to existing similar functions of the same order. It was also shown that if Bessel all-pole delay functions were used instead of Chebyshev, the resulting delays showed some improvement over the existing ones only in the cases of the overshoot and precursors in the step response.

The purpose of this communication is to give the results of a study of a similar modification of the sixth-order Chebyshev (ripple constant 0.01) and Bessel all-pole delay functions. Using again Budak's technique, new delay functions with five right-half s -plane zeros and six left-half s -plane poles are obtained. The resulting functions are adjusted to have the same half-power frequency, ω_{3dB} , as the well-known Padé delay function of the same order, thus

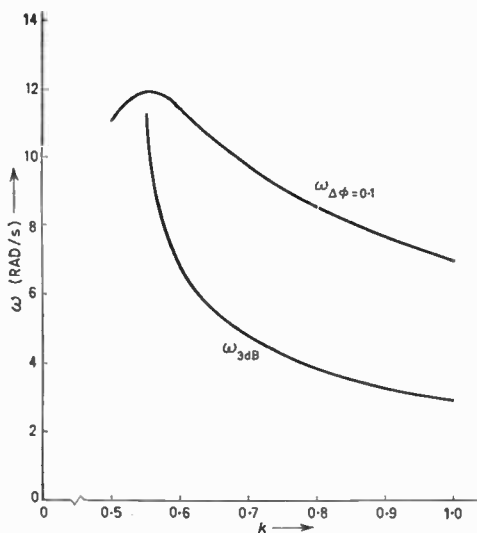


Fig. 1. Variation of ω_{3dB} and $\omega_{\Delta\phi=0.1}$ with k .

† West Ham College of Technology, Department of Electrical Engineering, London, E.15.

obtaining the functions $C-P_{5,6}$ and $B-P_{5,6}$, depending on whether the function is of Chebyshev or Bessel origin respectively.

Table 1 gives the poles and zeros of the functions $P_{5,6}$, $B-P_{5,6}$, $C-P_{5,6}$, and the corresponding values of the parameter k , through which the pole-zero locations are adjusted.‡

Table 1. Poles and zeros of $P_{5,6}$, $B-P_{5,6}$, $C-P_{5,6}$

Function	k	Zeros	Poles
$P_{5,6}$	0	$8.2985 \pm j0$	$-7.4906 \pm j1.6215$
		$7.7061 \pm j3.7401$	$-6.4705 \pm j4.9001$
		$5.6447 \pm j7.6935$	$-4.0388 \pm j8.3456$
$B-P_{5,6}$	0.5457	$8.0272 \pm j0$	$-7.7853 \pm j1.5895$
		$7.3783 \pm j3.8359$	$-6.8456 \pm j4.8127$
		$5.1171 \pm j7.8605$	$-4.6105 \pm j8.2329$
$C-P_{5,6}$	0.5508	$4.7382 \pm j0$	$-3.9851 \pm j2.2995$
		$4.5366 \pm j5.5583$	$-2.9425 \pm j10.9570$
		$3.5680 \pm j10.4000$	$-3.7642 \pm j6.7966$

In Table 2 some important quantities associated with the frequency and step response of these delay functions are given. Corresponding values for the parental functions $C_{0,6}$ and $B_{0,6}$ are also included. In the Table $\omega_{\Delta\phi=0.1}$ is the frequency at which the phase error $\omega - \phi(\omega)$ is 0.1 rad (1 second delays are considered). T_D/T_r is the ratio of the delay time to the rise-time and A_r the maximum value of the precursors in the step response.

‡ Deliyannis, T., 'Six new delay functions and their realization using active RC networks', *The Radio and Electronic Engineer*, 39, No. 3, pp. 139-44, March 1970.

Table 2. Some parameters associated with the frequency and step response for various delay functions

Function	ω_{3dB} (rad/s)	k	$\omega_{\Delta\phi=0.1}$ (rad/s)	T_D/T_r	A_r %	Overshoot %
$P_{5,6}$	11.2046	0	8.644	3.64	15.5	4.05
$B-P_{5,6}$	11.2046	0.5457	8.393	3.38	14.4	2.4
$C-P_{5,6}$	11.2046	0.5508	11.900	3.934	8	3.6
$B_{0,6}$	2.698	1	5.041	1.23	0	0.64
$Ch_{0,6}$	2.942	1	6.925	1.344	0	0.65

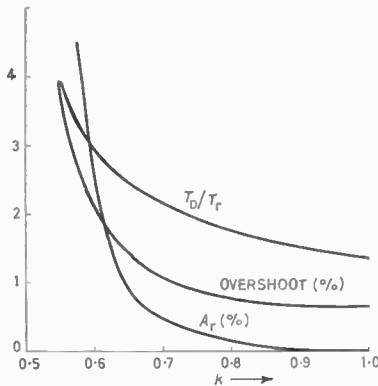


Fig. 2. Variation of overshoot, T_D/T_r and A_r with k .

It can be seen that, as in the case of 3, 4 order functions, $C-P_{5,6}$ shows superiority over $P_{5,6}$ and $B-P_{5,6}$ except for the overshoot, which is smaller in the case of $B-P_{5,6}$.

The quantities in Table 2 are plotted against k in Figs. 1 and 2 in the case of $C-P_{5,6}$, with k varying

between 0.5508, giving $C-P_{5,6}$, and 1, giving $C_{0,6}$. It can be seen that small overshoots and precursors go together with small T_D/T_r ratios and narrow bandwidths. For values of k below 0.5508 overshoot and precursors increase rapidly, and, although ω_{3dB} increases, the magnitude response curve becomes peaky and this degrades the phase response (Fig. 1).

Figures 1 and 2 can be used to determine the value of k and, therefore, the required delay function for certain design specifications. However, a word of caution is appropriate here: as k varies from 1 to 0.5506 the poles (zeros) move along radial lines away from (towards) the origin, starting from the poles (zeros) of $C_{0,6}$, ($C_{0,5}$). This is so because for each k , where $0 < k \leq 1$, the poles (zeros) of $C_{5,6}$ are the poles (zeros) of $C_{0,6}$ ($C_{0,5}$) divided by k (by $k-1$). Thus when realizing a $C_{5,6}$ function with k near unity, inconvenient component values may be required, since then the zeros will lie very far away from the origin as compared with the pole positions.

Manuscript first received by the Institution on 22nd December 1969 and in final form on 2nd February 1970. (Short contribution No. 133/CC 75).

© The Institution of Electronic and Radio Engineers, 1970

Gallium Arsenide-Phosphide Visible Lamps and Arrays

By

J. R. PETERS,

B.Sc.†

and

C. E. E. STEWART,

B.Sc.†

Reprinted from the Proceedings of the I.E.R.E. Conference on 'Lasers and Opto-Electronics' held at the University of Southampton on 25th to 28th March 1969.

This paper describes the fabrication and properties of forward biased GaAsP electroluminescent lamps and arrays. GaAsP, suitably doped with selenium, is grown as an epitaxial layer on GaAs substrates using the arsine-phosphine system. Planar techniques are then employed to fabricate the p-n junction by the diffusion of zinc into the epitaxial layer through a silicon dioxide mask. When forward biased these devices emit light at a wavelength lying in the range 660–690 nm, depending on the alloy composition. With an operating voltage of 1.7 V and a current density of 25 A/cm² (30 mA for 0.38 mm diameter devices), lifetimes up to 7000 hours have been measured with little deterioration in light output. By connecting the lamps on the epitaxial slice with a system of evaporated leads, 5×7 arrays have been made giving an alpha-numeric symbol within a rectangle measuring 6.1×8.6 mm.

1. Introduction

Semiconductor visible light sources have been known for some time, but due to their low brightness, difficulty of manufacture and high cost they have had very limited application. However, there is a growing requirement for very reliable light sources—indicator lamps and display systems—which operate at voltages compatible with transistor equipment, have long life, and which have low power requirements.

Of such sources which are at present available, those made from gallium phosphide¹ and from gallium arsenide-phosphide² are, at the moment, the most promising.

Gallium phosphide is an indirect band-gap material, and emits red light fairly efficiently via a combination of Zn and O levels, after doping with these elements, or green light much less efficiently when doped to produce near band-to-band recombination. Gallium phosphide is produced by Czochralski pulling, vapour or liquid epitaxy, and the p-n junction mainly by liquid epitaxial growth.

Gallium arsenide-phosphide, below about 40 mol% gallium phosphide, is predominantly a direct band-gap material. It emits red light fairly efficiently by band-to-band recombination from forward biased p-n junctions formed by shallow donors and acceptors. The solid solution is grown by vapour epitaxy, and the junction formed by diffusion.

In these laboratories, the arsenide-phosphide route was chosen for four main reasons:

- (i) The material is direct band-gap, with the possibility of fairly high electroluminescent

† Standard Telecommunication Laboratories Ltd., Harlow, Essex.

efficiency when adequate control has been established over the material growth.

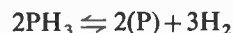
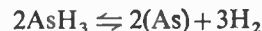
- (ii) The laboratory is well advanced in the growth of gallium arsenide by vapour epitaxy, and the growth of gallium arsenide-phosphide was seen as an extension of these techniques.
- (iii) Diffusion rather than epitaxy is involved in the junction making process. This opens the way to the use of planar methods, with the resulting possibilities of high yield, ease of contacting, and the progression to arrays of devices on a single slice, with evaporated and photolithographically defined contact patterns.
- (iv) The proposed processes are fairly easy to transfer to production.

2. Lamp Fabrication

2.1. Preparation of Material

Gallium arsenide-phosphide is grown as an epitaxial layer, approximately 100 μm thick, on suitably prepared {100} oriented n⁺ gallium arsenide substrates, by a method first described by Tietjen and others.³ In this system, 1% mixtures of arsine and phosphine in hydrogen are used as the sources of the Group V elements and are thermally decomposed at 850°C in the reaction tube. The gallium metal, which is contained in a silica boat maintained at 800°C in the reaction tube, is transported by reacting it with hydrogen chloride gas.

The reactions



occur at the high temperature end of the tube, and the reaction



occurs at the lower temperature end of the tube, where the substrates are situated. The free gallium, arsenic and phosphorus combine, resulting in epitaxial growth of gallium arsenide-phosphide on the gallium arsenide substrates. Hydrogen selenide in hydrogen is taken into the substrate zone to provide a suitable level of n-type selenium doping in the layer.

This system has two main advantages over other epitaxial systems which have been described for the alloy growth.^{4,5} These are:

- (i) The free arsenic and phosphorus do not come into contact with the gallium source, thereby avoiding the need to saturate the gallium with these elements before epitaxial growth can occur. As a result, the composition of the growing layer can be changed easily by changing the arsine and phosphine flow-rates.
- (ii) By using separate methods for the gallium and the arsenic-phosphorus transportation, independent control of the Group III/Group V ratio in the gas can be achieved.

When even fairly similar materials are grown epitaxially, one upon the other, crystal imperfections occur due to lattice parameter and thermal expansion mismatch between the layer and the substrate. By using the ability to vary the crystal composition easily, a less abrupt interface between the substrate and the layer can be achieved—initially growing gallium arsenide and then gradually increasing the phosphine flow until the required composition is established. Grading rates of about 1 mol% of gallium phosphide per micrometre have been used in this work.

We have found that variations of the Group III/Group V ratio affect the light-emitting properties of the epitaxial layer, and that for a given doping level in the crystal there is a minimum value for the ratio below which good luminescent material cannot be grown. The value of this minimum ratio increases rapidly with the crystal doping level. It is probable that the effect is due to variation in the stoichiometry of material grown under different vapour-phase compositions.

For these reasons, the hydride method of growth has been used almost entirely in our work. The majority of layers have been grown containing 37–40 mol% of gallium phosphide, a proportion just below that at which electroluminescent efficiency falls as a result of the effect of the indirect bandgap on the recombination mechanism.

2.2 Diffusion and Contacting

The diffusion to make the lamp is directed towards

a mesa or a planar structure. The planar structure has so many advantages that all devices except those made simply to evaluate the material are now made by this method.

The slice with the epitaxial layer is cleaned and provided with a silica masking layer 0.2–0.5 μm thick, usually by the oxidation of silane, which is a rapid and simple method, or by reactive sputtering. Windows are opened in the oxide by photolithographic means.

The p–n junction is made by the diffusion of zinc from zinc vapour, in a sealed, evacuated silica tube. Precautions are taken, by vacuum baking, to ensure the absence of water vapour in the tube, since this can act as a transport agent during the diffusion, resulting in pitting of the slice surface. The tube is sealed at a pressure of about 10⁻⁶ torr, enclosing the prepared slices and small weighed amounts of zinc and arsenic. The latter is necessary to prevent the decomposition of the slice surface and to control the zinc diffusion rate. The diffusion is carried out at 800°C for 5 minutes, resulting in a junction 1.2–1.5 μm deep.

The reverse side of the slice is lapped flat and provided with an overall ohmic contact by evaporation of a tin-gold alloy, while the slice is held at 600°C to produce alloying. A layer of titanium-gold or of aluminium is evaporated over the front of the slice, and the layer is then etched using photolithographic masks to produce peripheral contacts surrounding the devices, and any other required connection patterns. To make individual lamps, the slice is scribed and diced, and the dice are mounted by alloying into one of two types of encapsulation. Connection to the top contact is made by the ultrasonic bonding of aluminium wire 0.05 mm in diameter, and the encapsulation is completed with a hemispherical resin lens, which seals and protects the assembly. The resin lens also magnifies the emitting area, and increases the light output about threefold.

Planar arrays are mounted by alloying to a rectangular base, provided with the required number of lead-through wires.

3. Device Characteristics

The light output from the lamps is a fairly narrow wavelength band, with a half-peak width of about 16 nm, lying in the range 660–690 nm for phosphide contents of 40–37% (Fig. 1). At 665 nm the lamps give 47 lumens per emitted watt. There is much to be gained in brightness by increasing the phosphorus content and thereby decreasing the emitted wavelength, but there is a point at which the indirect band-gap dominates, and the efficiency drops dramatically. This point has not yet been established in the present system. It is variously reported at 40–45% gallium phosphide.^{2,6}

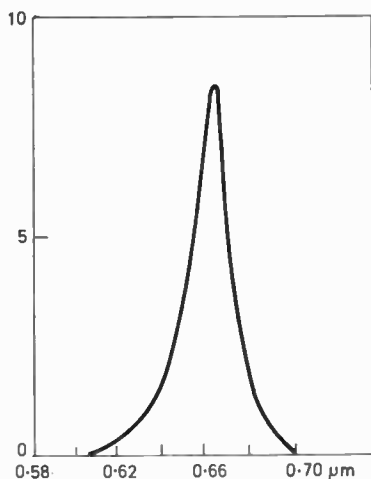


Fig. 1. Spectral distribution.

An external quantum efficiency of 0.15% has been achieved and a brightness of 900 footlamberts at 45 A/cm². The devices form useful indicator lamps at direct currents of 30–50 mA. A 1 mm diameter planar device with peripheral contact shows an increasing efficiency up to 100 mA (Fig. 2). Pulsed, the efficiency maximum is at 400–700 mA (Fig. 3) and a pulse brightness of 1400 footlamberts has been measured.

The electrical characteristics are very uniform from lamp to lamp. The dynamic resistance is 1.5–2.0 Ω. The operating voltage is 1.65–1.70 V at 30–100 mA. The lamps and arrays are thus compatible with transistor and integrated circuitry. Many lamps can be run at equal brightness from a common current supply without equalizing resistors, and this simplifies the use of lamps in array systems.

Life tests have been carried out on mesa and planar lamps for up to 7000 hours (Fig. 4). The lamps were run continuously at 25 A/cm² (30 mA for 0.38 mm diameter devices). The results are characterized by an initial 10–25% fall of measured output followed by a slow change, in the case of mesa devices. The planar lamps showed an initial 13% drop and virtually no change over the last 4000 hours.

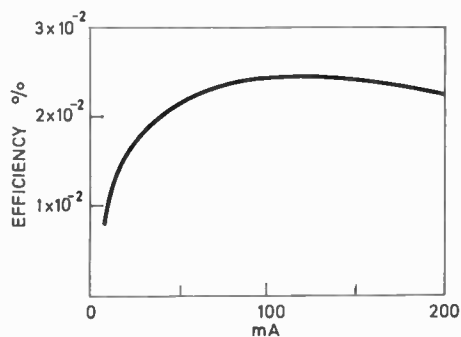


Fig. 2. Quantum efficiency vs. current (d.c.).

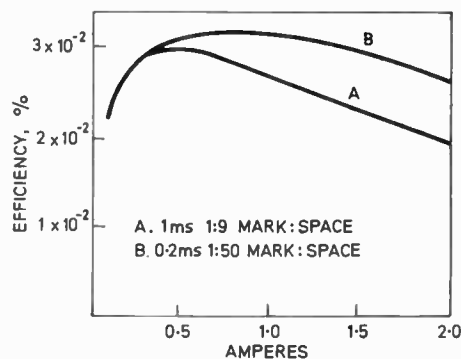


Fig. 3. Quantum efficiency vs. current (pulsed).

Gallium arsenide-phosphide lamps are fast, having an on-off time of 10 ns. They are useful for film marking, and using HP 3 film, a mark density of 0.9 above fog has been achieved using an 18 micro-coulombs input pulse.

Lamps in the miniature encapsulation have been mounted into close-packed 5 × 7 arrays, which have been used as alphanumeric indicators. These arrays are easily readable under normal illumination.

4. Factors Affecting Light-emitting Efficiency

Apart from the basic electroluminescent efficiency of the material, three further factors are important in the functioning and the efficiency of the lamps. These are current-crowding, absorption and light loss from internal reflection.

Lamps which have a single wire contact bonded to the p-type crystal surface always have a region around the contact which is brighter than the main surface of the device. The effect is also seen, though less markedly, in devices with peripheral contacts. This is due to the IR voltage drop in the p-type layer, parallel to the slice surface, and the consequent variation in current density across the p-n junction. The diffused p-type layer has a sheet resistivity of about 17 Ω per square. A mathematical estimate showed that the variation in current density to be expected across the

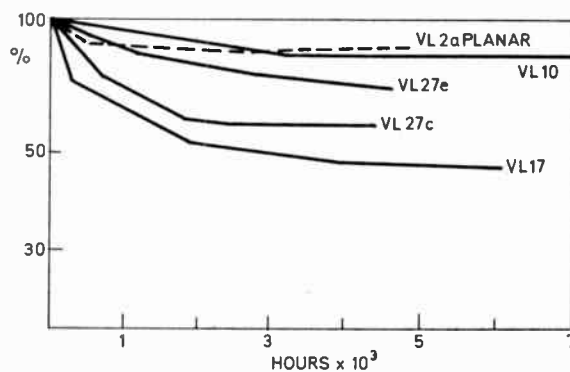


Fig. 4. Life-test. Percentage of initial output vs. time.

surface of a 1 mm diameter lamp with a peripheral contact could be 7 : 1 for a total current of 100 mA. The measured brightness variation across the diameter of such a device was in fact this ratio. The highest current density is under the contact, where the generated light is lost. It does not seem possible to decrease the sheet resistance of the diffused layer appreciably without increasing the junction depth and the absorption, but modified contact and device geometries may well result in improved current spreading and light output.

Light generated at the junction traverses the diffused p-type region before it is emitted from the device. Since the emission peak is near the band-edge wavelength, the shorter wavelength part of the band is relatively heavily absorbed, and lamps made in the same slice, with different junction depths have shown a displacement of the peak due to this preferential absorption.

The refractive index of gallium arsenide-phosphide is 3.5. Light generated inside the crystal is emitted only if it reaches the surface at an angle to the normal less than the critical angle, which is 16° . Thus less than 4% of the light reaching the surface can be transmitted. A threefold increase in the emitted light is achieved by using a resin hemisphere surrounding the device. This is the result of a slightly improved refractive index match to the crystal. A considerable improvement is possible if the hemisphere can be made of a high refractive index glass, which transmits in the visible range.

5. Planar Alphanumeric Arrays

Having established a reliable planar technology for the fabrication of lamps, it is a relatively straightforward step to connect the lamps on the slice by a system of evaporated leads to produce an array of devices suitable for an alpha-numeric readout.

Window masks for the diffusion and contact masks for the contact pattern of such an array have been made by a computer-controlled laser-machining process. This method of mask making has the advantage that from one computer program a series of masks can be made for arrays of a range of different sizes. 5×7 planar arrays have been made, with 0.66 mm square devices, giving an alpha-numeric symbol within a rectangle 6.1×8.6 mm (0.24×0.34 in). Evaporated metal leads were taken across the surface of the silica masking layer to contact pads along the two sides of the array rectangle. Ultrasonically-bonded aluminium wires complete the contact system to the array mount. (Fig. 5).

The lamps are very uniform in brightness across the slice, and the symbols can be read easily from a distance of 3–4 metres in bright room lighting. Four such arrays have been mounted together, and driven

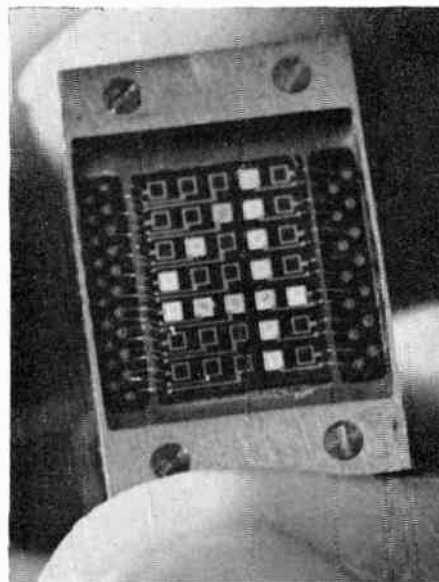


Fig. 5. Planar alpha-numeric array.

by an integrated circuit counter, decoder and d.t.l. encoder. They form a practical digital read-out system.

6. Conclusion

A planar technology has been established for making individual gallium arsenide-phosphide lamps. The lamps have uniform electrical characteristics and long life, making them useful as very reliable indicator lamps. They can be modulated at megahertz frequencies.

Planar alpha-numeric arrays have been made by fabricating 35 lamps in a 5×7 format, with associated evaporated lead pattern, on single slices of gallium arsenide-phosphide. The arrays are assembled in a rugged mount and can be driven by silicon integrated circuitry. They may well have a wide application in digital instruments of all kinds, calculators and computer peripherals.

7. References

1. Thomas, D. G., 'Gallium phosphide electroluminescence', *Brit. J. Appl. Phys.*, (*J. Phys. D.*), Ser. 2, 2, p. 637, 1969.
2. Maniska, H. and Pankove, J., 'Efficiency of $\text{GaAs}_{1-x}\text{P}_x$ electroluminescent diodes', *Solid State Electronics*, 10, p. 917, 1967.
3. Tietjen, J. and Amick, J., 'Preparation and properties of vapour deposited epitaxial $\text{GaAs}_{1-x}\text{P}_x$ using arsine and phosphine', *J. Electrochem. Soc.*, 113, p. 724, 1966.
4. Finch, W. and Mehal, E., 'Preparation of $\text{GaAs}_{1-x}\text{P}_x$ by vapour phase reaction', *J. Electrochem. Soc.*, 111, p. 814, 1964.
5. San-Mei Ku, 'Preparation and properties of vapour grown GaAs-GaP alloys', *J. Electrochem. Soc.*, 110, p. 991, 1963.
6. Pilkuhn, M. and Rupprecht, M., 'Electroluminescence and lasing action in $\text{GaAs}_{1-x}\text{P}_x$ ', *J. Appl. Phys.*, 36, p. 684, 1965.

Manuscript first received by the Institution on 26th February 1969 and in final form on 27th February 1970. (Paper No. 1321/CC76).

© The Institution of Electronic and Radio Engineers, 1970

Optical Harmonic Generation in Liquid Crystals

By

LAWRENCE S. GOLDBERG,

Ph.D.†

and

JOEL M. SCHNUR,

M.S.‡

Reprinted from the Proceedings of the I.E.R.E. Conference on 'Lasers and Opto-Electronics' held at the University of Southampton on 25th to 28th March 1969.

The non-linear optical properties of several cholesteric and nematic liquid crystals are studied in laser experiments on generation of second- and third-harmonic radiation. No second harmonic is observed in any of the liquid crystal mesomorphic phases, indicating that the local molecular ordering in these phases is centrosymmetric. The generality of this result to date diminishes the potential of liquid crystals as non-linear materials. Large intensity changes of third harmonic are observed at several phase transitions, and their possible origins are discussed. Tentative results are presented on experiments to utilize the high optical rotatory power of the cholesteric phase to obtain phase matching in third-harmonic generation.

1. Introduction

A large number of organic compounds known as liquid crystals undergo a state of molecular ordering intermediate between solid and liquid.¹ In this liquid crystalline or mesomorphic state physical properties characteristic of both are exhibited, for example optical birefringence and fluidity. According to their molecular ordering and the optical and physical properties that they display, three principal types of mesomorphic phases are identified: the nematic, in which the molecules lie on the average along a common direction; the cholesteric, similar to the nematic but in which the common direction spirals through the liquid; and the smectic, in which the molecules form a layered structure. In recent years, investigations of several unique linear optical properties of the cholesteric and nematic phases have led to such diverse applications as temperature sensing and electro-optic displays.²

This paper presents an investigation of the non-linear optical properties of liquid crystals in laser experiments on generation of optical harmonic radiation. The objectives were to explore the potential of liquid crystals as non-linear materials and to gain insight into aspects of their molecular structures. Measurements of second-harmonic (s.h.g.) and third-harmonic (t.h.g.) generation of light probe the non-linear polarization P_{NL} of the medium at optical frequencies to terms second and third order in electric-field strength E_ω .³ In the electric-dipole approximation P_{NL} may be written as

$$\begin{aligned} P_{NL} &= P_{2\omega}^{(2)} + P_{3\omega}^{(3)} \\ &= \chi^{(2)} E_\omega^2 + \chi^{(3)} E_\omega^3 \end{aligned}$$

† Naval Research Laboratory, Washington, D.C. 20390, U.S.A.

‡ Formerly with Naval Research Laboratory; now at Georgetown University, Washington, D.C. 20007, U.S.A.

where $\chi^{(2)}$ and $\chi^{(3)}$ are the respective second- and third-order susceptibility tensors. For a medium that contains a centre of symmetry or that is isotropic, the term $\chi^{(2)}$, and hence s.h.g., vanishes due to symmetry considerations analogous to those for piezoelectricity. A study of s.h.g. in liquid crystals can thus provide an important element of symmetry information on local molecular ordering in the mesomorphic state. The study of t.h.g., on the other hand, allows the investigation of their non-linear properties throughout all sample phases without such restrictions imposed by symmetry. Further, in certain of these liquid crystals one might hope to obtain increased conversion efficiency through phase matching of the harmonic generation process by utilizing the exceedingly high optical rotatory power of the cholesteric phase or the high birefringence in the orientable nematic phase.

2. Experimental Arrangement

The experiments were performed in several cholesteric and nematic materials with primary emphasis on cholesteryl nonanoate (CN), a derivative of cholesterol whose liquid crystalline behaviour is well understood.⁴ The purity of CN was of chromatographic grade, although standard grade material gave equivalent results. The experimental arrangement is shown in Fig. 1.

The liquid crystal was placed in a metal cell between fused-quartz windows separated by a metal spacer, of thickness varied from 0.025 mm to 1.7 mm. The sample cell was mounted within a temperature controlled circulating-water jacket with temperature monitored by a copper-constantan thermocouple attached to the cell adjacent to a window. The temperature stability was better than 0.05 degC. Prior to measurements, the sample was heated to a liquid, and then resolidified by slow cooling.

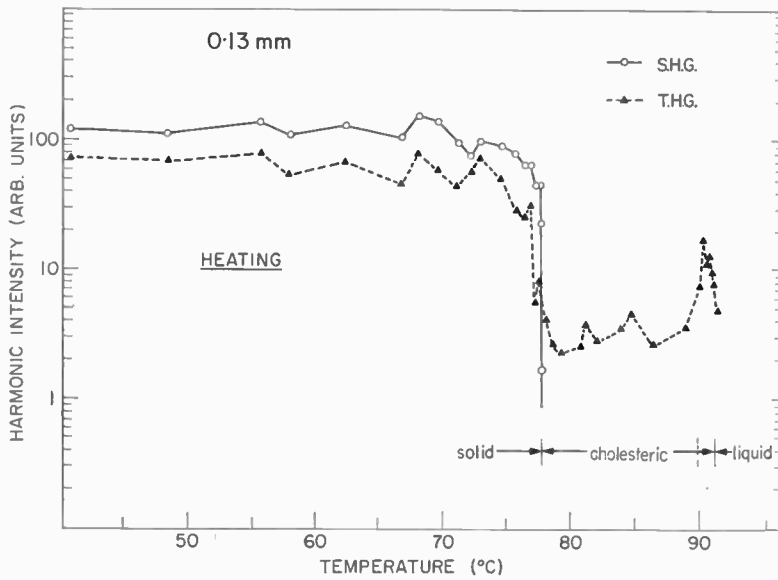


Fig. 3. Second-harmonic and third-harmonic generation in 0.13 mm-thick CN.

of CN between glass plates three distinct textures of the cholesteric phase may be observed. A homeotropic texture,⁴ cloudy with slight purple hue and no birefringence, appears briefly only on cooling from the isotropic liquid. Further cooling results in growth of characteristic focal-conic birefringent groups (Fig. 5(b)). A slight disturbance of the focal-conic texture, such as by displacement of the cover glass, produces the highly optically-active plane texture (Fig. 5(c)), comprised of uniform oriented areas with helix axis normal to the supporting glass surface.

A visual examination of thicker samples as those in Figs. 3 and 4, however, discloses an unexpected strong optical activity in the phase texture normally denoted as homeotropic (Fig. 5(d)). In the thick samples this phase texture is also observed on heating, and is turbid in appearance with no birefringent structures. Most notably, it displays strong optical activity and the Bragg-like scattering usually found only in the plane texture. The colour range of scattering extends with decreasing temperature from violet, to blue, green, and green-yellow before the growth of the focal-conic groups set in, about 2 degC below the transition from isotropic liquid. The scattering wavelength shows no apparent dependence on viewing direction, contrary to that found for the plane texture. It is likely that at this higher temperature the phase texture consists of small helical-structured scattering regions at random orientations through the bulk of the sample, with minimal long-range ordering effects from the supporting surface.

3.4.2. Third harmonic generation

The optically active plane texture was prepared in CN samples of various thicknesses. No significant changes in t.h.g. intensity were found while varying

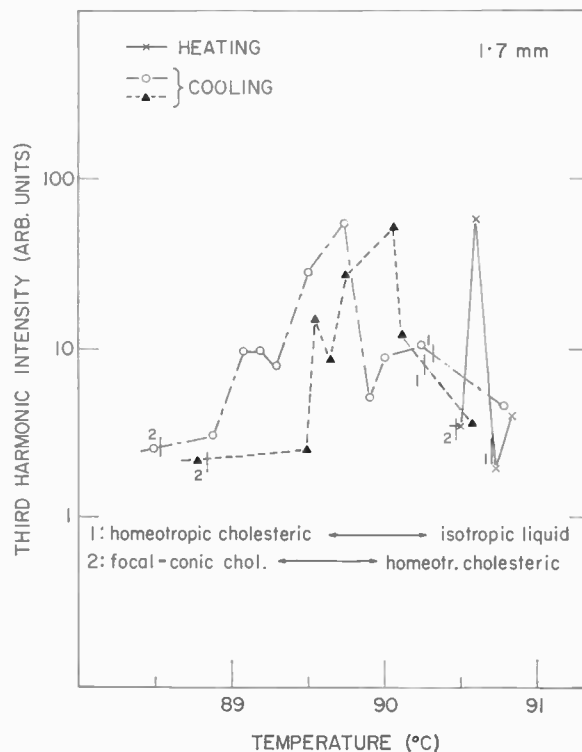
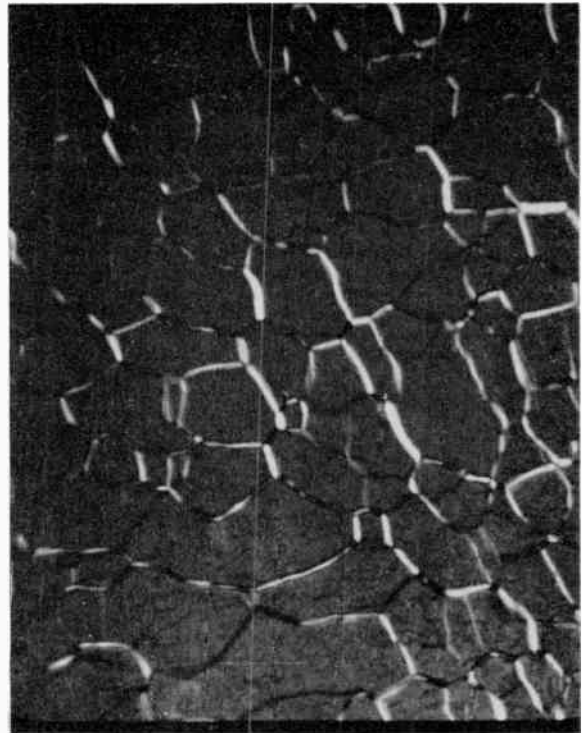


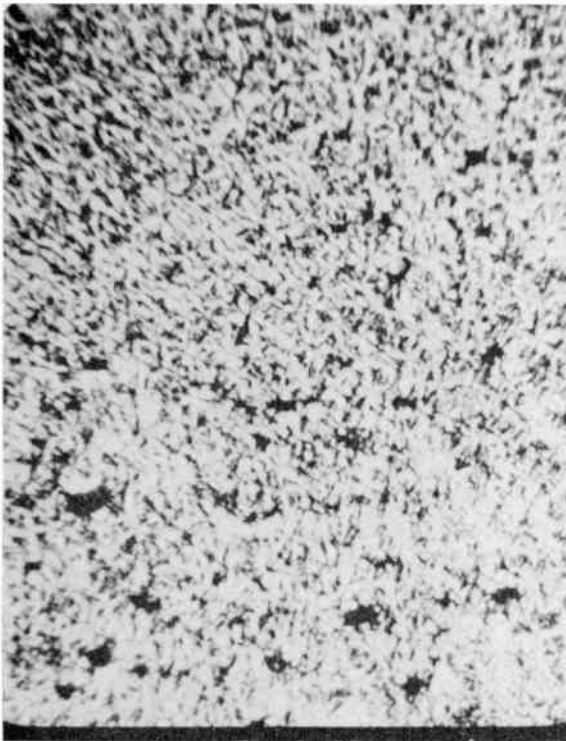
Fig. 4. Third-harmonic generation in 1.7 mm-thick CN, while heating and cooling through homeotropic region of cholesteric phase.



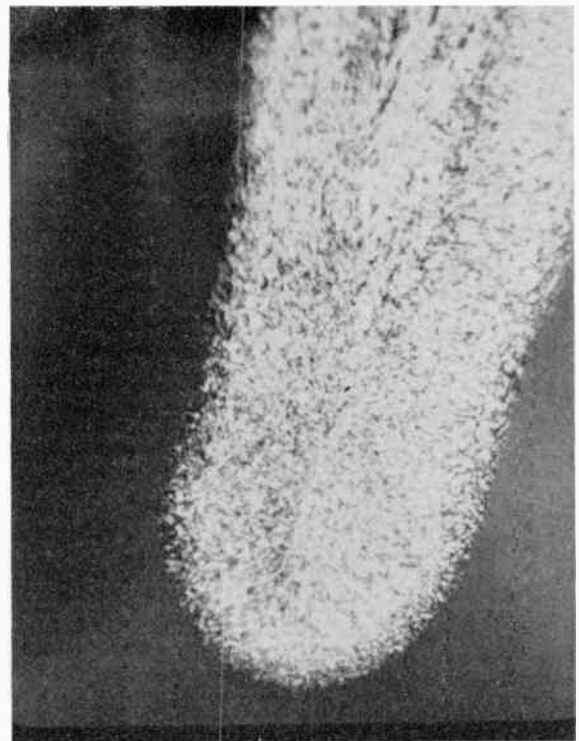
(a) smectic



(c) cholesteric: plane texture



(b) cholesteric: focal-conic texture



(d) cholesteric (1 mm thick): coloured homeotropic region with growth of focal-conics in centre.

Fig. 5. Mesomorphic phases of CN (polarizing microscope, $\times 320$ magnification).

the temperature throughout the plane-texture cholesteric phase and measuring at roughly $\frac{1}{4}$ degC intervals. However, in thick samples of CN, an apparent resonant increase in t.h.g. intensity could be observed in the high-temperature homeotropic region of the cholesteric phase, just prior to transition to the isotropic liquid. The t.h.g. data of Figs. 3 and 4 show this effect for 0.13 mm and 1.7 mm samples. An expanded temperature scale is used in Fig. 4 for several successive slow cooling and heating runs ($\frac{1}{3}$ degC/min) through this temperature region. Increases in t.h.g. intensity of over a factor of 20 were recorded in several of the discrete laser measurements. The temperature of the peak in intensity extended over less than $\frac{1}{4}$ degC and was difficult to stably reproduce. On some runs no intensity changes of note could be observed.

4. Discussion

4.1. Discussion of S.H.G.

A principal finding of this study is that no second harmonic was observed in any mesomorphic phase of the liquid crystals examined. In the first reported studies of s.h.g. in a cholesteric liquid crystal,^{9,10} there were conflicting results as to the observation of s.h.g. in the cholesteric phase. The present work and that of Durand and Lee,¹¹ who recently extended their initial study of s.h.g. to other cholesteric and nematic materials, find no evidence yet of an ordered mesomorphic state for which electric-dipole-allowed s.h.g. occurs. The absence of a second-order non-linearity is significant since it appears to preclude the use of liquid crystals for most non-linear applications. Further it indicates that the local molecular ordering in each of the mesomorphic phases is centrosymmetric. This conclusion lends support to considerations of close-packing models and to findings of X-ray structure analyses, which favour an anti-parallel orientation of the long, asymmetric molecules comprising the liquid crystals.¹²

4.2. Discussion of T.H.G.

The large changes in intensity of third harmonic that occur at several phase transitions in CN and other liquid crystals are very striking. An adequate account of this behaviour is made difficult, however, by the non-uniform nature of the liquid crystal material, in particular the polycrystalline-like textures and optical birefringence and their changes at phase transitions. This situation may be compared with the far more favourable problem of evaluating non-linear coefficients of a powdered material for which symmetry class, particle grain size, and refractive index data are known beforehand.¹³

Several possible contributing effects may nevertheless be considered. First, the symmetry of the medium

decreases in progressing from the unordered isotropic liquid through mesomorphic states of progressively higher molecular ordering to finally the crystalline solid. The changes in symmetry couple different coefficients of the non-linear-susceptibility tensor in producing t.h.g. Evidence of this effect is seen from changes in both magnitude and direction of polarization of the third-harmonic signal at several of the phase transitions. Second, the relation between coherence length of the third-harmonic radiation, involving the dispersion and birefringence of the medium, and an effective uniform 'grain' size within the polycrystalline-like phase appears significant in determining third-harmonic intensity. The relatively greater t.h.g. observed for CN in its solid phase as compared, for example, with cholesteryl myristate or palmitate appears to correspond with its much larger-scaled crystallized structure seen under a microscope. Third, some contributions to changes in the magnitude of the non-linear susceptibility may be expected from molecular interaction effects in the ordered phases.¹⁴

Finally, the results on t.h.g. in the cholesteric phase of CN give evidence, although tentative, for an increased coherence length or phase matching due to the high optical rotation in the medium. It is possible that the difficulties in clearly establishing this observation could be overcome by using a higher-repetition-rate laser to facilitate data acquisition.

5. Further Studies

There are several possible extensions of this work which could prove fruitful. (1) The generality of the s.h.g. results and the interesting t.h.g. behaviour should be checked in other liquid crystal systems of different molecular composition and mesophase behaviour. (2) In cholesteric or nematic materials application of an external electric or magnetic field may alter the molecular interactions to remove centrosymmetry and be detectable by s.h.g. or be otherwise observable with t.h.g. through changes in the third-order susceptibility. (3) Phase matching of t.h.g. may be obtainable in some nematic materials by utilizing the temperature-dependent birefringence in a nematic phase oriented by a magnetic field into relatively clear single-crystal-like regions. (4) The highly optically active cholesteric phase presents a unique system to pursue studies of phase matching in t.h.g. employing optical rotatory dispersion.

6. References

1. For general reviews on the subject, see: Gray, G. W., 'Molecular Structure and the Properties of Liquid Crystals', (Academic Press, London, 1962); Fergason, J. L., 'Liquid crystals', *Scientific American*, **211**, No. 2, pp. 76-85, February 1964.

2. Ferguson, J. L., 'Liquid crystals in nondestructive testing', *Applied Optics*, 7, No. 9, pp. 1729-37, September 1968; Heilmeyer, G. H. and Goldmacher, J. E., 'A new electric-field-controlled reflective optical storage effect in mixed-liquid crystal systems', *Applied Physics Letters*, 13, No. 4, pp. 132-3, August 1968.
3. Franken, P. A. and Ward, J. F., 'Optical harmonics and nonlinear phenomena', *Reviews of Modern Physics*, 35, No. 1, pp. 23-39, January 1963; Maker, P. D. and Terhune, R. W., 'Study of optical effects due to an induced polarization third order in the electric field strength', *Physical Review*, 137, No. 3A, pp. 801-18, February 1965.
4. Gray, G. W., 'The mesomorphic behaviour of the fatty esters of cholesterol', *J. Chem. Soc.*, pp. 3733-39, 1956.
5. Bey, P. P., Giuliani, J. F. and Rabin, H., 'Phase-matched optical harmonic generation in liquid media employing anomalous dispersion', *I.E.E.E. J. Quantum Electronics*, QE-4, No. 11, pp. 932-9, November 1968.
6. Goldberg, L. S. and Schnur, J. M., 'Optical second- and third-harmonic generation in cholesteryl nonanoate liquid crystal', *Applied Physics Letters*, 14, No. 10, pp. 306-8, May 1969.
7. Ferguson, J. L., 'Cholesteric structure—I, optical properties', *Molecular Crystals*, 1, No. 2, pp. 293-307, April 1966; Ferguson, J. L., Goldberg, N. N. and Nodalin, R. J., 'Cholesteric structure—II, chemical significance', *Molecular Crystals*, 1, No. 2, pp. 309-23, April 1966.
8. Rabin, H. and Bey, P. P., 'Phase matching in harmonic generation employing optical rotatory dispersion', *Phys. Rev.*-156, No. 3, pp. 1010-16, April 1967.
9. Freund, I. and Rentzepis, P. M., 'Second-harmonic generation in liquid crystals', *Phys. Rev. Letters*, 18, No. 11, pp. 393-4, March 1967.
10. Durand, G. and Lee, C. H., 'Sur l'origine de la generation d'harmonique lumineux dans un cristal liquide', *C.R. Acad. Sci., Paris*, 264, No. 20, Series B, pp. 1397-9, May 1967.
11. Durand, G. and Lee, C. H., 'On the origin of second harmonic generation of light in liquid crystals', *Molecular Crystals*, 5, No. 2, pp. 171-83, October 1968.
12. Vainshtein, B. K. and Christyakov, I. G., 'X-ray analysis of the structure of liquid crystals with the help of distribution functions', *Soviet Physics Doklady*, 8, No. 11, pp. 1044-7, May 1964 (English translation); Christyakov, I. G., 'Liquid crystals', *Soviet Physics Uspekhi*, 9, No. 4, pp. 541-73, January-February 1967 (English translation).
13. Kurtz, S. K. and Perry, T. T., 'A powder technique for the evaluation of nonlinear optical materials', *J. Appl. Phys.*, 39, No. 8, pp. 3798-813, July 1968.
14. Kielich, S., 'Higher-order elastic scattering of laser light', *Acta Physica Polonica*, 33, pp. 141-3, 1968; 'Multi-harmonic molecular light scattering in liquids', *Chemical Physics Letters*, 1, pp. 441-2, 1967.

Manuscript first received by the Institution on 20th January 1969 and in final form on 20th February 1970. (Paper No. 1322, CC77.)

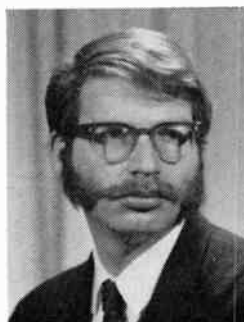
© The Institution of Electronic and Radio Engineers, 1970

The Authors



Dr. Laurence S. Goldberg graduated in physics from Washington University in 1961 and received the Ph.D. degree of Cornell University in solid state physics in 1966; his thesis was on the optical and e.s.r. phenomena of irradiation defect centres in alkali halides. In 1966-67 he carried out post-doctoral research at the University of Frankfurt, and since October 1967 he has been with

the Quantum Optics Branch of the Naval Research Laboratory, concerned with laser and n.l.o. research.



Joel M. Schnur obtained his first degree at Rutgers University, and his M.S. at Georgetown University, where he is now undertaking research into the thermodynamics of mesomorphic materials for a doctorate. In 1968-69 he was a research associate in the Quantum Optics Branch at the Naval Research Laboratory, and he is currently acting as consultant on aspects of liquid crystal

research with Display Sciences, of Upper Saddle River, New Jersey.

Performance Factor and Power Gain of Linear Active Two-Ports

By

Professor

S. VENKATESWARAN, B.Sc.,
M.A., Ph.D., D.I.C., C.Eng., M.I.E.E.†

and

V. P. NAMJOSHI, B.Tech.‡

Resistively mismatched, reactively tuned active two-ports can be designed for a given performance factor, n , by the analytical solution of appropriate equations. A previous paper provided a computer solution in the form of graphs for the range $1 \leq n \leq 10$ and a simple, closely accurate, analytical solution for $n \geq 10$. The present paper extends the computer solution from $n = 1$ to the limit of stability, where $n = \Pi$. It establishes that the root for optimum gain is the only positive real root if $\arg(p_{12}p_{21})$ is between 0 and π radians, and the only negative real root if $\arg(p_{12}p_{21})$ is between π and 2π radians.

1. Introduction

The operating power gain of an active two-port is given by

$$g = \frac{4|p_{21}|^2 \rho_s \rho_L}{|p_1 p_2 - p_{12} p_{21}|^2} \quad \dots\dots(1)$$

Here $\begin{bmatrix} p_{11} & p_{12} \\ p_{21} & p_{22} \end{bmatrix}$ is the general p -matrix of the device network in h -, z -, y - or g -matrix environment. Also

$$p = \rho + j\sigma \quad \dots\dots(2)$$

$$p_1 = p_{11} + p_s = \rho_1 + j\sigma_1; \quad p_2 = p_{22} + p_L = \rho_2 + j\sigma_2 \quad \dots\dots(3)$$

ρ_s and ρ_L are the source and load terminations respectively.

The performance factor¹⁻⁷, n , is a measure of the stability of the two-port network with ρ_s and ρ_L , while the 'inherent performance factor' n_i , is a particular value of n when $\rho_s = \rho_L = 0$.

$$n = \frac{\rho_1 \rho_2}{L}; \quad n_i = \frac{\rho_{11} \rho_{22}}{L} \quad \dots\dots(4)$$

where

$$p_{12} p_{21} = M + jN = L \angle \theta. \quad \dots\dots(5)$$

The maximum operating power gain of a two-port network, for a given value of $n > (1 + \cos \theta)/2$ or Π (Π is a normalizing factor, $(L + M)/2L$) is given by¹

$$g_{\max n} = 4F \frac{|p_{21}|}{|p_{12}|} \left(1 - \sqrt{\frac{n_i}{n}}\right)^2 \quad \dots\dots(6)$$

where

$$F = \frac{n}{[n(1 - \lambda_0^2) - \cos \theta]^2 + [2n\lambda_0 - \sin \theta]^2} \quad \dots\dots(7)$$

λ_0 is that particular real root of the cubic equation

$$\lambda^3 + \left(1 + \frac{\cos \theta}{n}\right)\lambda - \frac{\sin \theta}{n} = 0 \quad \dots\dots(8)$$

that makes the denominator of equation (7) a minimum.

The terminations for this maximum power gain are given by¹

$$\frac{\rho_s}{\rho_{11}} = \frac{\rho_L}{\rho_{22}} = \sqrt{\frac{n}{n_i}} - 1 \quad \dots\dots(9)$$

$$\sigma_s = \lambda_0 \rho_1 - \sigma_{11}; \quad \sigma_L = \lambda_0 \rho_2 - \sigma_{22} \quad \dots\dots(10)$$

Computer solution of λ_0 and F in the form of graphs was provided previously¹ for the range of n values between 1 and 10. This paper extends the range of n values below 1 to the limit of stability, where $n = (1 + \cos \theta)/2$ or Π . It establishes that the root for optimum gain is the only positive real root, if $\arg(p_{12}p_{21})$ is between 0 and π radians and the only negative real root, if $\arg(p_{12}p_{21})$ is between π and 2π radians.

2. Computer Solution

Equation (8) has been solved for values of n from 0.1 to 1.0 in steps of 0.1, for angle θ ranging between $\cos^{-1}(2n-1)$ to 180° in steps of 10° . If there is only one real root, it is λ_0 . When three real roots exist, one root is positive and the rest are negative. In this case, the positive root is λ_0 as it gives the maximum power gain. This is proved in Appendix 5.2.

Substitution of λ_0 in equation (7) yields the normalizing factor F of equation (6). Plots of λ_0 and F versus θ for various values of n between Π and 1.0 are given in Figs. 1 and 2 respectively. For angles between 180° and 360° or -180° and -0° , λ_0 is obtainable from

$$\lambda_0(-\theta) = -\lambda_0(\theta) \quad \dots\dots(11)$$

by inspection of the cubic equation (8) above. Equations (7) and (11) now give

$$F(-\theta) = F(\theta). \quad \dots\dots(12)$$

Figures 1 and 2 along with equations (6), (9) to (12) provide all the necessary data for designing resistively mismatched single stages with values of n between

† Department of Electrical Engineering, Indian Institute of Technology, Kanpur 16, India.

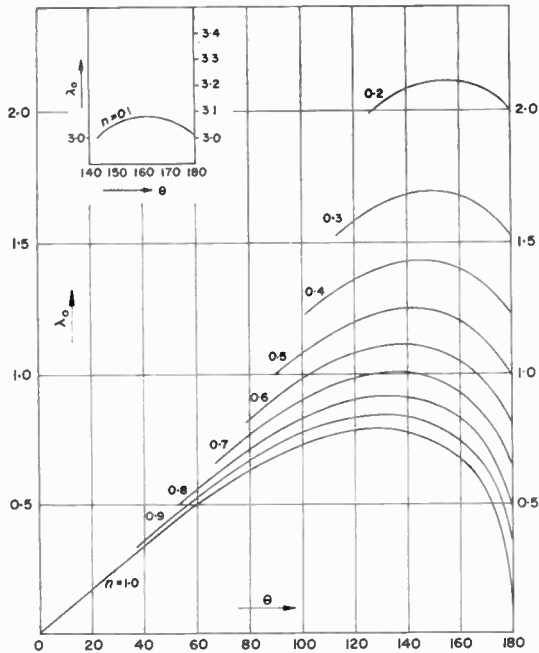


Fig. 1. Variation of λ_0 with θ for different values of the performance factor, n , ranging between $(1 + \cos \theta)/2$ and 1 in steps of 0.1.

Π and 1.0. For values of $n > 1$, with an example of actual design, refer to the earlier paper.¹

3. Acknowledgments

The authors wish to express their indebtedness to Dr. P. K. Kelkar, Director and the Computer Centre, Indian Institute of Technology, Kanpur, for the facilities provided.

4. References

1. Venkateswaran, S. and Namjoshi, V. P., 'Design of resistively mismatched single amplifier stages', *The Radio and Electronic Engineer*, 36, No. 1, pp. 61-6, July 1968.
2. Venkateswaran, S. and Boothroyd, A. R., 'Power gain and bandwidth of tuned transistor amplifier stages', *Proc. Instn. Elect. Engrs*, 106B, Suppl. 15, pp. 518-29, January 1960.
3. Boothroyd, A. R., 'The transistor as an active two-port network', *Scientia Electronica*, 7, pp. 3-15, March 1961.
4. Venkateswaran, S., 'An invariant stability factor and its physical significance', *Proc. Instn. Elect. Engrs*, 109C, pp. 98-102, 1962. (I.E.E. Monograph No. 468E, September 1961).
5. Spence, R., 'On the latitude of choice of tuned amplifier terminations', *Trans. Inst. Radio Engrs on Circuit Theory*, CT-9, pp. 336-9, December 1962.
6. Venkateswaran, S., 'Performance factor of linear two-port active networks', *The Radio and Electronic Engineer*, 35, No. 2, pp. 109-14, February 1968.
7. Venkateswaran, S., 'An invariant alignability factor and its significance', *The Radio and Electronic Engineer*, 35, No. 6, pp. 361-8, June 1968.

8. Venkateswaran, S. and Spence, R., 'Maximum power gain of an active two-port network', *Proc. I.E.E.E.*, 57, pp. 402-3, February 1963 (Letters).

5. Appendices

5.1. Number of Real Roots, their Signs and Magnitudes

Equation (8) has only one real root⁸ for $n \geq 1$, but for $n < 1$, it can either have one or three real roots. Rearranging equation (8),

$$\lambda = f(\lambda) = \frac{\sin \theta}{n + \cos \theta + n\lambda^2} = \frac{a}{\lambda^2 - b} \quad \dots\dots(13)$$

where

$$a = \frac{\sin \theta}{n} \quad \text{and} \quad b = -\left(\frac{n + \cos \theta}{n}\right) \quad \dots\dots(14)$$

Roots of equation (8) are values of λ common to the two equations:

$$y = \lambda \quad \text{and} \quad y = \frac{a}{\lambda^2 - b} \quad \dots\dots(15)$$

When $n \geq -\cos \theta$, b of equation (14) is ≤ 0 . Graphical solution of the real roots of equation (15) for positive a or $0 \leq \theta \leq \pi$ is illustrated by Fig. 3. It is easily verified that the only real root is positive. If θ changes sign, equation (11) is applicable and the only real root is negative.

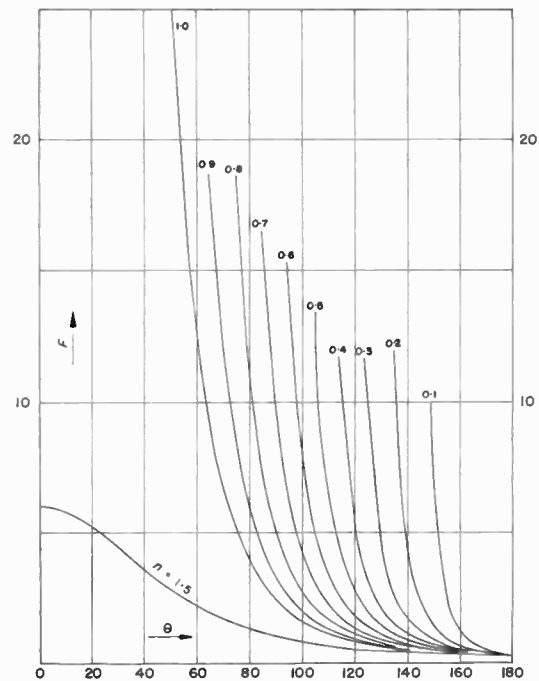


Fig. 2. Variation of F with θ for different values of the performance factor, n , ranging between $(1 + \cos \theta)/2$ and 1 in steps of 0.1.

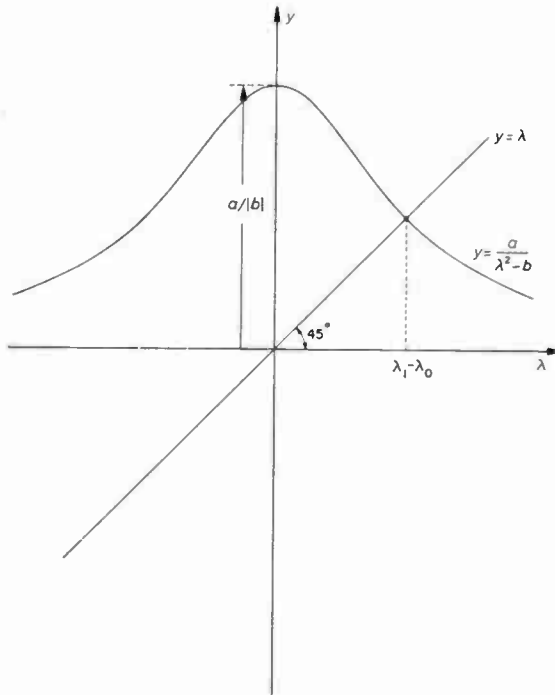


Fig. 3. Graphical solution of the real roots of the cubic equation, when a is positive and b is negative.

When $n < -\cos \theta$, b is > 0 . There will now be one or three real roots. Graphical solution of three real roots of equation (15) for $0 \leq \theta \leq \pi$ is illustrated by Fig. 4. If a/b is made sufficiently large, the middle inverted U curve shifts downwards to give only one real root for equation (8).

Let the λ -coordinates of the points of intersection A, B and C of Fig. 4 be λ_1 , λ_2 and λ_3 respectively. It is easily verified that

$$\lambda_1 > \sqrt{b}; \quad 0 > \lambda_2 > -\sqrt{b}; \quad 0 > \lambda_3 > -\sqrt{b} \quad \dots\dots(16)$$

Hence

$$\lambda_1 + \lambda_2 > 0; \quad \lambda_1 + \lambda_3 > 0 \quad \dots\dots(17)$$

$$\lambda_1 - \lambda_2 > 0; \quad \lambda_1 - \lambda_3 > 0 \quad \dots\dots(18)$$

When θ is negative, equation (11) is applicable, so that for $-0 \geq \theta \geq -\pi$,

$$\lambda_1 < -\sqrt{b}; \quad 0 < \lambda_2 < \sqrt{b}; \quad 0 < \lambda_3 < \sqrt{b} \quad \dots\dots(19)$$

$$\lambda_1 + \lambda_2 < 0; \quad \lambda_1 + \lambda_3 < 0 \quad \dots\dots(20)$$

$$\lambda_1 - \lambda_2 < 0; \quad \lambda_1 - \lambda_3 < 0 \quad \dots\dots(21)$$

5.2. Optimum Root, when there are three real roots

Substitution of λ_1 , λ_2 and λ_3 , the three real roots of cubic equation (8), in succession for λ_0 of equation (7), gives the three possible power gains. Of these, only

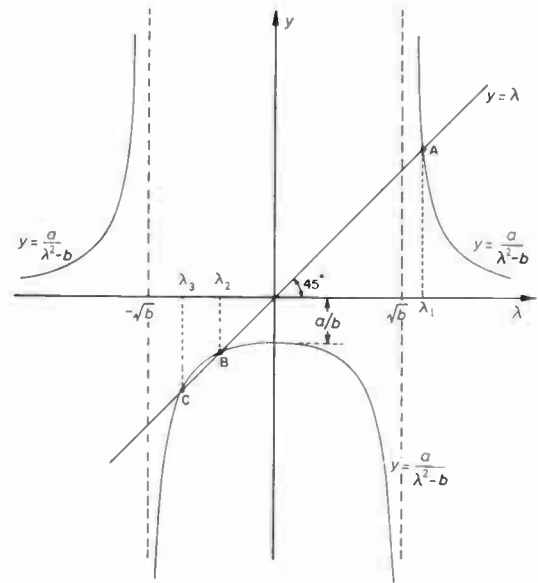


Fig. 4. Graphical solution of the real roots of the cubic equation, when a and b are both positive, while a/b is small.

one gives the maximum power gain of equation (6). Call the denominator of F , d_1 when λ_0 is replaced by λ_1 etc.; the following relations are obtained, after eliminating λ_1^4 etc., by use of cubic equation (8) multiplied by λ_1 etc.

$$d_1 = -n^2(b\lambda_1^2 + 3a\lambda_1) + n^2 - 2n \cos \theta + 1 \quad \dots\dots(22)$$

where a and b are defined by equations (14).

$$d_2 = -n^2(b\lambda_2^2 + 3a\lambda_2) + n^2 - 2n \cos \theta + 1 \quad \dots\dots(23)$$

$$d_3 = -n^2(b\lambda_3^2 + 3a\lambda_3) + n^2 - 2n \cos \theta + 1 \quad \dots\dots(24)$$

Hence

$$d_1 - d_2 = -n^2(\lambda_1 - \lambda_2)[b(\lambda_1 + \lambda_2) + 3a] \quad \dots\dots(25)$$

and

$$d_1 - d_3 = -n^2(\lambda_1 - \lambda_3)[b(\lambda_1 + \lambda_3) + 3a] \quad \dots\dots(26)$$

a is positive when $0 \leq \theta \leq \pi$ and b is positive, if there are three real roots (refer Appendix 5.1). Relations (17) and (18) with equations (25) and (26), make d_1 smaller than d_2 or d_3 . Hence λ_0 , the root that gives optimum power gain, equals the only positive real root, λ_1 .

For $-0 \geq \theta \geq -\pi$, a is < 0 and relations (20) and (21) with equations (25) and (26) apply. In this case, λ_0 , equals the only negative real root, λ_1 .

Manuscript first received by the Institution on 21st February 1969 and in revised form on 1st October 1969. (Short contribution No.134/CC78).

© The Institution of Electronic and Radio Engineers, 1970